e-ISSN: 2148-4171

12 cilt volume
2 sayı issue
2025 Haziran June

HITTITE JOURNAL OF SCIENCE AND ENGINEERING

HİTİT ÜNİVERSİTESİ YAYINLARI

HITTITE JOURNAL OF SCIENCE AND ENGINEERING

e-ISSN: 2148-4171

Volume 12

June 2025

Issue 2

LANGUAGE OF PUBLICATION

English

CONTACT ADDRESS

Hitit Üniversitesi Mühendislik Fakültesi, ÇORUM, TÜRKİYE
Tel: 0090 364 2191200 Fax: 0090 364 2191399
hjse@hitit.edu.tr | https://www.hjse.hitit.edu.tr

PUBLISHER

Hitit University Press

LOCKSS: http://dergipark.org.tr/hjse/lockss-manifest

OAI: https://dergipark.org.tr/ api/public/oai/hjse/?verb=ListRecords&metadataPrefix=oai_de

Dear Readers,

As the spring semester draws to a close and the summer break begins, many academics will take this opportunity to complete their ongoing research. This period also offers the valuable opportunity to attend scientific meetings, present new work, connect with fellow researchers, and build networks for future collaborations.

As Editor-in-Chief of the Hittite Journal of Science and Engineering (HJSE), I wish all academics a productive and restful break. May you all begin the new 2025-2026 Academic Year in good health and peace.

Working in a disciplined and team spirit, we have published the new issue of the Hittite Journal of Science and Engineering (2025-Volume 12, Issue 2). During the publishing stages of this issue, HJSE Team and Hitit University Publishing Office worked together. I want to thank HJSE team members, Hitit University Publishing Office, all our authors, and contributing reviewers of this issue.

As Editor in Chief, I also would like to thank to the President of Hitit University, Prof. Dr. Ali Osman Öztürk, for his support and interest in HJSE and to the Associate Editors of HJSE, namely Prof. Dr. Dursun Ali Kose and Assoc. Prof. Dr. Öncü Akyıldız and also the Section Editors of HJSE, namely Prof. Dr. Murat Hoşöz, Prof. Dr. Kazım Savaş Bahçeci, Prof. Dr. Cengiz Baykasoğlu and Prof. Dr. Akif Akgül as well as our Production Editors, Ömer Faruk Tozlu, Harun Emre Kıran and Hayati Töre for their invaluable efforts in making of the journal.

This issue of Hittite Journal of Science and Engineering covers two papers from mechanical engineering, one from electrical and electronic engineering, one from civil engineering and the last from transportation engineering. The first paper from mechanical engineering investigates the effects of water absorption behaviors on the hybrid glass/carbon fiber reinforced composite pipes with ±50° and ±70° winding angles that were subjected to hydrothermal aging in both distilled water and seawater environments for 120 days at 30°C. In the second paper related to mechanical engineering, a nonlinear model predictive control (NMPC) strategy was developed for the formation tracking of AGVs operating in a leader-follower configuration, and it is mentioned that the proposed method enables follower vehicles to track dynamically assigned positions in a geometric formation relative to a leader AGV that moves along a predefined figure-eight trajectory. As for the article in electrical and electronic engineering, the coefficients of the PI controller used for speed regulation of a DC motor were experimentally determined using the Particle Swarm Optimization (PSO) and Sine Cosine Algorithm (SCA) methods for three different reference values, including step, sinus with offset, and sinus without offset signals and four distinct control methods including open-loop control, PI control, PSO-PI control, and SCA-PI control. The paper from the discipline of civil engineering is based on the bibliometric analysis aiming to evaluate the publications on sustainable building renovation using the data obtained from the Web of Science (WoS) database, and it is mentioned in the paper that the data were created visual network maps using the VOSviewer program. The last paper, from transportation engineering, using the analytical hierarchy process (AHP) and TOPSIS methods, investigates the most suitable location for the installation of an electric vehicle (EV) charging station within the Erzincan Binali Yıldırım University Yalnızbag Campus. I hope the papers published in this issue (2025-Volume 12, Issue 2) will be helpful to researchers conducting research in the discipline of engineering mentioned above.

I would be very pleased to call on academics and researchers working in engineering to publish their best articles in the Hittite Journal of Science and Engineering.

Dr. Ali Kılıçarslan

Editor-in-Chief

CONTENTS

From Editor

Performance Analysis of Environmental Conditioning Effect on Crush Character of Hybrid Composite Pipes with Different Winding Angles
Özkan Özbek, Zeynal Abidin Oğuz, Ahmet Erkliğ, Ömer Yavuz Bozkurt **59**

Bibliometric Analysis of Publications on Sustainable Renovation of Buildings from 2001 to 2024
Sema Balçık, Ruşen Yamaçlı **69**

Optimization-Based Tuning of PI Controller Parameters for DC Motor Speed Control
Ahmet Top **81**

An Application on Electric Vehicle Charging Station Site Selection With Multi-Criteria Decision-Making Methods
Şeyma Sünbül, Ahmet Tortum **91**

Nonlinear MPC-Based Formation Control for Autonomous Ground Vehicles with Dynamic Geometric Patterns
Can Ulas Dogruer **101**

HITTITE JOURNAL OF SCIENCE AND ENGINEERING

e-ISSN: 2148-4171
Volume: 12 • Number: 2
June 2025

Performance Analysis of Environmental Conditioning Effect on Crush Character of Hybrid Composite Pipes with Different Winding Angles

Özkan Özbek[1] | Zeynal Abidin Oğuz[*2] | Ahmet Erkliğ[3] | Ömer Yavuz Bozkurt[3]

[1]Pamukkale University, Faculty of Engineering, Mechanical Engineering Department, 20160 Denizli, Türkiye.
[2]Adıyaman University, Besni Ali Erdemoğlu Vocational School, Mechatronics Department, 02040 Adıyaman, Türkiye.
[3]Gaziantep University, Faculty of Engineering, Mechanical Engineering Department, 27310 Gaziantep, Türkiye.

Corresponding Author

Zeynal Abidin Oğuz
E-mail: zoguz@adiyaman.edu.tr Phone: +90 554 845 42 05
RORID[1]: https://ror.org/01etz1309 RORID[2]: https://ror.org/02s4gkg68 RORID[3]: https://ror.org/020vvc407

Article Information

Article Type: Research Article
Doi: https://doi.org/10.17350/HJSE19030000352
Received: 27.02.2025
Accepted: 09.04.2025
Published: 30.06.2025

Cite As

Özbek Ö, et al. Performance analysis of environmental conditioning effect on crush character of hybrid composite pipes with different winding angles . Hittite J Sci Eng. 2025;12(2):59-67.

Peer Review: Evaluated by independent reviewers working in at least two different institutions appointed by the field editor.
Ethical Statement: Not available.
Plagiarism Checks: Yes - iThenticate
Conflict of Interest: Authors declare no conflict of interest.

CRediT AUTHOR STATEMENT

Özkan Özbek: Conceptualization, Data curation, Formal Analysis, Investigation, Methodology, Resources, Supervision, Writing – review and editing. **Zeynal Abidin Oğuz:** Conceptualization, Data curation, Formal Analysis, Investigation, Methodology, Supervision, Visualization, Writing – original draft & editing. **Ahmet Erkliğ:** Conceptualization, Data Curation, Formal Analysis, Methodology, Validation, Writing. **Ömer Yavuz Bozkurt:** Conceptualization, Data Curation, Formal Analysis, Methodology, Validation, Writing.

Performance Analysis of Environmental Conditioning Effect on Crush Character of Hybrid Composite Pipes with Different Winding Angles

Özkan ÖZBEK[1]|Zeynal Abidin OĞUZ*[2]|Ahmet ERKLİĞ[3]|Ömer Yavuz BOZKURT[3]

[1]Pamukkale University, Faculty of Engineering, Mechanical Engineering Department, 20160 Denizli, Türkiye.
[2]Adıyaman University, Besni Ali Erdemoğlu Vocational School, Mechatronics Department, 02040 Adıyaman, Türkiye.
[3]Gaziantep University, Faculty of Engineering, Mechanical Engineering Department, 27310 Gaziantep, Türkiye.

Abstract

The effects of hydrothermal aging in distilled water (DW) and seawater (SW) environments on the water absorption behavior and crush characteristics of hybrid glass/carbon fiber-reinforced composite pipes with ±55° and ±70° winding angles were evaluated. Specimens were kept for 120 days at 30°C, and water absorption was analyzed experimentally and theoretically. Results revealed that distilled water-aged samples exhibited higher maximum water absorption rates (2.5% for DW55 and 2.62% for DW70) compared to seawater-aged samples (2.37% for SW55 and 2.44% for SW70), attributed to the inhibitory role of ionic components in seawater. Lower winding angles consistently showed greater water absorption due to increased microstructural voids, facilitating water diffusion. Quasi-static axial compression tests demonstrated significant degradation in crush performance after aging. Unconditioned samples with 70° winding angles achieved the highest initial peak load (56.9 kN) and specific energy absorption (28.89 J/g). However, aging reduced these values, with seawater-aged samples (SW55) showing a 12.32% decrease in specific energy absorption compared to unconditioned counterparts. Crushing force efficiency (CFE) also declined, correlating with matrix plasticization and fiber/matrix interface weakening. Notably, hybrid pipes with 55° winding angles exhibited superior energy absorption (30.44 J/g for U55), emphasizing the role of fiber orientation in load distribution.

Keywords: Hybrid composites, Hydrothermal aging, Winding angle, Fickian diffusion, Crush performance, Energy absorption

INTRODUCTION

Composites have numerous better qualities compared to conventional materials. Since these materials are formed by combining different components, they can simultaneously carry opposing properties such as high strength and lightness. In particular, high specific strength (strength/density ratio) and specific stiffness (stiffness/density ratio) values make composites indispensable in sectors where lightweight and durable materials are critical, such as aerospace, automotive and construction. In addition, their properties such as corrosion resistance, fatigue life and chemical resistance are superior to traditional metals and alloys [1,2]. For this reason, composite materials are widely preferred in order to increase performance and efficiency in modern engineering applications. Composite pipes offer significant advantages over pipes manufactured with traditional materials in industrial and industrial applications. These pipes stand out with their features such as high corrosion resistance, lightness, long life and low maintenance costs. Especially in sectors such as petrochemical, energy, water and wastewater management, composite materials provide a more durable and economical solution than metal pipes in pipelines exposed to aggressive chemicals and harsh environmental conditions. In addition, the high mechanical strength and low thermal conductivity of composite pipes minimize energy losses and increase system efficiency. Therefore, composite pipes are of great importance in terms of the sustainability and performance of modern industrial infrastructures. Testing the sensitivity of composite pipes to environmental aging is critical to assessing the long-term performance and reliability of these materials. Environmental factors (humidity, water, UV rays, temperature changes, chemical exposure, etc.) can affect the mechanical properties of composite materials, causing structural changes. Such aging effects can change the load-bearing capacity, leak-tightness, and overall service life of pipes [3,4]. Therefore, accelerated aging tests performed in laboratory environments help predict the durability and performance of composite pipes by simulating their behavior under different environmental conditions. These tests enable improvements in the design and material selection of pipes, ensuring their safe and sustainable use in industrial applications.

Zuo et al. [5] evaluated the crashworthiness of carbon fiber reinforced plastic (CFRP) composite tubes under thermal and hydrothermal aging conditions were experimentally investigated. CFRP tubes were subjected to thermal aging at temperatures of 25°C, 70°C, 100°C and 160°C and to hydrothermal aging at 25°C and 70°C. As a result of the experiments, it was observed that the impact strength of CFRP tubes decreased significantly with increasing temperature. For example, specific energy absorption (SEA) decreased by 35% at 70°C, 86% at 100°C and 94% at 160°C. As a result of hydrothermal aging, water absorption reached 1.4118% at 70°C, and this reduced the average crushing load of CFRP tubes by 25%. Microscopic examinations showed that temperature and humidity significantly affected the bonding state between the fiber and the resin.

The behavior of glass reinforced epoxy (GRE) composite pipes with [±55°]4 winding angle at multiaxial stress rates under accelerated hydrothermal aging conditions was experimentally investigated by Krishnan et al. [6]. The pipes were aged by exposure to water at 80°C for 1500 h and then subjected to multiaxial cyclic loading tests at five different stress rates. Axial and circumferential strength reductions of up to 14% were observed in the aged pipes. Scanning electron microscope (SEM) images revealed a significant separation between the epoxy resin and glass fibers in the aged samples. The results show that hydrothermal aging significantly affects the mechanical properties of GRE pipes, and especially the axial strength is damaged more.

Fitriah et al. [7] investigated the effects of hydrothermal aging on the compressive strength of glass fiber reinforced epoxy (GRE) composite pipes. Pipes with three different winding angles (±45°, ±55°, ±63°) were aged for 500, 1000 and 1500 hours in tap water at 80°C and compression tests were conducted at different temperatures such as 25°C, 45°C

and 65°C in accordance with ASTM standard. The results showed that the strength of the pipes decreased significantly as temperature and aging time increased, but the strength increased as the winding angle decreased. For example, the strength of the pipes with ±45° angle at 25°C decreased from 118.9 MPa to 64.6 MPa, while the strength of the pipes with ±63° angle decreased from 59.4 MPa to 37.2 MPa. The experimental results were predicted by the Berbinau model and agreement was achieved with a maximum deviation of 25%.

Sepetçioğlu et al. [8] searched the effect of hydrothermal aging on the mechanical properties was investigated by adding 0.25% graphene nanoplatelets (GnP) to basalt fiber reinforced epoxy composite pipes (BFRP). Mechanical properties such as water absorption, hardness, density and environmental tensile strength were tested in accordance with ASTM standards in samples aged in distilled water at 80 °C for 15, 30, 45 and 60 days. Aging showed that the mechanical properties of BFRPs decreased significantly due to water absorption and temperature-induced stresses; for example, the environmental tensile strength of unaged unreinforced samples decreased from 677.9 MPa to 430.6 MPa at the end of 60 days, while this decrease was from 694.7 MPa to 449.1 MPa in GnP reinforced samples. GnP reinforcement reduced mechanical losses by strengthening the fiber-matrix interfacial bonds. Additionally, the hydrophobic properties of GnP reduced water absorption and contributed to the preservation of mechanical properties.

Kara et al. [9] assessed the impact character and mechanical properties of hydrothermally aged multiwalled carbon nanotube (MWCNT) reinforced carbon composite pipes with ±55° winding angle were investigated. For aging conditions, fluid, temperature and aging time were selected as distilled water, 80°C and 3 weeks, respectively. The samples subjected to ring tensile test (ASTM D 2290) and low-velocity impact tests at 5, 10, 15 J energy levels after aging. The results showed that MWCNT reinforcement increased the tangential tensile strength of the composite pipes, but this strength decreased with the aging process. For example, after 3 weeks of aging, the tangential tensile strength decreased by 17% in MWCNT-reinforced samples and by 13% in samples without MWCNT reinforcement. In low-velocity impact tests, MWCNT reinforcement increased the impact resistance, but the aging process negatively affected this resistance. In particular, the maximum contact force decreased by 26% in particulated pipes after 3 weeks of aging. The aging process increased the damage mechanisms such as delamination and matrix cracks in the samples and decreased the impact durability of the material. It was discovered that MWCNT reinforcement increased the mechanical characteristics of pipes, however aging largely removed this benefit.

Oğuz et al. [10] studied the the crushing character of hybrid and non-hybrid composite pipes under hydrothermal aging process. Composite pipes are created using glass, basalt and carbon fibers. For aging conditions, fluid, temperature and aging time were selected as purified water/seawater, 30°C and four months. The water absorption data were defined both theoretically and experimentally. The results revealed that basalt pipes had the highest water absorption rate (10.45% in distilled water, 8.44% in seawater), while glass pipes had the lowest water gain rate (1.45% in distilled water, 1.29% in seawater). The mass change rates of hybrid samples remained between these values depending on the fiber types they contained. The aging process adversely affected the crushing character of the samples, and especially the load carrying capacity and energy absorption decreased significantly because of the deterioration at the fiber/matrix interface. For example, while unaged carbon fiber reinforced pipes showed a specific energy absorption of 35.3 J/g, this value decreased by 24-29.3% in aged hybrid CB pipes. Hybrid pipes were particularly effective in improving the performance of pipes with low crushing properties. Hybrid constructions were therefore proposed as a potential advantage for pipelines that may be subjected to severe environmental conditions.

Özbek et al. [11] investigated the different aging conditions effect on the mechanical properties of glass/basalt hybrid pipes after 2500 h aging exposure. Aging negatively affected the mechanical properties; specific energy absorption values decreased by 3.26–11% (distilled water) and 7.31–18.23% (seawater) in glass fiber reinforced samples. The highest specific energy absorption value of 32.9 J/g was observed in the unaged 55% angle glass fiber sample. Aging decreased the load carrying capacity and increased the brittleness of the material, but hybrid samples exhibited a more stable crushing behavior.

In this study, hybrid glass/carbon fiber reinforced composite pipes with ±50° and ±70° winding angles were subjected to hydrothermal aging in both distilled water and seawater environments for 120 days at 30°C, and the effects of water absorption behaviors on the crush properties were investigated. Although there are various studies in the literature on water absorption mechanisms and mechanical performances of composite pipes after aging, most studies have focused on structures containing only single fiber type or short-term aging conditions. In this study, experimental and theoretical water absorption models were derived by considering hybrid fiber content and different winding angles, and their effects on specific energy absorption, load carrying capacity and fracture mechanisms were investigated in detail. In particular, the role of fiber type and winding angle on mechanical weakening due to water absorption was revealed, and the effects of long-term hydrothermal aging on the crush properties of hybrid composite pipes were evaluated more comprehensively. In this respect, the study provides an original contribution to the literature by providing important engineering data for maritime, pipelines and applications requiring structural safety.

MATERIALS & METHODS

Materials

In this study, the fiber reinforcements in the pipe samples were used as carbon roving fiber with a 7 µm filament diameter (Dost Kimya A. Ş., Turkey) and glass fiber roving having a 17 µm filament diameter (Plasto A. Ş., Turkey). To create the matrix phase of the samples, EPIKOTE MGS LR160 resin (Dost Kimya A. Ş., Turkey), and EPIKURE MGS LH260S

Curing Agent (Dost Kimya A. Ş., Turkey) were considered and they were mixed in a stoichiometric weight ratio of 100:35, respectively. The mechanical and physical properties of these materials are given in Table 1.

Table 1 The properties of raw materials [17]

Material	Linear Density (tex)	Tensile Strength (MPa)	Tensile Modulus (GPa)	Elongation at Break (%)	Specific Density (g/cm³)
Carbon Fiber	800	3950	238	1.5	1.77
Glass Fiber	2400	1970	79	3.5	2.56
Epoxy (neat)	-	70-80	3.2-3.5	5.0-6.5	1.18-1.20

Sample Preparation

For all sample fabrication, the filament winding technique which is schematically seen in Figure 1 was used. Interply fiber hybridization is the presence of different fibers in different layers and offers non-homogeneous performance between layers. However, intraply fiber hybridization means winding more than one different filament on the same layer and means having the same fibers in each layer. Therefore, intraply fiber hybridization was planned in the study. Firstly, the fiber reinforcements passing through rollers and resin bath were oriented with the desired parameters. To create intraply fiber hybridization, fiber bundles were stacked side by side. Then, wet fibers were wrapped around a mandrel with the help of motion codes given to the machine. After the winding process, a release agent film was covered, and curing at room temperature was applied for a day. After this period, the pipes were kept at 40°C for 2 hours to perform post-curing [21]. Finally, the samples by cutting with a diamond sawing process were prepared at the desired dimensions with 49.5±1 mm in length. Additionally, their inner and outer diameters were measured as 46.3±0.2 mm and 54.4±0.6 mm, respectively. Five composite pipes were tested for each sample group.

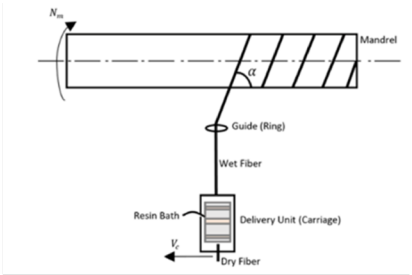

a)

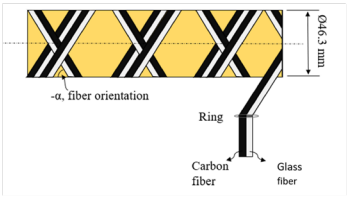

b)

Figure 1 Fabrication of composite pipes; a) filament winding technique [22], b) intraply fiber hybridization [20]

Hydrothermal aging

In this work, pipes were hydrothermally aged for 120 days at 30°C in both saltwater and distilled water. In compliance with ASTM D5229/D5229M-14, the aging procedure was conducted. Purchased sea salts were used to create a seawater solution with a salinity of 3.5%. A 400 L/h circulation pump and an adjustable thermostat with a ±1°C tolerance was used to maintain temperature uniformity in the aging chamber. In this manner, it was ensured that the samples were exposed to identical circumstances at every stage of the aging process and that the ambient temperature stayed constant. Prior to aging, the specimens had been dried until their weight remained consistent. The hybrid glass/carbon fiber tubes used for every specimen group were then submerged in saltwater and distilled water. Throughout the age procedure, specimens were removed from the aging chamber at specific times, their weights were determined using an accurate analytical scale, and the water droplets on their surfaces were meticulously wiped. Weight change calculation was done with two different methods. First, the amount of water present at a certain aging time is calculated:

$$M_f = \frac{(m_t - m_i)}{m_i} \times 100 \quad (1)$$

where m_t, and m_i are the sample's initial weights before and after aging, respectively, and M_f is the percentage of water at that time t.

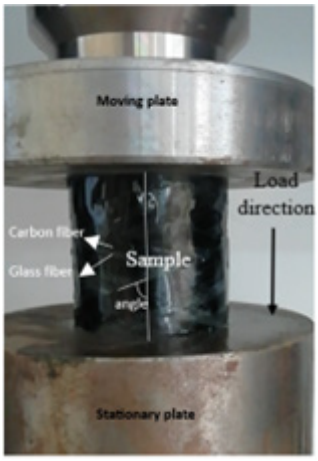

Figure 2 Quasi-static axial compression on Shimadzu AG-X Series testing machine

Fickian's law is used in this work to calculate the sorption of water of the aged samples since it establishes the amount of water uptake in composite materials. The formula is written as:

$$\frac{M_{\%}}{M_m} = 1 - \frac{8}{\pi^2} \sum_{n=0}^{\infty} \frac{1}{(2n+1)^2} \exp\left(\frac{-(2n+1)^2 \pi^2 D t}{h^2}\right) \quad (2)$$

where D is the diffusion coefficient, h is the sample thickness, $M_{\%}$ is the water amount at time, t, and M_m is the amount of water saturation. The following formula can be used to determine D's value:

$$D = \pi\left(\frac{h}{4M_m}\right)^2\left(\frac{M_2-M_1}{\sqrt{t_2}-\sqrt{t_1}}\right)^2 \quad (3)$$

where denotes the linear part of the line and M_2 - M_1 is the slope of the graph of the water intake throughout the first ageing phase.

Quasi-static Axial Compression

The unconditioned and aged pipes were exposed to the quasi-static axial compression loads to define the crushing properties of glass/carbon intraply fiber hybrid reinforced composite pipes. The tests were conducted on the Shimadzu AG-X Series universal testing machine with a frame capacity of 300 kN as shown in Figure 2. 5 mm/min stroke movement was applied for loading rate. The compression amount was adjusted to 35 mm which means approximately 70% stroke efficiency. During the ex periments, the samples we re photographed at various stages (after initial peak (5 mm), during crush (15 mm and 25 mm) and before densification (35 mm)) to examine fracture behaviors under crushing.

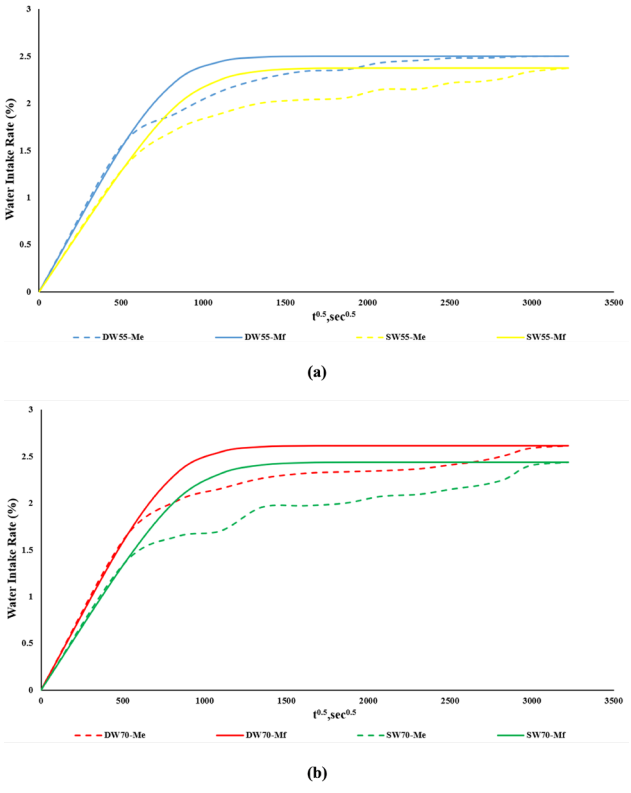

Figure 3 Water intake ratio of pipes different environment conditions a) 55° b) 70° winding angle

The load and displacement values taken by the test device were used for the calculation of the crushing parameters such as mean crushing load, initial peak load, crushing force efficiency, and energy absorption [14]. The total energy absorption, E which is the area under the load-displacement diagram from starting of the test to the end (s_f = 35 mm) was calculated by Eqn. (4):

$$E = \int_0^{S_f} P\left(s\right)ds \quad (4)$$

Mean crushing load, P_m which is a useful indicator to make a reliable comment on crushing was calculated by Eqn. (5):

$$P_m = \frac{\int_0^{S_f} P\left(s\right)ds}{S_f} \quad (5)$$

Crushing force efficiency, CFE is the ratio of mean crushing load to initial peak load (P_i) as seen in Eqn. (6):

$$\mathrm{CFE} = 100(P_m/P_i) \quad (6)$$

The specific energy absorption considering the mass of the samples is seen as the most reliable parameters in crushing experiments. It was calculated by Eqn. (7):

$$E_s = \frac{E}{m_c} \quad (7)$$

RESULTS & DISCUSSIONS

Water Gain Character

Experimental (M_e) and theoretical (M_f) water absorption models obtained after aging of composite pipes in different environments for 55° and 70° winding angle are shown in Figure 3 a) and b) respectively, showing the water uptake rates versus time. In general, the water absorption trend shows a rapid increase at the beginning and then tends to reach saturation. This shows that the material absorbs water rapidly at the beginning, but the amount of water it can absorb becomes limited over time. This behavior also coincides with the theoretical model in accordance with Fick's law. Although there is a general agreement between the experimental results and the theoretical model, there are also differences at some points. These differences may be due to variations in the microstructure of the material or small deviations in the experimental conditions. Further, the differences can be associated with the factors such as microstructure, fiber/matrix interface, and voids of hybrid composite materials may affect the water sorption behavior. The theoretical model may not fully reflect these heterogeneities [9-11].

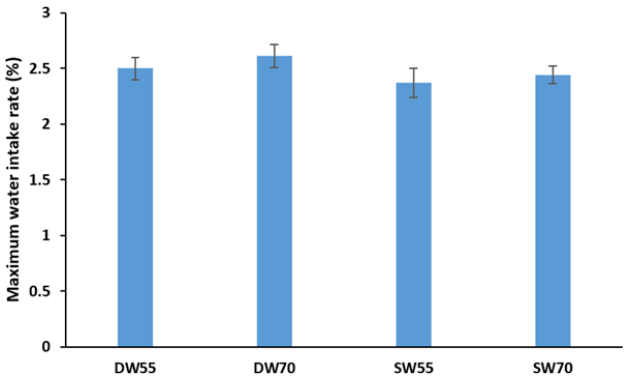

Figure 4 Maximum water intake rate of pipes under different conditions with winding angle

Maximum water intake rates based on aging conditions and winding angles is illustrated in Figure 4. This graph makes it evident that varying aging circumstances and winding angles have a direct impact on the maximum water intake rates of pipes. The maximum water absorption rates of the hybrid composite samples were measured as 2.5%, 2.62%, 2.37%, and 2.44% for DW55, DW70, SW55, and SW70, respectively. Samples aged in distilled water exhibited higher water absorption rates compared to samples aged in seawater. This can be explained by the purity of distilled water and its ability to penetrate the internal structure of the material more effectively. Salt and other ionic components in seawater affected the structure of the material and limited water absorption. Seawater may have reduced the water absorption capacity by creating chemical interactions on the polymer matrix and fiber/matrix interface of the material [12,13]. In addition, samples with a winding angle of 55° exhibited higher water absorption rates compared to samples with a winding angle of 70°. This can be explained by the fact that the lower winding angle causes the formation of more voids and pores in the microstructure of the material. These voids allow easier diffusion of water molecules within the material [10,11]. The main differences between seawater and pure water are due to the presence of ionic components, especially sodium chloride (NaCl). In this study, the lower water absorption of samples aged in seawater (3.5% salinity) compared to pure water (Figure 4) is consistent with the findings in the literature. Oğuz et al. [10] reported that salt ions interact with the polymer matrix as a result of aging hybrid composite pipes in seawater, causing changes in osmotic balance and inhibiting water diffusion. Similarly, Sepetçioğlu et al. [8] stated that ions in seawater accumulate in the microcavities of the composites, physically limiting the penetration of water into the internal structure, thus reducing the maximum water absorption rate by 15-20%. This mechanism explains the low water absorption observed in samples aged in seawater in this study. The high water absorption in samples aged in pure water (DW55: 2.5%, DW70: 2.62%) is related to the freer occurrence of Fickyen diffusion due to the absence of ionic inhibitors. Fitriah et al. [7] showed that the high polarity of pure water increased the swelling of the epoxy matrix, triggered the formation of microcracks, and this accelerated water absorption. In addition, the increased microvoid density in samples with low winding angle (55°) [10,11] shortened the diffusion path of water and increased the absorption rate. These findings are consistent with the effect of fiber orientation on microstructural heterogeneities emphasized by Miki et al. [18] and Wang et al. [19] in the literature.

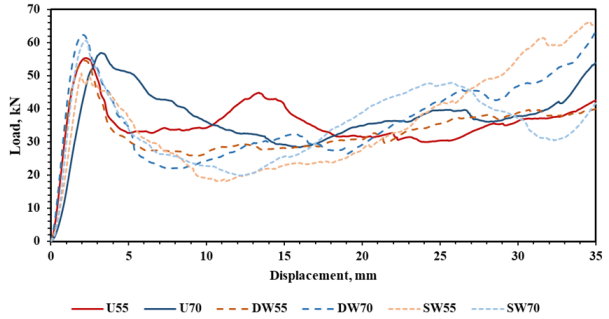

Figure 5 Load-displacement curves of the samples

Crushing Test Results

Load-displacement response and failure modes

The load-displacement graph of the unconditioned and aged pipes with varying winding angles are depicted in Figure 5. The load values initiated with a linear increase up to the first peak point where the short inter/intralaminar crack begins. Then, dramatic decreases were seen, particularly in aged samples. Here, the unconditioned samples showed a better load-bearing capability against crushing loads. So, it can be said that the aging process had a negative effect in the post-crushing zone. This can be associated with the lower interaction between fiber and matrix [15]. According to the literature, aging might be the reason for the matrix fragmentations and weakening fiber/matrix interphases which decreases the mechanical performance of the samples [11,12]. Examining the winding angle revealed that increases in angle led to increases in the first elastic region's load responses. However, a complicated behavior was seen in the post-crushing stage due to intraply fiber hybridization.

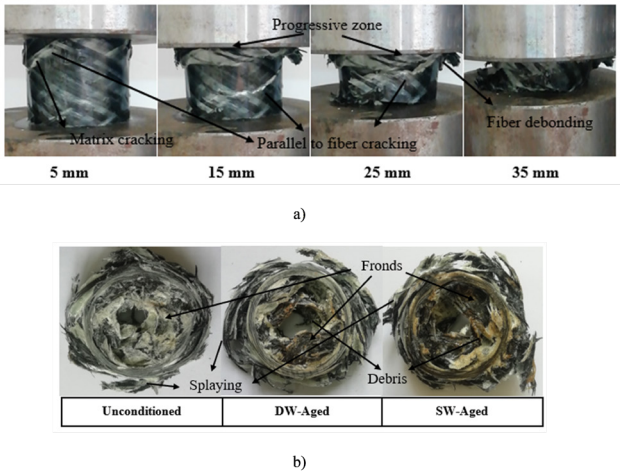

Figure 6 Fracture characteristics; a) crushing history, b) crushed samples

The crushing history of the samples is seen in Figure 6(a). As a result of intraply fiber hybridization, a parallel to fiber cracking because of the presence of glass fiber was seen in the samples. This was the reason for the sharp drop in load values after the first peak load. Also, progressive crushing mode which starts from one end of the sample to the other end is observed. The failures began with matrix fragmentations and were followed by delamination. Then, fiber cracking was observed as a failure mode. The samples exposed to crushing loads are given in Figure 6(b). Outer fiber splaying behaviors are observed due to the debonding of the fibers. Aged samples exhibited more debris as a result of weak fiber/matrix interphase. Additionally, frond formations, especially inner region of the samples, occurred due to parallel fiber cracking. As seen in Figure 6(b), aged samples showed more destructive fracture characteristics because of the degradation of the matrix phase. This may be attributed to the matrix plasticization due to the effects of different environmental conditions [11].

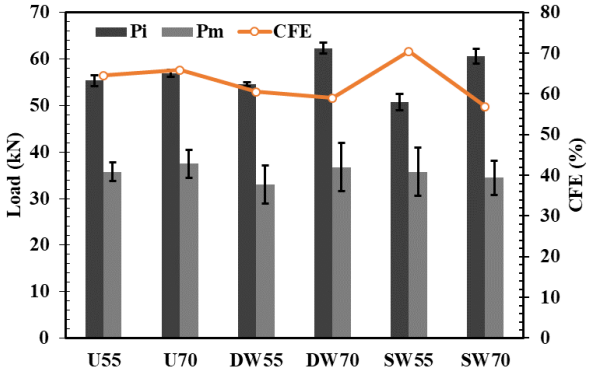

Figure 7 Loading responses of the samples

Loading Characteristics

Figure 7 shows the samples' loading characteristics in terms of initial peak load, mean crushing load, and crushing force efficiency. While the U70 samples had a maximum initial peak load of 56.9 kN, SW55 exhibited a minimum of 50.7 kN. At the same winding angle, U55 with 55.36 kN showed 1.4% and 9.2% more initial load response than DW55 and SW55, respectively. Additionally, the maximum mean crushing load of 37.5 kN was achieved from U70 samples which is 1.9% and 8.7% higher than DW70 and SW70, respectively. So, it can be said that exposure to distilled, and seawater environments decreased the load-bearing capabilities of the unconditioned glass/carbon intraply fiber-reinforced composite pipes. This may be explained by the water absorption of the samples led to matrix fragmentations, non-homogeneity in load distribution, and so local stress concentrations [16]. The performance loss in the samples aged in pure water (SEA in DW55: 28.49 J/g) is related to the polar structure of water causing matrix swelling and microcrack formation. Fitriah et al. [7] showed that pure water creates thermal stresses in the epoxy resin, leading to internal structural heterogeneities, which trigger sudden load drops during crushing. In addition, the high SEA value (30.44 J/g) obtained in the unaged samples (U55) can be explained by the fact that the fiber orientation (55°) optimizes the load distribution and increases energy dissipation. Wang et al. [19] emphasized that low winding angles provide more effective response of the fibers to axial load and this supports the progressive crushing mode. As a result, the corrosion and chemical degradation effects of seawater and the physical swelling mechanisms of pure water affect the crushing behavior of composites in different ways. Studies in the literature [6,10,16] provide critical clues on how these processes can be modulated depending on the design parameters (e.g. fiber orientation, hybridization). In particular, since low wrapping angles (55°) optimize energy absorption but increase the risk of water exposure, the integration of hybrid strategies such as protective coatings or nano-filler reinforcements [8] can be recommended in marine applications. This study provides the experimental and theoretical basis of this balance and provides guidance for industrial optimization.

Energy absorption

Figure 8 displays the unconditioned and aged pipe samples' overall and specific absorbance of energy values. While the maximum value in absorbance of energy was observed from the U70 samples (1311.56 J), the best specific energy absorption of 30.44 J/g was achieved from the U55 samples. These results indicated the importance of mass in the determination of the crushing characteristics of the composites. As seen in Table 2, which shows the crushing indicators of the samples, the mass values of the samples were different due to aging, water absorption, and the content of the composites. So, specific energy absorption was accepted as the main parameter in crushing parameters and was the best way to make a reliable discussion on the results [17]. U55 showed 6.84% and 12.32% higher specific energy absorption than DW55 and SW55, respectively. Also, it was 5.36% more than U70 (28.89 J/g). It was seen that an increase in winding angle cause to drop of the specific energy absorption because of the fiber orientation's closeness to the loading direction [17]. In literature, many studies devoted to fiber orientation had serious effects on the mechanical behaviors of the composites [18,19]. In addition, it is known that salt in seawater creates a partial "barrier effect" on the polymer matrix and reduces the mobility of water molecules [12,13]. Krishnan et al. [6] experimentally proved that NaCl in seawater reduces the plasticization tendency of epoxy resin and provides a more stable structure at the fiber/matrix interface, which slows down water absorption. However, it is also emphasized that salt can also lead to corrosion and chemical degradation [16]. This contradictory effect can be interpreted as the main reason for the mechanical performance loss observed in the samples aged with seawater in this study. The effects of hydrothermal aging in seawater and pure water environments on the crushing performance of hybrid composite pipes are shaped by the synergistic interactions of both ionic components and fiber orientation. In the study, a decrease of 12.32% in specific energy absorption (SEA) of samples aged in seawater (SW55) is consistent with the findings in the literature related to corrosion and fiber/matrix interface deterioration. For example, Sebaey [16] reported that NaCl in seawater triggers galvanic corrosion in composites, weakening the fiber/matrix bond, and this situation increases delamination during crushing. Similarly, Oğuz et al. [10] stated that salt ions accelerate hydrolysis reactions in the epoxy matrix, leading to plasticization, and this process reduces the load carrying capacity. These mechanisms explain the low CFE (70.44%) and SEA (27.10 J/g) values observed in SW55 samples.

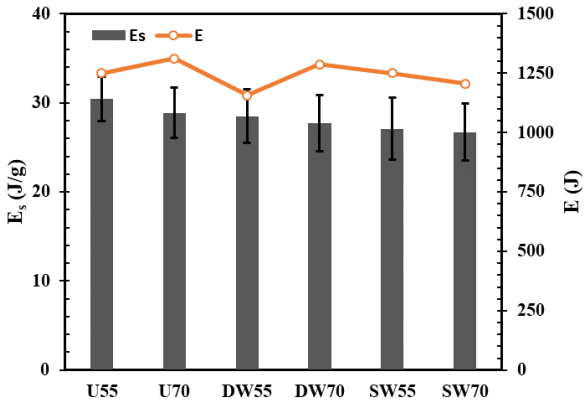

Figure 8 Energy absorption values of the samples subjected to different environmental conditions

Table 2 Summarization of the crushing indicators

	Angle (°)	P_m (kN)	P_i (kN)	CFE (%)	m_{crush} (g)	E (J)	E_s (J/g)
Unconditioned	55	35.7	55.4	64.52	28.52	1250.26	30.44
	70	37.5	56.9	65.83	32.10	1311.56	28.89
DW Aged	55	33.1	54.6	60.53	28.09	1156.90	28.49
	70	36.8	62.3	58.99	33.52	1287.31	27.72
SW Aged	55	35.7	50.7	70.44	32.29	1250.00	27.10
	70	34.5	60.6	56.89	32.27	1206.37	26.70

CONCLUSION

The water adsorption performance and crushing durability of hybrid glass/carbon fiber reinforced composite pipes with ±55° and ±70° winding angles under the impacts of hydrothermal aging in distilled water (DW) and seawater (SW) environments were thoroughly assessed in this work. Peak intake of water percentages was greater in specimens aged in distilled water than in samples aged in seawater (DW55: 2.5%, DW70: 2.62%; SW55: 2.37%, SW70: 2.44%). It was found that the primary cause of this discrepancy was the ionic elements in seawater, which inhibit water transport by generating chemical reactions at the fiber/matrix interface. Because of the increased microstructural voids, specimens with a smaller winding angle (55°) exhibited greater water absorption. The effect of microstructural heterogeneities (void distribution, interfacial distortions) was demonstrated by variations of up to 0.5%, despite the fact that theoretical Fickian models generally agreed with experimental trends. Mechanical characteristics were significantly lost as a result of hydrothermal aging. The maximum initial peak load (56.9 kN) and average crushing load (37.5 kN) were obtained from unaged 70° winding angle samples. These results, however, declined with aging, in samples aged in seawater (SW55), specific energy absorption dropped from 30.44 J/g to 27.10 J/g, a 12.32% decrease. In aged specimens, the CFE dropped (DW55: 60.53%, SW55: 70.44%), which was linked to matrix plasticization and a compromised fiber/matrix interaction. The maximum specific energy absorption (30.44 J/g, U55) was obtained by hybrid tubes with a winding angle of 55°, underscoring the crucial role that fiber orientation plays in load distribution and energy dissipation. The findings emphasize how crucial it is to optimize winding angles and hybrid designs in order to minimize mechanical losses brought on by aging, particularly in harsh settings like pipelines and ships. Low winding angles (55°) boost energy absorption but increase water exposure, therefore design decisions must be balanced.

References

1. Kosedag E. Effect of artificial aging on 3-point bending behavior of glass fiber/epoxy composites. J Reinf Plast Compos. 2023; 42(21-22):1147-53.
2. Demircan G, Kisa M, Ozen M, Acikgoz A, Işıker Y, Aytar E. Nano-gelcoat application of glass fiber reinforced polymer composites for marine application: Structural, mechanical, and thermal analysis. Mar Pollut Bull. 2023; 194:115412.
3. Kosedag E, Caliskan U, Ekici R. The effect of artificial aging on the impact behavior of SiC nanoparticle-glass fiber-reinforced polymer matrix composites. Polym Compos. 2022; 43(2):964-76.
4. Doğan NF, Oğuz ZA, Erkliğ A. An experimental study on the hydrothermal aging effect on the free vibration properties of hybrid aramid/glass/epoxy composites: Comparison of sea water and distilled water. Polym Compos. 2023; 44(10):6902-12.
5. Zuo W, Luo Q, Li Q, Sun G. Effect of thermal and hydrothermal aging on the crashworthiness of carbon fiber reinforced plastic composite tubes. Compos Struct. 2023; 303:116136.
6. Krishnan P, Majid MA, Afendi M, Yaacob S, Gibson AG. Effects of hydrothermal ageing on the behaviour of composite tubes under multiaxial stress ratios. Compos Struct. 2016; 148:1-11.
7. Fitriah SN, Majid MA, Ridzuan MJM, Daud R, Gibson AG, Assaleh TA. Influence of hydrothermal ageing on the compressive behaviour of glass fibre/epoxy composite pipes. Compos Struct. 2017; 159:350-60.
8. Sepetcioglu H, Gunoz A, Kara M. Effect of hydrothermal ageing on the mechanical behaviour of graphene nanoplatelets reinforced basalt fibre epoxy composite pipes. Polym Polym Compos. 2021;29(9_suppl): S166-77.
9. Kara M, Ak S, Uyaner M, Gunoz A, Kepir Y. The effect of hydrothermal aging on the low-velocity impact behavior of multi-walled carbon nanotubes reinforced carbon fiber/epoxy composite pipes. Appl Compos Mater. 2021; 28:1567-87.
10. Oğuz ZA, Özbek Ö, Erkliğ A, Bozkurt ÖY. Hydrothermal aging effect on crushing characteristics of intraply hybrid composite pipes. Eng Struct. 2023; 297:117011.
11. Özbek Ö, Oğuz ZA, Bozkurt ÖY, Erkliğ A. Crashworthiness characteristics of hydrothermally aged intraply glass/basalt composite pipes. Mar Struct. 2024; 97:103656.
12. Oguz ZA, Erklig A, Bozkurt ÖY. Degradation of hybrid aramid/glass/epoxy composites hydrothermally aged in distilled water. J Compos Mater. 2021;55(15):2043-60.
13. Oğuz ZA, Erkliğ A, Bozkurt ÖY. Effects of hydrothermal seawater aging on the mechanical properties and water absorption of glass/aramid/epoxy hybrid composites. Int Polym Process. 2021; 36(1):79-93.
14. Quaresimin M, Ricotta M, Martello L, Mian S. Energy absorption in composite laminates under impact loading. Compos Part B Eng. 2013; 44(1):133-40.
15. Fitriah SN, Majid MA, Ridzuan MJM, Daud R, Gibson AG, Assaleh TA. Influence of hydrothermal ageing on the compressive behaviour of glass fibre/epoxy composite pipes. Compos Struct. 2017; 159:350-60.
16. Sebaey TA. Crashworthiness of GFRP composite tubes after aggressive environmental aging in seawater and soil. Compos Struct. 2022; 284:115105.
17. Özbek Ö, Bozkurt ÖY, Erkliğ A. An experimental study on intraply fiber hybridization of filament wound composite pipes subjected to quasi-static compression loading. Polym Test. 2019; 79:106082.
18. Miki M, Murotsu Y, Tanaka T. Optimum fiber angle of unidirectional composites for load with variations. AIAA J. 1992; 30(1):189-96.
19. Wang HW, Zhou HW, Gui LL, Ji HW, Zhang XC. Analysis of effect of fiber orientation on Young's modulus for unidirectional fiber reinforced composites. Compos Part B Eng. 2014; 56:733-9.
20. Özbek Ö, Oğuz ZA. Crushing behaviors of intraply carbon/basalt hybrid composite pipes under seawater and distilled water aging environments. In: International Scientific Research and Innovation Congress -II; 2024. p. 2509-23.
21. https://www.dostkimya.com/tr/urunler/epoksi-sistemler//mgs-

laminasyon-epoksi-recine-l160 (Date of visit: 08.04.2025)
22. Özbek, Ö., Bozkurt, Ö. Y., & Erkliğ, A. (2022). Development of a trigger mechanism with circular cut-outs to improve crashworthiness characteristics of glass fiber-reinforced composite pipes. Journal of the Brazilian Society of Mechanical Sciences and Engineering, 44, 1-14.

HITTITE JOURNAL OF SCIENCE AND ENGINEERING

e-ISSN: 2148-4171
Volume: 12 • Number: 2
June 2025

Bibliometric Analysis of Publications on Sustainable Renovation of Buildings from 2001 to 2024

Sema Balçık*[1] | Ruşen Yamaçlı[2]
[1]Sivas Cumhuriyet University, Department of Urban and Regional Planning, 58140, Sivas, Türkiye.
[2]Eskisehir Technical University, Department of Architecture, 26555, Eskisehir, Türkiye.

Corresponding Author
Sema Balçık
E-mail: semabalcik@cumhuriyet.edu.tr Phone: +90 346 219 1560 / 3393
RORID[1]: https://ror.org/04f81fm77 RORID[2]: https://ror.org/00gcgqv39

Article Information
Article Type: Review
Doi: https://doi.org/10.17350/HJSE19030000353
Received: 0 1.12.2024
Accepted: 10.04.2025
Published: 30.06.2025

Cite As
Balçık S, Yamaçlı R. Bibliometric analysis of publications on sustainable renovation of buildings from 2001 to 2024. Hittite J Sci Eng. 2025;12(2):69-79.

Peer Review: Evaluated by independent reviewers working in at least two different institutions appointed by the field editor.
Ethical Statement: Not available.
Plagiarism Checks: Yes - iThenticate
Conflict of Interest: Authors declare no conflict of interest.

CRediT AUTHOR STATEMENT
Sema Balçık: Conceptualization, Data curation, Formal Analysis, Investigation, Methodology, Resources, Supervision, Writing – review and editing. **Ruşen Yamaçlı:** Conceptualization, Data curation, Formal Analysis, Investigation, Methodology, Supervision, Visualization, Writing – original draft & editing.

Bibliometric Analysis of Publications on Sustainable Renovation of Buildings from 2001 to 2024

Sema Balçık*[1] |Ruşen Yamaçlı[2]

[1]Sivas Cumhuriyet University, Department of Urban and Regional Planning, 58140, Sivas, Türkiye.
[2]Eskisehir Technical University, Department of Architecture, 26555, Eskisehir, Türkiye.

Abstract

Sustainable architecture is becoming increasingly important today, and designs that take into account environmental conditions come to the fore, especially in the life cycle of the existing building stock and in the processes of building new buildings. The principles of sustainable architecture aim to produce buildings that cause the least damage to the environment and consume the least amount of natural resources, minimize the damage to the environment in the existing building stock, and provide sustainable qualities through renovation processes. Not demolishing the existing building stock, not destroying the energy embedded in buildings, not creating waste, and not harming the environment is a sustainable architectural approach. In addition, by renovating buildings to increase their sustainable quality, they are made more sensitive to the environment. This study aims to evaluate the publications on sustainable building renovation by bibliometric analysis method. Within the scope of the study, data obtained from the Web of Science (WoS) database were used. The study retrieved 1058 publications published between 2001 and 2024 from the Web of Science database on November 17, 2024. The data obtained as a result of bibliometric analysis were created visual network maps using the VOSviewer program. This study emphasizes the importance of sustainable renovation of buildings and efficient consumption of resources within the scope of sustainable development. Within the scope of the study, quantitative data on the development of the subject in the world in line with the bibliometric analysis method are included. In this direction, suggestions have been developed on what needs to be done to increase sustainable building renovation studies.

Keywords: Sustainable architecture, Sustainable renovation, Sustainable renovation of buildings, Bibliometric analysis, VOSviewer

INTRODUCTION

The concept of sustainability, which should be given importance and included in every field today, is best known as meeting the needs of the present while not preventing future generations from meeting their needs (WCED, 1987). For this reason, when we consider the rapidly increasing consumption habits, it is necessary to focus on producing sustainable solutions in all areas of life.

The field of architecture should include the principles of sustainability in all its steps with its human-oriented approaches, resource utilization, and the quality of life that needs to be sustained. The principles of sustainable architecture are expressed by Belek and Yamaçlı (2023) as focusing on human-centered design, protecting natural resources, and planning the life cycle. As one of the steps of sustainable architecture, the reuse and sustainable renovation of buildings also allows the protection of natural resources and the re-planning of buildings in a human-centered and sustainable way.

In cities, there is a trend towards strengthening and reusing buildings instead of new construction to ensure energy efficiency and reduce environmental impacts, and existing buildings are seen as a resource reserve. Reuse ensures waste reduction, resource recovery, and efficient use (Rodrigues & Freire, 2021). According to Elefante (2007), the most environmentally sustainable buildings are those that already exist, and repurposing these structures yields significant resource and energy conservation.

Buildings account for approximately 40% of energy consumption (European Commission, 2020). Considering this situation, sustainable renovation of buildings should become a necessity in these days when we face the dangers of depletion of natural resources. In their research, Menna et al. (2022), state that sustainable retrofitting of existing buildings constitutes an important step in sustainable architecture steps to achieve climate and energy goals. Trachte and Salvesen (2014), stated that sustainable renovation of buildings is an option that improves comfort and quality of life for users, as well as contributing to the environment through energy efficiency.

Sustainable renovation of buildings constitutes an important sustainable architecture approach and has become an increasingly important concept. The act of building a building means the use of a lot of materials, a labor-intensive process, and the intervention of a new area in nature. While the reuse of the building eliminates these harmful steps, its sustainable renovation will increase respect for nature in the life process. For this reason, more studies on sustainable renovation of buildings should be conducted and recommendations should be developed.

Bibliometric studies reveal documents related to a specific subject. The bibliometric analysis method, which is widely used in many different fields, provides a quantitative examination of different variables such as publication years, types, languages, countries, and citation analysis (McBurney & Novak , 2002). This research study seeks to delineate the current state of international literature regarding sustainable building refurbishment from 2001 to 2024. This date range has been determined based on the oldest publication accessed after the categories were identified during the subject-specific search in the Web of Science (WoS) database. The aim is to identify the qualitative characteristics such as the fields of study within the scope of the subject, keywords that would indicate the trend of the subject, the languages of the publications, and the countries where they were published, as well as the quantitative characteristics such as the years of publication, the number of publications, and the number of citations. The study employed bibliometric analysis to elucidate the focus of research and its contemporary significance for the notion of sustainable building refurbishment.

In line with the purpose of the study, the qualitative research method was primarily used, and the importance of the topic

of sustainable building renovation was emphasized. Then, using the bibliometric analysis method, data on the studies produced by searching the keyword "sustainable renovation of buildings" in the Web of Science (WoS) database were accessed (Web of Science, 2024). As a result of the search, the studies were visualized through tables and the VOSviewer program with the data obtained within the scope of category, year, type, journals, indexes, countries producing the most studies, publication languages, contributions to sustainable development goals, and keywords. This program enables the analysis and visualization of scientific publication studies and citation networks (VOSviewer, 2023). As a result of the study, recommendations were developed based on the findings obtained from the analysis of the tables and visualizations produced within the scope of sustainable building renovation.

MATERIAL AND METHODS

The material of the research study consists of data obtained through the bibliometric analysis method. Within the scope of the study, the concept of sustainable renovation of buildings is first explained. Then, the Web of Science (WoS) database was selected to obtain data on studies on sustainable renovation of buildings. This database stood out among analytical information and scientific citation search platforms. The selection of the Web of Science database for the analysis was based on the quality and reliability of the research, its advanced search indicators, and its comprehensive data on different disciplines and transitions (Dirik, Eryılmaz, & Erhan, 2023). The data obtained from the Web of Science database was used to conduct a bibliometric analysis of the concept of sustainable renovation of buildings. Bibliometric analysis is widely used to evaluate and analyze large volumes of scientific data and is a method that enables understanding the relationship between the number of citations and publications, keywords, and topic occurrences in the current topic to obtain an overview of the researched topic, to identify knowledge gaps within the scope of the topic, to derive new ideas for research, and to indicate intended contributions to the field (Donthu, Kumar, Mukherjee, Pandey, & Lim, 2021). The data of the studies obtained through the database were evaluated using the VOSviewer program developed by Nees Jan van Eck and Ludo Waltman (Dereli, 2024) at the Center for Science and Technology Studies at Leiden University.

Van Eck and Waltman (2010), the founders of the VOSviewer software, state that the software should be used to create bibliometric maps and that this software provides advantages and important contributions to researchers by using different techniques in the analysis. In addition to the Vosviewer program for bibliometric analyses, there are also software programs such as Citespice, BibExcel, Gephi, Scimat, and Histcite for visualization. Among these, VOSviwer is more commonly preferred for analyses such as citation analysis, co-citation, and bibliographic coupling in the structuring of bibliometric networks (Öztürk & Kurutkan, 2020). By evaluating large amounts of bibliographic data, the VOSviewer program allows the invisible concepts in publications to be depicted in the form of maps, to be understandable by transforming them into a visual representation, and to apply thresholds to categorize this data (Mokhtari , Mirezati , Saberi , Fazli , & Kharabati-Neshin , 2019). It provides an advantage in the process of analysis to examine and visualize the structures and dynamics of publications. The steps that constitute the method of the study are shown in Figure 1.

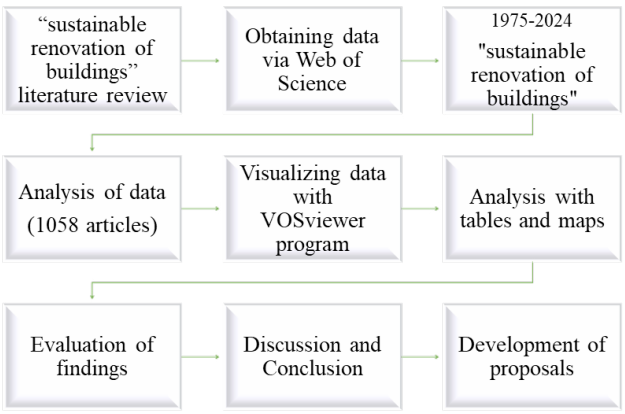

Figure 1 Methodology of the study

In order to obtain the studies conducted between 1975-2024 in the Web of Science (WoS) database within the scope of sustainable renovation of buildings, "All Fields" was selected in the search section and "sustainable renovation of buildings" was typed as the keyword. The Web of Science (WoS) database includes publications from 1975 onwards. The term "buildings" in the context of renovation encompasses the complete current building inventory, without differentiating between heritage structures. The search through WoS was conducted on November 17, 2024. As a result of this search, 1,720 studies were found. The analysis was limited to articles and when "article" was selected as the document type, 1,139 results were obtained. When only architecture is selected as a category, 67 article studies are revealed. For this reason, the category with at least 10 studies produced in this field was marked. The 21 selected categories and the number of studies are shown in Table 1 and it is seen that the discipline of architecture ranks 8th in terms of the number of studies. It is seen that the highest number of studies is in the field of Construction Building Technology with 370 studies. As a result of the search in line with the selected categories, 1 study from the year 2025 was excluded and bibliometric analysis was performed with 1,058 studies.

The reuse of buildings makes use of the available energy in the building stocks stored in our cities. Guidettia & Ferrara (2023), state that in addition to the available energy, the reuse of these buildings should be emphasized in terms of creating the built environment in the future. In addition to the sustainable nature of their reuse, another step is to improve the energy consumption of buildings during their life cycle. According to the European Commission report, buildings are the largest consumers of energy in Europe, and their renovation has an important role in achieving energy and climate targets (2024).The ratios mentioned in the report are shown in Figure 2.

Table 1 Distribution of the articles produced according to categories

Categories	Number
Construction Building Technology	370
Green Sustainable Science Technology	359
Energy Fuels	333
Engineering Civil	269
Environmental Sciences	257
Environmental Studies	225
Engineering Environmental	103
Architecture	67
Urban Studies	34
Economics	31
Materials Science Multidisciplinary	31
Thermodynamics	27
Engineering Multidisciplinary Management	25
Public Environmental Occupational Health	20
Physics Applied	19
Regional Urban Planning Multidisciplinary	18
Sciences	17
Chemistry Multidisciplinary	15
Engineering Chemical	12
Water Resources	12
	11

According to the Commission's report (2024), approximately 40% of the energy consumed in the EU is used in buildings. The majority of the energy consumed in homes is used for heating, cooling, and hot water, accounting for around 80%. Buildings are responsible for 90% of energy-related greenhouse gas emissions.

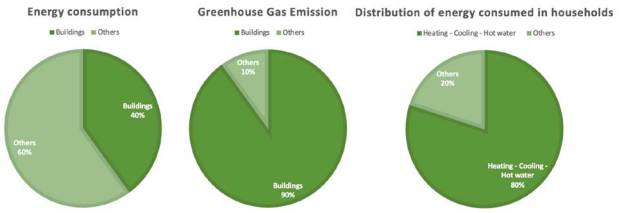

Figure 2 The role of buildings in energy consumption and greenhouse gas production in the EU (adapted from European Commission (2024) report)

Within the scope of sustainable development, architecture aims to contribute to the continuity of life, the efficient use of natural resources, the consideration of spatial and environmental comfort, and the proper management of waste (Çiğan & Yamaçlı, 2020, s. 554-571). The reuse of buildings, utilizing their embedded energy, and being sensitive during sustainable renovation processes represent a sustainable approach. The efficient use of energy and water resources in buildings, the shift towards renewable energy sources, the importance given to material selection, the management of waste, and the reduction of its formation are processes that increase the environmental sensitivity of structures.

Many studies have been carried out within the scope of reuse and sustainable renovation of buildings, and especially in recent years, the importance of this issue, which also contributes to sustainable development, has been increasing. The use of existing structural elements of buildings, creating a basis for new functions, eliminating the processes of demolishing buildings and building a new structure will allow savings in energy and materials (Doğru, 2017). When the results of the articles dealing with the scenarios emerging in the concepts of new building construction and renovation of buildings are evaluated, it is revealed that renovation processes should be preferred in line with the global warming problem (Leichter & Piccardo, 2024). Apostolopulos et al. (2023), in a study that reveals that sustainable retrofitting of buildings is concretely positive, state that due to the high energy consumption rates of buildings, renovation of building stocks is a mandatory approach to achieve sustainability goals. However, Jimenez-Pulido, Jimenez-Rivero, and Garcia-Navarro (2022), emphasize the importance of building renovation processes in line with Europe's carbon neutrality target (by 2050) and the need to develop innovative technologies. In this context, Riuttala, Harala, Aarikka-Stenroos, and Huuhka (2024), in a study investigating the reuse of more customized and concrete building components, state that building component reuse is a critical tool to achieve sustainability goals in the construction industry by reducing resource consumption, waste generation, and associated emissions. Caruso et al. (2024) emphasize that the renovation and improvement of buildings should aim to minimize the impacts of the building's life cycle by choosing materials that are resistant to natural disasters, reduce energy needs, and low-energy materials. Sustainable building renovation studies aim to provide improvements in the building envelope, extend the life cycle, provide energy efficiency, save on materials, and reduce greenhouse gas emissions (Amoruso, Sonn, & Schuetze, 2022). Balçık and Yamaçlı (2024) recommend increasing studies on water efficiency, waste management, user habits, and country policies within the scope of renovating buildings with sustainable qualities.

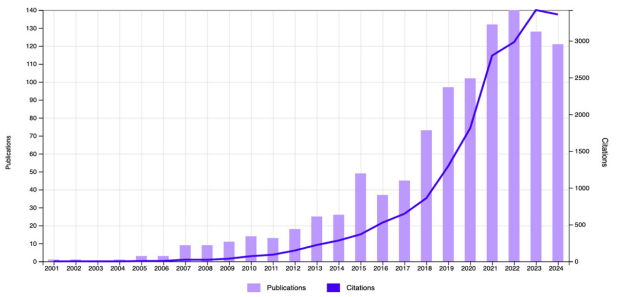

Figure 3 Publication and Citation Graph between 2001-2024.

Considering the energy consumption and greenhouse gas emission rates in buildings, it is seen that it is inevitable to make improvements to life cycle processes and to renew the buildings with sustainable qualities. In this study, which

aims to reveal the current state of the literature within the scope of this subject and to raise awareness, data from 1058 studies conducted between 1975 and 2024 were used. In line with the analysis of the data, it is seen that the first study on sustainable renovation of buildings was produced in 2001, and most studies with 140 studies were conducted in 2022. Figure 3 shows the publication and citation graph of the studies conducted between 2001 and 2024.

Table 2 Distribution of studies according to years

Years	Number
2024	121
2023	128
2022	140
2021	132
2020	102

Looking at the distribution of studies and citations produced within the scope of the sustainable renovation of buildings by years, 121 studies were produced in 2024, 128 in 2023, 140 in 2022, 132 in 2021, and 102 in 2020 (Table 2). The highest number of citations was made in 2023 (3148).

Table 3 Distribution of studies according to categories

Categories	Number
Construction Building Technology	370
Green Sustainable Science Technology	359
Energy Fuels	333
Engineering Civil	269
Environmental Sciences	257

The analysis shows that 96 studies were produced in 96 categories on sustainable renovation of buildings. For this reason, the categories were limited within the scope of the study and those that produced at least 10 studies were selected. Within these categories, the most studies were produced in the fields of Construction Building Technology with 370 studies, Green Sustainable Science Technology with 359 studies, Energy Fuels with 333 studies, Civil Engineering with 269 studies and Environmental Sciences with 257 studies (Table 3). In the field of Architecture, 67 articles were published and ranked 8th among the categories (Table 1).

Table 4 Distribution of studies according to publication types

Types	Number
Article	1058
Declaration	19
Early Access	16
Book Chapter	11
Withdrawn publication	1

In the research conducted with the keyword sustainable renovation of buildings, 1720 results were obtained in the WoS database, and the scope of the study was limited according to publication types and categories. In the analysis of the study, in which article-type studies were included in the scope of the study, there were 1058 articles, 19 proceedings, 16 early access publications, and 11 book chapters in line with the determined categories (Table 4).

Table 5 Distribution of studies according to the journals in which they were published

Journals	Number
Sustainability	142
Sustainable Cities and Society	85
Energy and Buildings	72
Buildings	54
Energies	45

Upon examining the publications in which the studies studied in the article were published, it was observed that 142 articles appeared in Sustainability, 85 in Sustainable Cities and Society, 72 in Energy and Buildings, 54 in Buildings, and 45 in Energies (Table 5).

Table 6 Distribution of studies according to the indexes in which they were published

Indexes	Number
Science Citation Index Expanded (SCI-EXPANDED)	800
Social Sciences Citation Index (SSCI)	347
Emerging Sources Citation Index (ESCI)	156
Arts & Humanities Citation Index (A&HCI)	47
Conference Proceedings Citation Index – Science (CPCI-S)	18

When the academic studies analyzed are considered according to the indexes in which they were published, there are 800 studies with the "Science Citation Index Expanded (SCI-EXPANDED)" index, 347 studies with the "Social Sciences Citation Index (SSCI)" index, 156 studies with the "Emerging Sources Citation Index (ESCI)" index, 47 studies with the "Arts & Humanities Citation Index (A&HCI)" index, and 18 studies with the "Conference Proceedings Citation Index-Science" index. Table 6 shows the distribution of studies according to their indexes.

Table 7 Distribution of studies according to the countries where they were published

Countries	Number
Italy	170
People's Republic of China	154
Sweden	98
Spain	93
United States of America	80

When the academic studies are categorized by country, Italy is shown to have the highest number of studies. Italy has 170 studies, China has 154, Sweden has 98, Spain has 93, and the

United States has 80 (Table 7). The UK and the Netherlands scored 6th and 7th with 50 and 46 studies, respectively, while Turkey has 18 studies on sustainable building rehabilitation.

Analysis of academic works by publication language reveals that the predominant language of publication is English. There are 1,031 studies in English, 9 in German and Spanish, and 6 in Italian (Table 8). There is one publication each in Croatian, Dutch, and French.

Table 8 Distribution of studies by language of publication

Language	Number
English	1031
German	9
Spanish	9
Italian	6
Croatian	1

When the studies analyzed within the scope of the article are evaluated according to Sustainable Development Goals, 793 studies were produced for Sustainable Cities and Communities (11), 749 for Climate Action (13), 732 for Accessible and Clean Energy (07), 325 for Industry, Innovation, and Infrastructure (09), and 253 for Responsible Production and Consumption (12). Table 9 shows the distribution of the studies produced for the top five sustainable development goals with the highest contribution. Within the scope of all studies, there are publications for all goals except for only 2 sustainable development goals (Gender Equality (05) and Peace, Justice, and Strong Institutions (16)).

Table 9 Distribution of studies according to Sustainable Development Goals

Sustainable Development Goals	Number
Sustainable Cities and Communities (11)	793
Climate Action (13)	749
Accessible and Clean Energy (07)	732
Industry, Innovation and Infrastructure (09)	325
Responsible Production and Consumption (12)	253

Using the data obtained as a result of the analysis of the Web of Science (WoS) database, tables were created according to the years, categories, types, journals, indexes, countries, and languages of publication. After the tables, the study data were visualized using the VOSviewer program. The VOSviewer program contributed to the analysis of publications, citations, distribution by countries, keywords, authors, information about publications, and the creation of visual network maps. The statements shown in the maps are represented by a circle. The size of the circles is determined by the weight of the expression, quantitatively its size. The larger the weight, the larger the circle. The lines between the statements express their connectedness (Eck & Waltman, 2024).

First, the keywords used by the authors were analyzed and visualized through the VOSviewer program. In the co-occurrence analysis/keywords analysis, when 3567 words were limited to at least 3 common words, 279 word results were mapped (Figure 4). The map shows the keywords as circles. While the circle of the most frequently used keyword is the largest, the circles become smaller as the number of uses decreases.

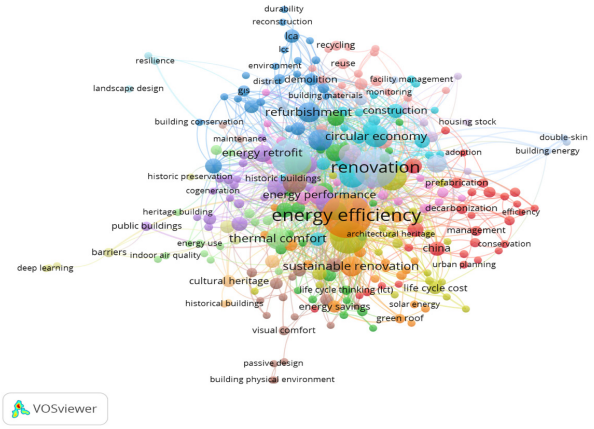

Figure 4 Network map of the most frequently used keywords

Energy efficiency (111), renovation (85), sustainability (74), building renovation (62), and life cycle assessment (40) are the most frequently used keywords. Table 10 shows the distribution of the most frequently used keywords.

Table 10 Distribution of the most frequently used keywords

Keywords	Number
energy efficiency	111
renovation	85
sustainability	74
building renovation	62
life cycle assessment	40
buildings	31
building stock	24
refurbishment	23
circular economy	29
energy consumption	27

Within the scope of visualization through the VOSviewer program, the frequency of use of keywords in year intervals is seen with the “overlay visualization” option. In the visual shown in Figure 5, while the keywords in the darkest colors were used before 2016, the color tone lightens as it approaches the present day, and it is seen that the keywords in yellow are frequently used in 2022 and after.

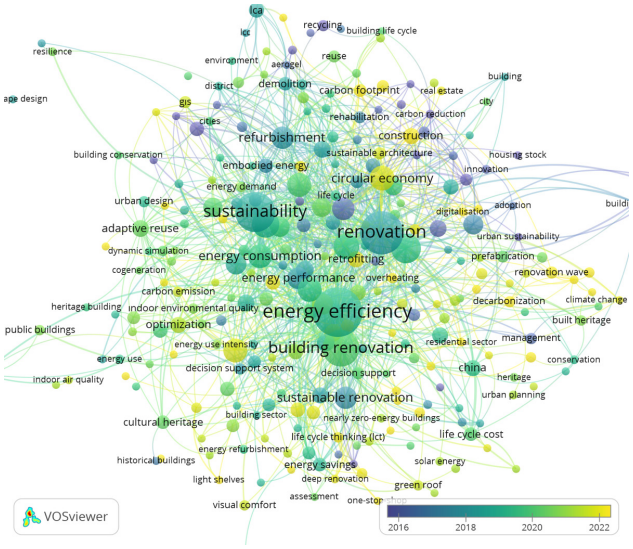

Figure 5 Visualization of the most frequently used keywords by year

In recent years, the keywords thermal comfort, circular economy, nzeb (nearly zero-energy buildings), overheating, and renovation wave have emerged. The keywords are visualized as in Figure 3, with the most frequently used ones representing the largest circles. Another visual obtained within the scope of visualization through the program is the density analysis of keywords with the "density visualization" option (Figure 6). The intensity of the use of the keywords on the blue background is understood by the size of the yellow spots. It is clear from this visualization that the keywords energy efficiency, sustainability, renovation, and building renovation stand out.

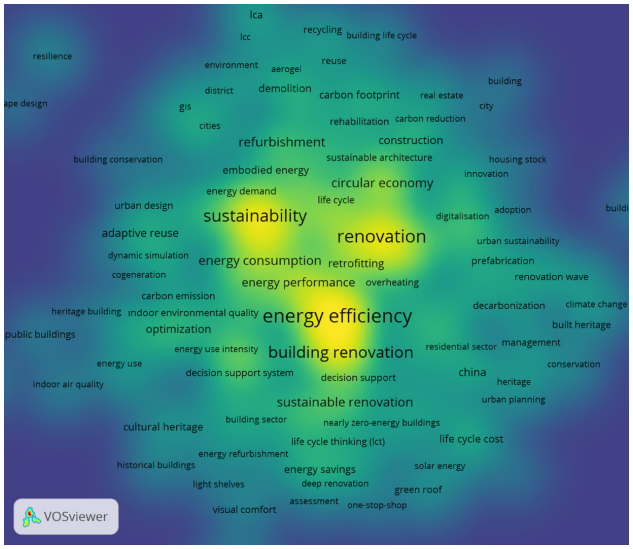

Figure 6 Visualization of the density of the most frequently used keywords

For the analysis of researchers producing studies within the scope of sustainable renovation of buildings, citation and author options were selected in the VOSviewer program. When 3210 researchers were limited to have at least 2 publications and at least 2 citations, 396 authors were analyzed. As a result of the analysis, the authors who produced the most publications (Table 11) and received the most citations emerged. In Figure 7, the authors who produced the most publications are visualized with the VOSviewer program.

Table 11 Authors who produced the most publications and the number of publications

Authors	Number of Publications	Number of Citations
Mjornell, Kristina	13	237
Serrano-Jimenez, Antonio	10	192
Habert, Guillaume	10	303
Femenias, Paula	9	212
Barrios-Padura, Angela	8	153
Attia, Shady	8	301
Vanoli, Giuseppe Peter	8	139
Malmqvist, Tove	7	191
Marini, Alessandra	7	211
Passoni, Chiara	7	211

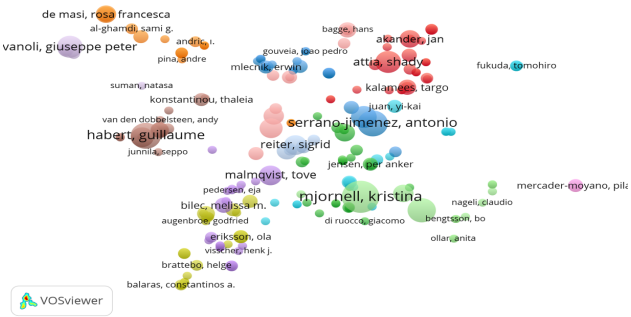

Figure 7 Visualization of authors who produced the most publications

Analysis of writers in the architecture category reveals that most have a maximum of two publications. Of the 158 authors who published in the architectural category, only those with at least one publication and one citation were considered, resulting in the inclusion of 98 authors in the analysis. Table 12 displays the publication and citation counts for the initial five writers.

Table 12 Authors who produced the most publications in the field of architecture and the number of publications

Authors	Number of Publications	Number of Citations
Pushkar, Svetlana	2	35
Verbitsky, Oleg	2	35
Arumagi, Endrik	1	30
Kalamees, Targo	1	30
Kallavus, Urve	1	30

In the same way, the most cited authors were analyzed by

selecting the citation and author options in the VOSviewer program. The most cited authors are shown in Table 13 as a result of the analysis of 396 authors obtained by limiting at least 2 publications and at least 2 citations. Mjornell, Kristina, who has the most publications (13) within the scope of the subject, ranks 11th with 237 citations.

Table 13 Most cited authors and number of citations

Authors	Number of Citations	Number of Publications
Bilec, Melissa M.	421	5
Bocken, Nancy	374	2
Habert, Guillaume	303	10
Attia, Shady	301	8
Juan, Yi-Kai	289	4
Jensen, Per Anker	270	4
Maslesa, Esmir	268	3
Balaras, Ca	253	2
Dascalaki, E.	253	2
Almeida, Manuela	245	4

In line with the data of the studies on sustainable renovation of buildings, an analysis of citations by countries (citations/countries) was made. In the program, 66 countries were analyzed over 84 countries when the minimum number of publications and the minimum number of citations of a country were limited to 2. In the analysis, it is seen that Italy, which has the highest number of publications (170), ranks first again with 3284 citations. Italy ranks next in China with 2283 citations, the United States with 2141, Sweden with 2135, and Spain with 1824. The most cited countries are visualized in Figure 8 with the VOSviewer program. As with the number of publications, the UK and the Netherlands follow these countries in 6th and 7th place, respectively. The 18 publications made in Turkey received 160 citations.

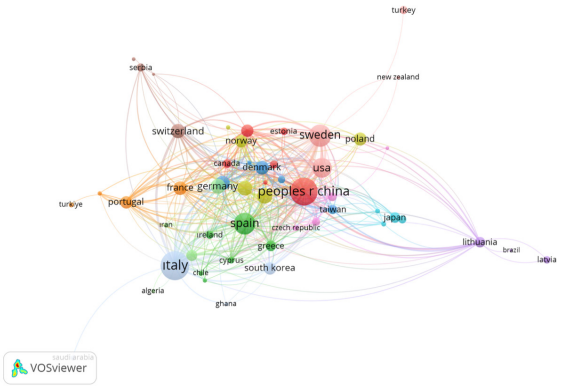

Figure 8 Visualization of the most cited countries

For the analysis of the sources co-cited in the study, the co-citation analysis/cited source options were selected. 21625 sources were limited to those with at least 10 citations. Among the 348 sources analyzed as a result of the limitation, the journals that stand out with the highest number of citations are Energy Buildings (3753), Building and Environment (1743), Journal of Cleaner Production (1282), Renewable and Sustainable Energy Reviews (1105), and Energy Policy (1070). Figure 9 shows the map of the most co-cited sources visualized with the VOSviewer program.

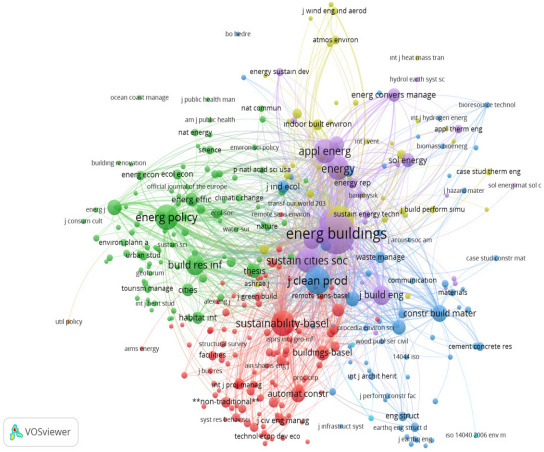

Figure 9 Visualization of the most co-cited sources

For the analysis of the most cited studies within the scope of sustainable renovation of buildings, citation/document options were selected. The 1058 publications examined within the scope of the study were limited to at least 10 citations, and 491 publications were analyzed. Table 14 shows the most cited publications, and Figure 10 shows the visual network maps.

Table 14: Most cited publications and number of citations

Yazar	**Çalışma**	**Atıf Sayısı**
Gonzalez (2006)	Assessment of the decrease of CO_2 emissions in the construction field through the selection of materials: Practical case study of three houses of low environmental impact	281
Güneralp (2017)	Global scenarios of urban density and its impacts on building energy use through 2050	279
Leising (2018)	Circular Economy in the building sector: Three cases and a collaboration tool	267
Juan (2010)	A hybrid decision support system for sustainable office building renovation and energy performance improvement	247
Power (2008)	Does demolition or refurbishment of old and inefficient homes help to increase our environmental, social and economic viability?	230

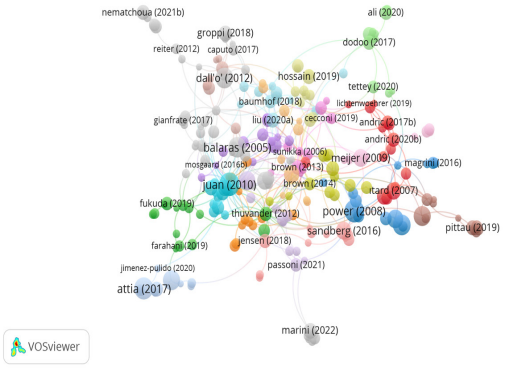

Figure 10 Visualization of the most cited publications

FINDINGS

The research study on papers concerning sustainable renovation of building has yielded conclusions regarding publication trends. The characteristics of the studies have been analyzed to elucidate the situation of publication output about the keywords. In the Web of Science (WoS) database, 1720 studies were found by searching with the keyword sustainable renovation of the building. Then, by limiting the category and year options, the research study was continued with 1058 publications. The category, year, type, journals, indexes, countries that produced the most studies, languages of publication, contributions to sustainable development goals, and keywords of these publications were interpreted with the help of tables and the VOSviewer program.

In the analyses made within the scope of sustainable renovation of buildings:
- It has been observed that studies in the article type stand out.
- It is seen that Italy is the leading country with the highest number of studies, followed by China, Sweden, Spain and the United States of America.
- It was found that the studies were mostly published in the journal Sustainability and were mostly scanned in index Science Citation Index Expanded (SCI-EXPANDED).
- The most commonly used keywords were energy efficiency, renovation, sustainability, building renovation, and life cycle assessment.
- When we look at the dates of the research conducted within the scope of the subject, it is seen that studies have been developed since 2001, but have increased as we approach the present day. The most studies within the scope of this subject were conducted in 2021 and 2022.
- Within the scope of the subject, publications were produced in 7 different languages in total, and the most publications were made in English.

Mjornell, Kristina is the author who has produced the most publications in the analysis of the study, and she is working in the field of Building Physics at RISE Research Institutes in Sweden, producing studies on sustainable renovation. The most cited work was produced by Gonzalez, MJ (González & Navarro, 2006), who aimed to quantify the total amount of CO2 emissions saved by the method applied to the choice of materials in the life cycle of a building and showed the possibility of reducing CO2 emissions. Gonzalez, MJ works at the Department of Construction and Rural Roads at the Polytechnic University of Madrid, Spain, where he produces papers on building and construction technologies and sustainable construction. Bilec, Melissa M., the most cited author, works in the field of Civil and Environmental Engineering at the University of Pittsburgh, United States, in the areas of environmental sciences, ecology, construction, and building technology.

The authors in the field of architecture Pushkar, Svetlana Verbitsky, Oleg in their joint LEED-NCV3 Silver and Gold Certified Projects In The Us: An Observational Study (2018) and LEED-NC 2009 Silver To Gold Certified Projects In The Us In 2012-2017: An Appropriate Statistical Analysis (2019), aimed to identify trends in Silver and Gold LEED for New Construction and Major Renovations (LEED-NCv3) certified projects. In Israel he produces studies in the field of architectural research.

One of the most cited studies in this context is “Assessment of the decrease of CO2 emissions in the construction field through the selection of materials: Practical case study of three houses of low environmental impact.” In the field of Civil Engineering; “Global scenarios of urban density and its impacts on building energy use through 2050” is in the field of Environmental Sciences and Ecology, focusing on the environmental impacts of buildings, carbon dioxide emissions, and energy consumption. These concepts, along with the most commonly used keywords such as energy efficiency, sustainability, and life cycle, indicate the trend of the subject.

DISCUSSION AND CONCLUSION

In the study, the concept of sustainable renovation of buildings was established, and its importance was emphasized first. Then, it is aimed to investigate the publication studies made in line with this concept and to examine the quantitative characteristics of the publications. In order to obtain the publications to be examined, the Web of Science (WoS) database, which covers qualified and reliable studies and provides access to comprehensive data collection from different disciplines, was utilized.

Sustainable renovation of buildings is an issue that needs to be considered on an international scale and constitutes an inevitable application area, especially due to the increasing building stocks in cities today. Along with the discipline of architecture, studies are being developed in many different fields within the scope of renewal technologies and processes of buildings. It is important to develop innovative technologies that will minimize the environmental damage of buildings and raise awareness.

The significant increase in research on the sustainable renovation of buildings over time constitutes one of the most important findings of the study. It has been determined that these studies, which began in 2001, reached their highest number with 140 publications in 2022. Additionally, the

identification of the most cited publications on sustainable renovation through bibliometric analysis and the provision of a comprehensive overview of the general state of the literature in this field are also among the significant findings. The trend of the most cited studies in the field of construction includes factors such as reducing CO2 emissions, material selection, having a low environmental impact, and energy use in buildings, indicating that sustainable building renovation is becoming increasingly important within the scope of global issues and that more research needs to be conducted. Therefore, it is necessary to increase publications in the field of architecture that contribute to this topic.

In this study, within the scope of sustainable renovation of buildings, not only architecture but also the studies produced by related disciplines are included, and it is aimed to reveal the latest situation and to create a basis for future studies on this subject. In this sense, all relevant disciplines, and especially the discipline of architecture, which is responsible for all stages such as building construction, life process, and demolition, have important duties. When looking at the categories in which work is being done, it is necessary to increase the number of studies in the field o f a rchitecture, which is currently less represented. The design of policies that will bring together architecture and different disciplines will contribute to the development of new technologies and applications.

It is observed that the majority of the studies conducted within the scope of sustainable building renovation (approximately 97%) are published in English. It is recommended that countries also publish high-quality works in their own languages on this subject. In addition to this, it should be emphasized that the studies should be produced with sustainable development goals in mind, and their contribution to sustainable development should be emphasized.

References

1. Amoruso, F. M., Sonn, M.-H., & Schuetze, T. (2022). Carbon-neutral building renovation potential with passive house-certified components: Applications for an exemplary apartment building in the Republic of Korea. *Building and Environment*, 1-23.
2. Apostolopoulos, V., Mamounakis, I., Seitaridis, A., Tagkoulis, N., Kourkoumpas, D. S., Iliadis, P., . . . Nikolopoulos , N. (2023). An integrated life cycle assessment and life cycle costing approach towards sustainable building renovation via a dynamic online tool. *Applied Energy* , 1-21.
3. Balçık, S., & Yamaçlı, R. (2024). Sürdürülebilir Bina Yenileme Yöntemleri Üzerine Bir İnceleme. *Online Journal of Art and Design*, 164-178.
4. Belek, A. N., & Yamaçlı, R. (2023). Ekolojik Binaların Sürdürülebilir Tasarım Kriterleri ve Değerlendirme Süreci. Journal of Architecture and Life, 529-550.
5. Caruso, M., Buttazzoni, M., Passoni, C., Labò , S., Marini , A., & Pinho, R. (2024). An updated multi-criteria decision- making method for the sustainable renovation of buildings including environmental, economic and social life-cycle metrics. *Journal of Building Engineering*, 1-15.
6. Çiğan, A., & Yamaçlı, R. (2020). Doğal Enerji, Sürdürülebilir Kalkınma ve Mimarlık Politikaları. *Düzce University Journal of Science & Technologj,* 554-571.
7. Dereli, A. B. (2024). Vosviewer ile Bibliyometrik Analiz. *Communicata*, 1-7.
8. Dirik, D., Eryılmaz, İ., & Erhan, T. (2023). Post-Truth Kavramı Üzerine Yapılan Çalışmaların VOSviewer ile Bibliyometrik Analizi. *Sosyal Mucit Academic Review*, 164-188.
9. Donthu, N., Kumar, S., Mukherjee, D., Pandey, N., & Lim, W. M. (2021). How to conduct a bibliometric analysis: An overview and guidelines. *Journal of Business Research*, 285-296.
10. Doğru, M. (2017). *Yeşil Binaların Bütüncül Enerji Verimliliği Yaklaşımı.* ecobuild: https://www.ecobuild.com.tr/post/2017/07/25/ye%C5%9Fil-binalar%C4%B1n-b%C3%BCt%C3%BCnc%C3%BCl-enerji-verimlili%C4%9Fi-yakla%C5%9F%C4%B1m%C4%B1
11. Eck, N. J., & Waltman, L. (2010). Software survey: VOSviewer, a computer program for bibliometric mapping. *Scientometrics*, 523-538.
12. Eck, N. J., & Waltman, L. (2024). *VOSviewer Manual.* Access Date: 28.11.2024: https://www.vosviewer.com/documentation/Manual_VOSviewer_1.6.16.pdf
13. Elefante, C. (2007). The Greenest Building Is...One That Is Already Built. The Journalof the National Trust for Historic Preservation, 26-38.
14. European Commission. (2020, October 14). *Renovation Wave: doubling the renovation rate to cut emissions, boost recovery and reduce energy poverty.* ec.europa.eu: https://ec.europa.eu/commission/presscorner/detail/en/IP_20_1835
15. European Commission. (2024). *Energy Performance of Buildings Directive*. https://commission.europa.eu/: https://energy.ec.europa.eu/topics/energy-efficiency/energy-efficient-buildings/energy-performance- buildings-directive_en
16. González, M. J., & Navarro, J. G. (2006). Assessment of the decrease of CO2 emissions in the construction field through the selection of materials:: Practical case study of three houses of low environmental impact. *Building and Environment*, 902-909.
17. Guidettia, E., & Ferrara, M. (2023). Embodied energy in existing buildings as a tool for sustainable intervention on urban heritage. *Sustainable Cities and Society*, 1-15.
18. Jiménez-Pulido, C., Jiménez-Rivero, A., & García-Navarro, J. (2022). Improved sustainability certification systems to respond to building renovation challenges based on a literature review. *Journal of Building Engineering*, 1-29.
19. Leichter, M., & Piccardo, C. (2024). Assessing life cycle sustainability of building renovation and reconstruction: A comprehensive review of case studies and methods. *Building and Environment*, 1-19.
20. McBurney , M. K., & Novak , P. L. (2002). What Is Bibliometrics and Why Should You Care? *Proceedings. IEEE International Professional Communication Conference*, (s. 108-114). Portland, OR, USA,.
21. Menna, C., Felicioni, L., Negro, P., Lupisek, A., Romano, E., Prota, A., & Hajek, P. (2022). Review of methods for the combined assessment of seismic resilience and energy efficiency towards sustainable retrofitting of existing European buildings. *Sustainable Cities and Society*, 1-19.
22. Mokhtari , H., Mirezati , S. Z., Saberi , M. K., Fazli , F., & Kharabati-Neshin , M. (2019). A Bibliometric Analysis and Visualization of the Scientific Publications of Universities: A Study of Hamadan University of Medical Sciences during 1992-2018. *Webology*,

197-2011.
23. Öztürk, N., & Kurutkan, M. N. (2020). Kalite Yönetiminin Bibliyometrik Analiz Yöntemi ile İncelenmesi. *Journal of Innovative Healthcare Practices (JOINIHP)*, 1-13.
24. Pushkar, S., & Verbitsky, O. (2018). LEED-NCV3 Silver and Gold Certified Projects In The Us: An Observational Study . *Journal of Green Building*, 67-83.
25. Pushkar, S., & Verbitsky, O. (2019). LEED-NC 2009 Silver To Gold Certified Projects In The Us In 2012-2017: An Appropriate Statistical Analysis. *Journal of Green Builgind*, 83-107.
26. Riuttala, M., Harala, L., Aarikka-Stenroos, L., & Huuhka, S. (2024). How building component reuse creates economic value – Identifying value capture determinants from a case study . *Journal of Cleaner Production*, 1-13.
27. Rodrigues, C., & Freire, F. (2021). Environmental impacts and costs of residential building retrofits – What matters? Sustainable Cities and Society, 1-14.
28. Trachtea, S., & Salvesenb, F. (2014). Sustainable renovation of non residential buildings, a response to lowering the environmental impact of the building sector in Europe. *Energy Procedia*(48), 1512-1518.
29. VOSviewer. (2023). *VOSviewer version 1.6.19*. Access Date: 12.10.2023: https://www.vosviewer.com/
30. WCED. (1987). *"Our Common Future".* The World Commision on Environment and Development.: http://www.un-documents.net/our-common-future.pdf
31. Web of Science. (2024). *Access Date: 17.11.2024*. 11 2024 tarihinde www.webofscience.com: https://www.webofscience.com/wos/woscc/summary/78e1a39c-82d7-4824-aafa-0155a725c33e-012ba93e9a/relevance/1

HITTITE JOURNAL OF SCIENCE AND ENGINEERING

e-ISSN: 2148-4171
Volume: 12 • Number: 2
June 2025

Optimization-Based Tuning of PI Controller Parameters for DC Motor Speed Control

Ahmet Top
Fırat University, Faculty of Technology, Department of Electrical and Electronic Engineering, Elazığ, Türkiye.

Corresponding Author
Ahmet TOP
E-mail: atop@firat.edu.tr Phone: +90 0424 237 00 00
RORID[1]: https://ror.org/05teb7b63

Article Information
Article Type: Research Article
Doi: https://doi.org/10.17350/HJSE19030000354
Received: 0 1.12.2024
Accepted: 10.04.2025
Published: 30.06.2025

Cite As
Top A. Optimization-Based Tuning of PI Controller Parameters for DC Motor Speed Control . Hittite J Sci Eng. 2025;12(2):81-90.

Peer Review: Evaluated by independent reviewers working in at least two different institutions appointed by the field editor.
Ethical Statement: Not available.
Plagiarism Checks: Yes - iThenticate
Conflict of Interest: Authors declare no conflict of interest.

CRediT AUTHOR STATEMENT
Ahmet Top: Conceptualization, Data curation, Formal Analysis, Investigation, Methodology, Resources, Supervision, Writing – review and editing.

Optimization-Based Tuning of PI Controller Parameters for DC Motor Speed Control

Ahmet TOP

Fırat University, Faculty of Technology, Department of Electrical and Electronic Engineering, Elazığ, Türkiye.

Abstract

Direct current (DC) motors are widely used in industrial applications due to their numerous advantages, such as high efficiency, cost-effectiveness, and adaptability. Therefore, accurate control of these motors is equally crucial. The most popular controller for regulating the speed of a DC motor is the conventional Proportional-Integral-Derivative (PID) controller. However, determining the parameters of a DC motor, developing a mathematical model, and subsequently identifying or experimentally selecting control parameters is a laborious and time-consuming process. In this study, the coefficients of the PI controller used for speed regulation of a DC motor were determined using the Particle Swarm Optimization (PSO) and Sine Cosine Algorithm (SCA) methods. The study was conducted experimentally for three different reference values and four distinct control methods, with the resulting data visualized using MATLAB. Step, sinus with offset, and sinus without offset signals were selected as reference values. The control methods employed included open-loop control, PI control, PSO-PI control, and SCA-PI control. When the results of open-loop control and optimization-based PI control were compared, it was observed that steady-state errors decreased by 91.25% and 90.41% for step reference with PSO and SCA, respectively; by 84.7% and 80.58% for sinus with offset reference with PSO and SCA, respectively; and by 76.72% and 74.75% for sinus without offset reference with PSO and SCA, respectively. Additionally, the motor demonstrated a more stable tracking of the reference values. When the PI control results were compared with PSO-PI and SCA-PI control, the steady-state error was found to decrease by an mean of 9.74% for the same reference values.

Keywords: DC motor control, PID controller, PSO,SCA, Arduino

INTRODUCTION

Motors that can be powered directly by a DC (direct current) source and convert electrical energy into mechanical energy are known as DC motors. They come in a variety of forms, including Brushed DC Motor [1], Servo Motors [2], Stepper Motors [3], Brushless DC (BLDC) Motors [4], and more. Their prices are also relatively low compared to AC Motors [5]. Furthermore, DC motors can be operated with simple and stable control algorithms. High efficiency and high initial torque in the event of abrupt load increases are further benefits [6]. On the other hand, brushless DC motors have become popular as a replacement for DC motors, which have drawbacks like the need for frequent maintenance, rapid mechanical wear of the outputs, glare, noise pollution, and the impact of the brush on efficiency [7]. Because of their benefits, including their lack of noise, low maintenance requirements, quick dynamic response, excellent torque characteristics, and effective operation, brushless DC motors may be preferred [8].

These days, DC motors are used extensively and are considered crucial to support human activity. Examples of frequently utilized systems are industrial applications [9], running a conveyor machine to transport an object [10], pumping water from below the surface to the top [11], utilizing a fan to cool the room [12], robotics [13,14], and electric vehicles [15]. Because of this, it's critical to employ a suitable control method when controlling motor speed, particularly when facing variable and non-linear loads and input disturbances [16]. The DC motor system has been fitted with many controllers, including the PI Controller [17], PID Controller [18,19], ANFIS Hybrid PID Controller [20], Fractional Order PID [21], Fuzzy Logic Controller [22], Model Reference Adaptive Control (MRAC) [23], and Integral state feedback [24]. The most popular among these is the PID controller [25-27]. PID has several benefits, including an easy-to-implement hardware or software architecture, robust resistance, good stability, and simplicity of structure [28,29]. It is used in numerous systems, including temperature control [30], airplane systems [31], robots [32], etc. The main problem often discussed in PID is parameter tuning [33,34]. In other words, to obtain optimal system performance, the proportional gain (Kp), integral gain (Ki), and derivative gain (Kd) parameter values are determined [35,36]. One of the techniques used for this is parameter determination by trial and error [37]. However parameters are hard to set with this method, as the parameter search takes a long time, the control precision is poor, and the parameters that are employed are not ideal.

Many smart methods for adjusting PID parameters have been employed by researchers recently, including Learning-Based Optimization [38], Artificial Bee Colony Algorithms [39,40], Gray Wolf Optimization [41], Firefly Algorithms [42], Differential Evolution [43], Genetic Algorithms [44], Sine Cosine Algorithms [45,46], and Water Wave Optimization [47]. When compared to other methods, parameter optimization utilizing the PSO method yields stable results, according to some research references [48].

The majority of research published in the literature on DC motor control has been performed in simulation. In experimental studies, only step references were used. It has not been shown that PSO or SCA can be effective in time-varying references for motors. In this study, the speed control of a DC motor with a PSO-based PI and SCA-based PI controller has been carried out experimentally for more than one reference. Step, offset sine and non-offset sine signals were selected as references. Open loop control, PI control, PSO-PI, and SCA-PI control were used as control methods. The reason for selecting the sinus reference is that different values of reference data can be obtained in real time. In the experiments conducted using the Arduino Due development board, the performance of the motor was first examined by performing open-loop control. Then, the steady-state error of the system was measured by performing PI control with different parameter values. In cases where the error value was greater than the specified threshold value, parameter determination was performed with PSO/SCA for a certain number of iterations. Error rates

were re-evaluated by performing PI control again with these parameters. Since step reference is generally chosen in the literature, step, offset sine, and non-offset sine were preferred as references in this study. The results obtained with the Arduino IDE serial port were transferred to the MATLAB program and the graphs drawn here. The results obtained show that PSO and SCA are quite effective in obtaining PI parameters to reduce the steady-state error in motor speed.

MATERIAL AND METHOD

PID Control

Proportional (P), Integral (I), and Derivative (D) controllers, or PID controllers for short, are typically used to regulate the speed of the DC motor. The PID controller is widely recognized as the most commonly utilized method in various nonlinear control systems [49]. The PID controller concept is essentially a straightforward three-term controller that reduces steady-state error and enhances stability [50]. For many control problems, this controller provides the most effective and straightforward solution, addressing both transient and permanent state responses. The PID controller's transfer function is typically expressed as the "gain notation" given by Equation (1) or the "time constant notation" given by Equation (2).

$$T(s) = K_p + K_i\frac{1}{s} + K_d s \quad (1)$$

$$T(s) = K_p\left(1 + \frac{1}{T_i s} + T_d s\right) \quad (2)$$

Where T_i is the integral time constant, T_d is the derivative time constant. K_p is the proportional gain, K_i is the integral gain, and K_d is the derivative gain, When any of the gain values are set to zero, the controller type may change. For example, if K_d=0, it becomes a PI controller. While proportional control increases the response speed of the system, integral control corrects the steady-state error as it takes the integral of the error. Derivative control, on the other hand, detects rapid changes by taking the derivative of the error, that is, the slope of the error signal, and is thus effective in transient overshoots. Because the motor speed's transient state would not be considered and the steady-state error would be addressed, PI control was employed in this study.

Particle Swarm Optimization (PSO)

Particle Swarm Optimization is a swarm-based optimization algorithm inspired by the social behavior of birds and fish and developed by transferring it to computer simulations. It was introduced by Eberhart and Kennedy in 1995 [51]. Each individual in this approach is referred to as a particle [52].

The general procedure of the PSO algorithm is as follows: In the first stage, the initial positions of the particles are generated randomly. In the second stage, the fitness values of these positions are calculated using a fitness function. The fitness function is used to obtain these fitness values. In the third stage, the best position of each particle for the relevant iteration ($p_{best,i}$) and the position of the best of the swarm so far (g_{best}) are identified. To make this determination, the fitness values calculated in the second stage are used. In the fourth stage, the speed and position of each particle are updated according to $p_{best,i}$, and g_{best}. A weight coefficient (inertia weight) is used to update the speed. In the fifth stage, the best solution obtained through these updates is stored in memory and the algorithm proceeds to the next iteration. This iterative process continues until the stopping criterion is met. Equations 3 and 4 show the speed and position update equations, and Figure 1(c) shows the workflow diagram of the algorithm.

$$v_{t+1} = wv_t + c_1 r_1(p_{\text{best}} - p_t) + c_2 r_2(g_{\text{best}} - p_t) \quad (3)$$

$$p_{t+1} = p_t + v_{t+1} \quad (4)$$

where v_{t+1} is the current speed of the particle, w is the inertia weight, v_t is the previous speed of the particle, r_1 ,r_2 are random numbers generated within the range (0,1), c_1,c_2 are the learning coefficients, p_t is the previous position of the particle, p_{t+1} is the updated position of the particle [53].

Among the studies on PID controllers, the commonly used fitness functions are integral of absolute error (IAE), integral of time-weighted absolute error (ITAE), integral of squared error (ISE), and integral of time-weighted squared error (ITSE) [54]. These fitness functions are expressed in Equations 5-8. Because the ISE and IAE criteria treat all errors equally, without accounting for time, they can result in a response with a long settling time and a relatively small overshoot [55]. To address this issue, an integral of time-weighted absolute error (ITAE) is used as a fitness function in this paper [56].

$$\text{IAE} = \int_0^T \left|e(t)\right| dt \quad (5)$$

$$\text{ITAE} = \int_0^T t\left|e(t)\right| dt \quad (6)$$

$$\text{ISE} = \int_0^T e^2(t)\, dt \quad (7)$$

$$\text{ITSE} = \int_0^T te^2(t)\, dt \quad (8)$$

Where t is the time and $e(t)$ is the difference between the set point and the controlled variable.

Sine Cosine Algorithm (SCA)

The Sine Cosine Algorithm (SCA) is a newly developed population-based metaheuristic optimization technique introduced by Mirjalili. It mimics the behavior of mathematical sine and cosine functions [57]. In recent years, various versions of SCA, such as USMN-SCA [58], MTV-SCA [59], IC-SCA [60], and others, have been extensively studied and applied in DC motor control [57,61] as well as in renewable energy systems [62] and buck converter [63] optimizations. Solutions are updated based on the sine or cosine function, as represented in Equation 9.

$$R_i^{t+1} = \begin{cases} R_i^t + r_1 \cdot \sin(r_2) \cdot \left|r_3 Y_i^t - R_i^t\right| & r_4 < 5 \\ R_i^t + r_1 \cdot \cos(r_2) \cdot \left|r_3 Y_i^t - R_i^t\right| & r_4 \geq 5 \end{cases} \quad (9)$$

Here, Ri represents the current solution position, t denotes the current iteration, and Y_i indicates the target solution. The

parameter r_1 is referred to as the transformation parameter, which determines the region of the next solution. The range of the sine and cosine functions in Equation 9 is adaptively adjusted using Equation 10.

$$r_1 = b\left(1 - \frac{t}{T}\right) \quad (10)$$

where t is the current iteration, T is the total number of iterations, and b>0 is a constant. In Equation 9, $r_2 \in [0,2\pi]$ is a random variable used to determine the movement direction of the next solution (i.e., either towards or away from Y_i). Additionally, r_3 provides random weights as a stochastic factor to either increase (r_3>1) or decrease (r_3>1) the influence of Y_i on defining the distance. The term r_4 in Equation 9 is used to switch between sine and cosine functions [57]. To ensure accurate comparison with PSO, the time-weighted absolute error is used as a fitness function in this algorithm.

System Software

The Arduino Due development board was used to create the optimization and control algorithm and to facilitate bidirectional information exchange with the hardware. The software was written in the Arduino IDE (Integrated Development Environment) interface according to the workflow diagram in Figure 1. Specifically, Figure 1(a) shows the main program, Figure 1(b) shows the test subprogram, Figure 1(c) shows the PSO subprogram, and Figure 1(d) shows the SCA subprogram. After initially performing the necessary assignments and adjustments, the algorithm generates random parameters for speed control of the motor with the PI controller. These parameters are sent to the test subprogram and ensuring the motor operates for a specific period. During this period, the transient state is disregarded, and the absolute value of the difference between the steady-state reference speed (V_{ref}) and the measured motor speed (V_{est}) is taken. After completing the subprogram, these error values are divided by the number of samples as in Equation 11 and the mean absolute error (MAE) value is determined.

$$\text{MAE} = \frac{1}{N}\sum_{k=1}^{N}\left|e\left(k\right)\right| \quad (11)$$

where e is the error value, N is the total number of samples, and k is the number of samples. In this study, the MAE value was set to 1 rpm for sine without offset, while it was accepted as 0.5 rpm for other reference values. This is because the errors at the zero crossing points in the sine without offset are high. According to the algorithm, the system will control motor speed with randomly determined parameters if the MAE value is less than the threshold value. However, if it exceeds the threshold value, the optimization subprogram will be executed for the specified number of iterations. For the parameters found with optimization, the error status is rechecked by returning to the test subprogram, and motor control is provided using these parameters. The motor continues to move until the button specified for exit is pressed. PI parameter information, reference speed data, and instantaneous motor speed data were taken from the Arduino IDE serial port and entered into the MATLAB program, where the data was graphed.

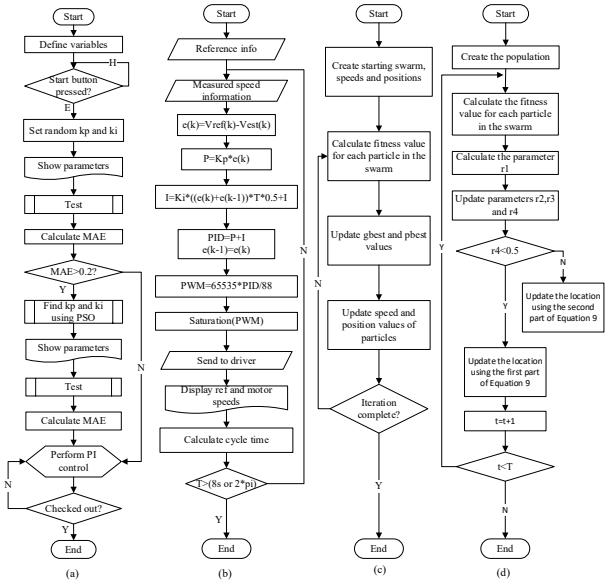

Figure 1 System software workflow diagram: a) main program, b)test subprogram, c) PSO subprogram and d) SCA subprogram

Hardware

Direct current motors have advantages such as excellent torque and speed characteristics, quick response to dynamic changes, high power-to-weight ratio, no requirement for current excitation, and low operating noise. For these reasons, they are widely used in industrial applications and robotics [64]. In this study, a 12 V DC motor with a reducer with a conversion ratio of 131.1:1 and an encoder with a resolution of 64 PPR was used. To generate voltage for this motor based on PWM (Pulse Width Modulation) values received from an Arduino Due, a SparkFun Monster Motor Driver Module containing two VNH2SP30-E H-bridge integrated circuits was used. This driver module allows the control of motors with a maximum voltage of 16 V, a continuous current draw of 14 A, and a maximum PWM frequency of 20 kHz

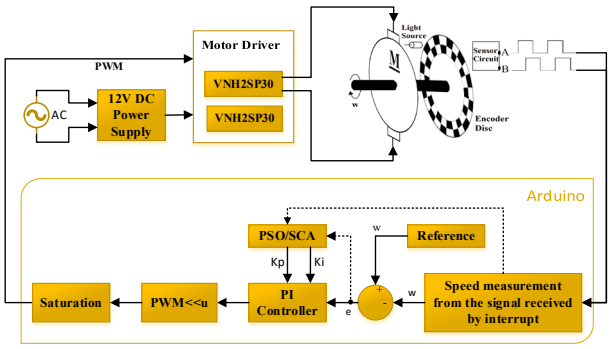

Figure 2 General block diagram of the system

Figure 2 illustrates the general schematic structure of the system, while Figure 3 shows the physical setup. The motor is powered by a 12 V voltage source, whereas the Arduino is powered via a computer connection. To enhance the precision of motor operation, the Arduino's PWM output resolution was increased from 8 bits to 16 bits, and the PWM frequency was set to 15 kHz.

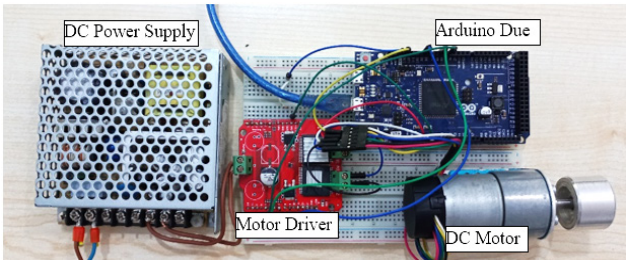

Figure 3 System setup

The motor encoder is powered by the Arduino. The signals from the encoder are transferred to the interrupt pin, where instantaneous speed measurements are conducted within the interrupt subprogram in the Arduino. The measured speed value is then compared with the reference value in the program to calculate the error value.

EXPERIMENTAL RESULTS

In this study, the results were analyzed for three distinct reference values and four different control methods for the speed control of a DC motor. Step, offset sine, and non-offset sine signals were chosen as reference values. For these references, motor speed control was implemented using open-loop control, a PI controller, a PSO-based PI controller, and an SCA-based PI controller. The steady-state MAE (Mean Absolute Error) was calculated by disregarding the transient states for the step and offset sine references, whereas for the non-offset sine reference, the MAE of the entire signal was considered to highlight the differences at zero-crossing points. Initially, as shown in Figure 4, the open-loop speed control results of the motor were obtained for a step reference value of 25 rpm.

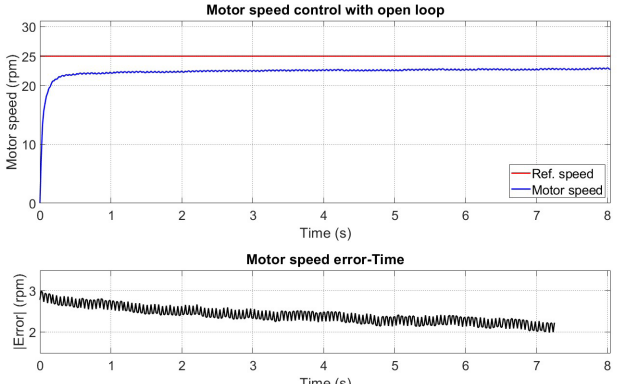

Figure 4 Motor speed control with an open loop for 25 rpm setpoint

When the open loop speed control of the motor was examined, it was observed that the motor reached a steady state in 0.66 seconds without overshoot, However, it remained constant at an mean of 22.60 rpm during the steady state, resulting in a steady state error of 2.40 rpm.

Closed loop control was achieved using the PI controller based on feedback received from the DC motor encoder. Since the motor parameters were unknown, the PI coefficients could not be determined directly. Consequently, the results obtained with different integral and proportional coefficients for PI control are shown in Figure 5.

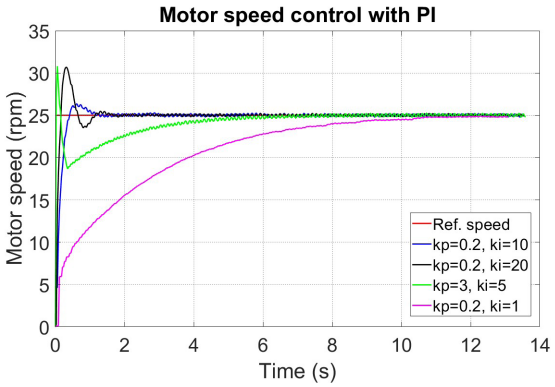

Figure 5 Motor speed control with different PI parameters for 25 rpm setpoint

When the results in Figure 5 are examined, it is observed that when the proportional and integral coefficients are low, the system does not exceed the reference value, but takes a long time to reach the steady state. Conversely, increasing the proportional coefficient and integral coefficient can accelerate the system response, but may lead to overshoots in transient states. To further improve this result, the appropriate parameter should either be calculated through mathematical modeling or determined experimentally via trial and error. However, since both methods are time-consuming when applied to different motors, PSO and SCA were used to find the appropriate parameters.

In the created algorithm, the MAE is first calculated using randomly determined parameters over a specific time or period. If this error value exceeds the threshold, adjustments are made using PSO or SCA. The motor speed results for PI parameters determined using PSO and SCA are shown in Figures 6 and 7, respectively. To ensure clarity, error graphs were plotted from the moment the speed reached the reference value, while the MAE was calculated only after the steady-state time was achieved.

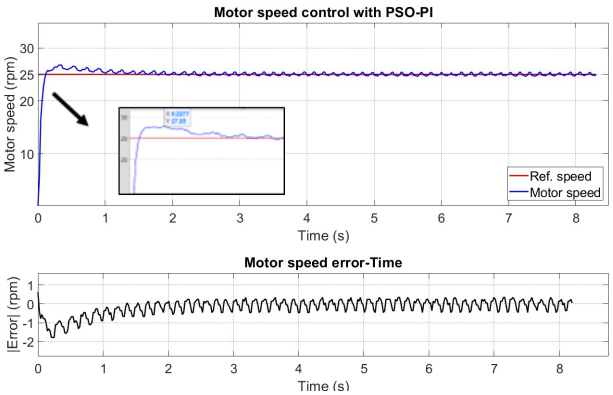

Figure 6 Motor speed control with PSO-PI for 25 rpm setpoint

The PI parameters obtained through PSO are kp=0.83 and ki=3.31. Upon evaluating the performance with these parameters, the motor exhibits a rise time of 0.1242 seconds,

an overshoot of 7.12% at 0.3312 seconds, and reaches a steady state after 1.7595 seconds. Subsequently, the motor operates with an average steady-state error of 0.21 rpm.

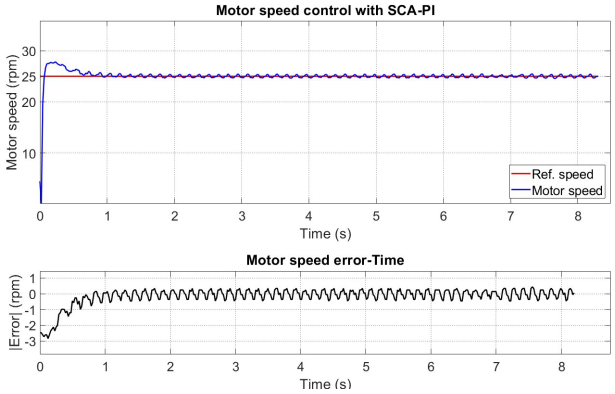

Figure 7 Motor speed control with SCA-PI for 25 rpm setpoint

The PI parameters found with SCA are kp=1 and ki=8.37. Upon analyzing the results with these parameters, the motor exhibits a rise time of 0.062 seconds, an overshoot of 7.4% at 0.22 seconds, and reaches steady state after 1.09 seconds. Subsequently, the motor operates with an average steady-state error of 0.23 rpm.

When the same control applications were applied to the reference value of 30+15Sin(wt), the results depicted in Figures 8-11 were obtained.

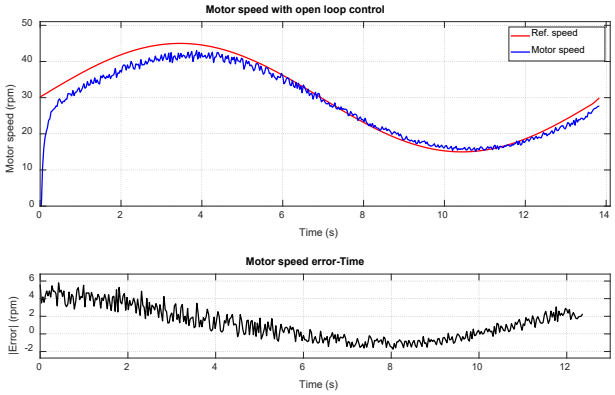

Figure 8 Motor speed control with an open loop for 30+15Sin(wt) rpm setpoint

In open-loop control, the system began tracking the reference value at 0.39 seconds, without exhibiting any overshoot during the transient state. The motor then continued its movement with an mean absolute speed of 1.70 rpm. Furthermore, as illustrated in the graph, the reference signal is followed with a noticeable delay.

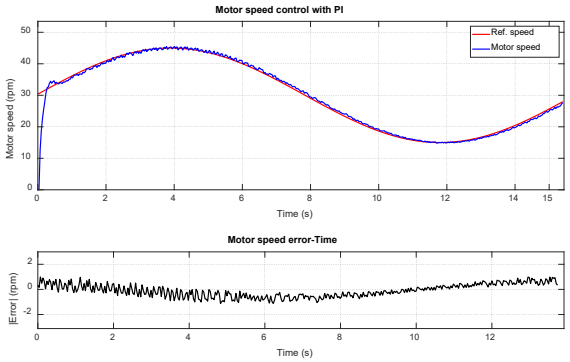

Figure 9 Motor speed control with PI for 30+15Sin(wt) rpm setpoint

For the PI control, the user set kp=0.5 and ki=23.75., and The results obtained with these parameters are shown in Figure 9. The motor speed reached its rise time at 0.27 seconds and exhibited an overshoot of 5.77% at 0.37 seconds. The motor successfully followed the sine reference with an average error of 0.443 rpm.

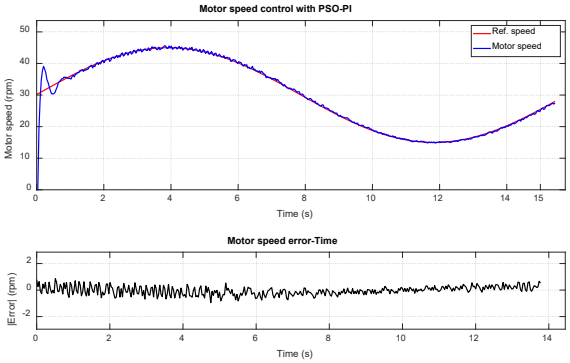

Figure 10 Motor speed control with PSO-PI for 30+15Sin(wt) rpm setpoint

After ten iterations, PSO algorithm determined the proportional parameter to be 0.92 and the integral coefficient to be 60.03. Upon evaluating the performance of the PI control with these coefficients, the motor exhibited an MAE of 0.268 rpm. The system achieved a rise time of 0.102 seconds and a peak time of 0.204 seconds, before reaching steady state at 1.29 seconds. During the peak time, the motor experienced an overshoot of 24.56%.

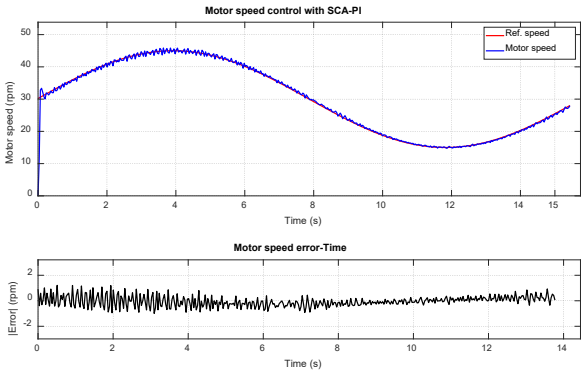

Figure 11 Motor speed control with SCA-PI for 30+15Sin(wt) rpm setpoint

After ten iterations, SCA found the proportional parameter to be 7.28 and the integral coefficient to be 55.9. When the results of the PI control performed with these coefficients were examined, the motor moved with an MAE of 0.338 rpm. The system reached a rise time of 0.068 seconds and a peak time of 0.102 seconds, before attaining steady state at 0.476 seconds. During the peak time, the motor experienced an overshoot of 8.34%.

For bidirectional motion control of the motors, the reference signal 25Sin(2wt) was applied to the motor, and control was performed using open-loop, PI, PSO-PI, and SCA-PI methods. The results obtained for each control method are presented in Figures 12, 13, 14, and 15, respectively. Two periods were considered for each control method, and the mean absolute errors were calculated. Due to the low pulse per revolution (PPR) of the encoder, speed information cannot be obtained with high accuracy, especially at low speeds, as the period of the encoder signal increases. Consequently, errors may occur at the zero-crossing points of the signal.

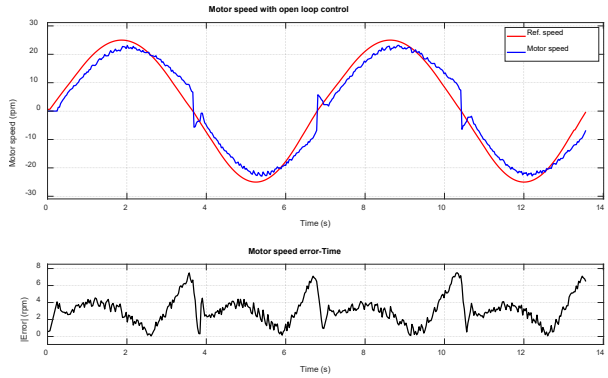

Figure 12 Motor speed control with an open loop for 25Sin(2wt) rpm setpoint

In open-loop control, the motor followed the reference with a delay of 0.22 seconds and an mean error of 3.054 rpm.

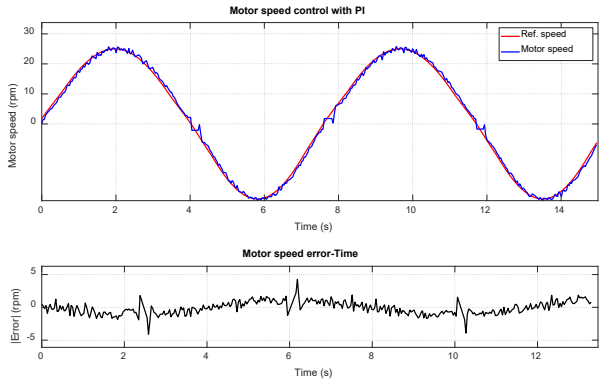

Figure 13 Motor speed control with PI for 25Sin(2wt) rpm setpoint

The experimental values produced by the user are Kp = 2.8 and Ki = 55.12. The results obtained from the closed-loop PI controller of the motor with these values are shown in Figure 13. Upon examining these graphs, it is observed that the motor follows the reference value with an mean error of 0.787 rpm, with no delay in the signal. However, jumps are present at the zero-crossing points.

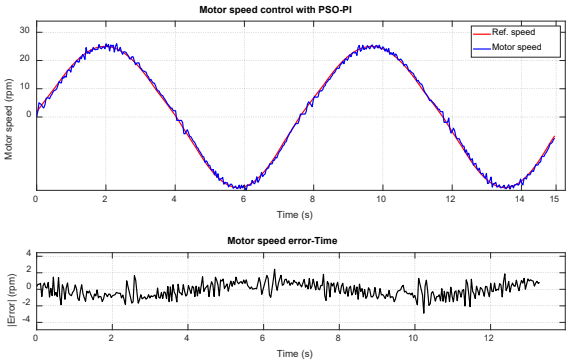

Figure 14 Motor speed control with PSO-PI for 25Sin(2wt) rpm setpoint

Since the MAE exceeded the threshold value, the parameters were recalculated using Particle Swarm Optimization (PSO), resulting in kp = 7.23, and ki = 69.21. Upon examining the control results obtained with these values, it is observed that the reference is tracked with an error of 0.712 rpm, with no delay in the signal. Additionally, the zero-crossing points occur with reduced error compared to previous results.

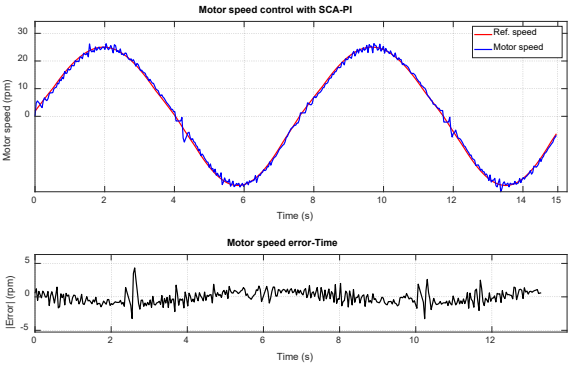

Figure 15 Motor speed control with SCA-PI for 25Sin(2wt) rpm setpoint

Since the MAE was above the threshold value, the parameters were calculated using SCA, yielding kp = 8.87, and ki = 63.35. When the control result obtained with these values is examined, it is observed that the reference is tracked with an error of 0.771 rpm, there is no delay in the signal and zero crossing points occur with less error. The results obtained with the controllers for all three references are given in Figures 16, 17, and 18.

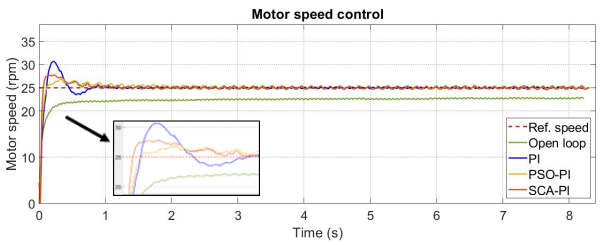

Figure 16 Motor speed control for 25rpm setpoint

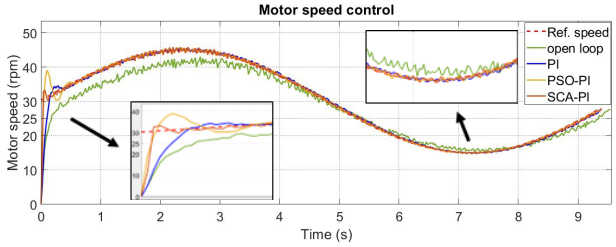

Figure 17 Motor speed control for 30+15Sin(wt) rpm setpoint

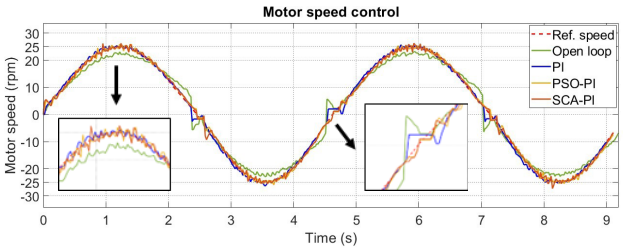

Figure 18 Motor speed control for 25Sin(2wt) rpm setpoint

When analyzing the above results, it is observed that in the DC motor controls performed with the PI parameters obtained through experimental studies using SCA and PSO, SCA provides superior performance in the transient state, while PSO proves to be more effective in reducing steady-state error.

CONCLUSION

In this study, the Particle Swarm Optimization (PSO) algorithm and the Sine Cosine Algorithm (SCA) were employed to determine the optimal proportional-integral (PI) controller parameters for the speed control of a DC motor. The experimental study utilized using three different reference values: step reference, offset sine, and non-offset sine. Additionally, bidirectional control of the motor was achieved with the non-offset sine reference. A comparative analysis was conducted on the data obtained from open-loop control, PI control with experimentally determined parameters, and PI control using the proposed optimization methods. The results demonstrated that the PI controller when optimized with the proposed methods, produced effective outcomes.

An analysis of the experimental results presented in Table 1 and the associated graphs revealed steady-state errors of 2.40 rpm, 1.70 rpm, and 3.05 rpm for step, offset sine, and non-offset sine reference values, respectively, under open-loop control. Furthermore, the motor speed failed to reach the reference speed in the open-loop control scenario. For PI control with experimentally determined coefficients, it was observed that some parameter configurations yielded fast responses accompanied by overshoots, while others resulted in slower responses with no overshoot.

When the PI parameters were optimized using PSO, the steady-state error values for the step, offset sine, and non-offset sine reference cases were reduced to 0.21 rpm, 0.26 rpm, and 0.71 rpm, respectively. Similarly, with SCA-based optimization, the error values were 0.23 rpm, 0.33 rpm, and 0.77 rpm for the same reference cases. Notably, in the DC motor speed control implementations using PSO-optimized parameters, the mean absolute error was consistently below, indicating that the motor successfully tracked the reference values with high accuracy.

Table 1 Steady-state errors of control methods according to different setpoints

Control Method / Reference	Open loop	PI	PSO-PI	SCA-PI
e_{ss}(rpm) for Step Reference	2.40	0.2 (for kp=0.8, ki=5)	0.21	0.23
e_{ss}(rpm) for Sinus with offset ref.	1.70	0.44	0.26	0.33
e_{ss}(rpm) for Sinus without offset ref.	3.05	0.78	0.71	0.77

In the operation with a sinusoidal reference without offset, it was determined that the fluctuations at the zero-crossing points of the motor speed were caused by the low resolution of the DC motor encoder. Since feedback information was obtained with fewer samples for this reference value, the instantaneous speed was measured with greater oscillation. In contrast, more stable results were obtained with a fixed reference due to the higher sampling rate used during the measurement. Since the steady-state error was considered as the primary control performance criterion and derivative control was not included to improve the transient regime, overshoots during the transition phase were not evaluated as a success metric. Experimental studies demonstrated that 10 iterations for 10 particles reduced the error to an acceptable level; therefore, the mean absolute error (MAE) was not reassessed in either optimization result. However, to enhance usability in different systems, the optimization cycle can be repeated until the error from the PSO and SCA outputs reaches an acceptable level, or the optimization process can continue until the desired error level is achieved instead of relying on a fixed number of iterations.

References

1. Chotai J, Narwekar K. Modelling and position control of brushed DC motor. In: International Conference on Advances in Computing, Communication and Control (ICAC3); 2017. p. 1–5.
2. Kumar, P., Chatterjee, S., Shah, D., Saha, U.K., & Chatterjee, S. On comparison of tuning method of FOPID controller for controlling field controlled DC servo motor. Cogent Engineering, 2017; vol. 4, no. 1.
3. Shekhawat AS, Rohilla Y. Design and control of two-wheeled self-balancing robot using Arduino. In: Proceedings of the International Conference on Smart Electronics and Communication (ICOSEC); 2020. p. 1025–1030.
4. Shekhar S, Saha PK, Thakura PR. Optimal PID tuning of BLDC drive using LQR technique. In: Proceedings of the 2019 IEEE International Conference on Intelligent Systems and Green Technology (ICISGT); 2019. p. 57–61.
5. Köse F, Kaplan K, Ertunç M. PID ve bulanık mantık ile DC motorun gerçek zamanda STM32F407 tabanlı hız kontrolü. In: Otomatik Kontrol Ulusal Toplantısı; 2013 Sep 26–28; Malatya, Türkiye.

6. Siemens Training Education Program. STEP 2000 Series. Basics of DC drives and related products.
7. Oguntoyinbo, O. PID control of brushless dc motor and robot trajectory planning and simulation with matlab/simulink, Vaasan Ammattikorkeakoulu University Of Applied Sciences Degree Programme of Inform. 2009.
8. Yedamale P. Brushless DC motor fundamentals. Chandler (AZ): Microchip Technology Inc.; 2003.
9. Okoro, I. S., & Enwerem, C. O. Robust control of a DC motor. Heliyon, 2020; vol. 6, no. 12, https://doi.org/10.1016/j.heliyon.2020.e05777.
10. Dezaki, M. L., Hatami, S., Zolfagharian, A., & Bodaghi, M. A pneumatic conveyor robot for color detection and sorting. Cognitive Robotics. 2022; vol. 2, pp. 60–72, https://doi.org/10.1016/j.cogr.2022.03.001.
11. Ahmed, M. M., Hassanien, W. S., & Enany, M. A. Modeling and evaluation of SC MPPT controllers for PVWPS based on DC motor. Energy Reports. 2021; vol. 7, pp. 6044–6053, https://doi.org/10.1016/j.egyr.2021.09.055.
12. Hendra, H., Pebriyanto, S., Hernadewita, H., Hermiyetti, H., & Yoserizal, Y. Applying Programmable Logic Control (PLC) for Control Motors. Blower and Heater in the Rubber Drying Processing, Jurnal Ilmiah Teknik Elektro Komputer dan Informatika. 2021; vol. 7, no. 1, pp. 131–141, https://doi.org/10.26555/jiteki.v7i1.20514.
13. Auzan, M., Hujja, R. M., Fuadin, M. R., & Lelono, D. Path Tracking and Position Control of Nonholonomic Differential Drive Wheeled Mobile Robot, Jurnal Ilmiah Teknik Elektro Komputer dan Informatika. 2021; vol. 7, no. 3, pp. 368–379. https://doi.org/10.26555/jiteki.v7i3.21017.
14. Maarif, A., Puriyanto, R. D., & Hasan, F. R. T. Robot Keseimbangan Dengan Kendali Proporsional-Integral-Derivatif (PID) dan Kalman Filter. IT Journal Research and Development. ITJRD. 2020; vol. 4, no. 2, pp. 117–127.
15. Ashokkumar, R., Suresh, M., Sharmila, B., Panchal, H., Gokul, C., Udhayanatchi, K. V. et al. A novel method for Arduino based electric vehicle emulator. International Journal of Ambient Energy. 2021; 43(1), pp. 4299-4304. https://doi.org/10.1080/01430750.2020.1860129.
16. Kocaoğlu S, Kuşçu H. PIC ile DC motorun hız ve konum kontrolü için gerekli PID parametrelerinin belirlenmesi ve bir uygulama. In: Otomatik Kontrol Ulusal Toplantısı (TOK); 2012.
17. Chaouch S, Hasni M, Boutaghane A, Babes B, Mezaache M, Slimane S, Djenaihi M. DC-motor control using Arduino-Uno board for wire-feed system. In: 2018 International Conference on Electrical Sciences and Technologies in Maghreb (CISTEM); 2018 Oct. p. 1–6.
18. Gasparesc G. PID control of a DC motor using LabVIEW interface for embedded platforms. In: 12th International Symposium on Electronics and Telecommunications (ISETC); 2016. p. 145–148.
19. Adel Z, Hamou AA, Abdellatif S. Design of real-time PID tracking controller using Arduino Mega 2560 for a permanent magnet DC motor under real disturbances. In: 2018 International Conference on Electrical Sciences and Technologies in Maghreb (CISTEM); 2018 Oct. p. 1–5.
20. Guo, Y., & Mohamed, M. E. A. Speed Control of Direct Current Motor Using ANFIS Based Hybrid P-I-D Configuration Controller, IEEE Access. 2020; vol. 8, pp. 125638–125647.
21. Hekimoglu B. Optimal Tuning of Fractional Order PID Controller for DC Motor Speed Control via Chaotic Atom Search Optimization Algorithm. IEEE Access. 2019; vol. 7, pp. 38100–38114.
22. Tir Z, Malik O, Hamida MA, Cherif H, Bekakra Y, Kadrine A. Implementation of a fuzzy logic speed controller for a permanent magnet DC motor using a low-cost Arduino platform. In: 2017 5th International Conference on Electrical Engineering - Boumerdes (ICEE-B); 2017 Oct. p. 1–4.
23. Akbar, M. A., Naniwa, T., & Taniai, Y. Model reference adaptive control for DC motor based on Simulink. In: 2016 6th International Annual Engineering Seminar (InAES); 2016 Aug. p. 101–106.
24. Ahmad M, Khan A, Raza MA, Ullah S. A study of state feedback controllers for pole placement. In: 2018 5th International Multi-Topic ICT Conference (IMTIC); 2018 Apr. p. 1–6.
25. Somwanshi, D., Bundele, M., Kumar, G., & Parashar, G. Comparison of fuzzy-PID and PID controller for speed control of DC motor using LabVIEW. in Procedia Computer Science. 2019; vol. 152, pp. 252–260.
26. Varshney, A., Gupta, D., & Dwivedi, B. Speed response of brushless DC motor using fuzzy PID controller under varying load condition. Journal of Electrical Systems and Information Technology. 2017; vol. 4, no. 2, pp. 310–321.
27. Ma'arif, A., Nabila, H., & Wahyunggoro, O. Application of Intelligent Search Algorithms in Proportional-Integral-Derivative Control of Direct-Current Motor System. İn: The 2019 Conference on Fundamental and Applied Science for Advanced Technology; 2019, vol. 1373, no. 1, pp. 1–10.
28. Joseph, S. B., Dada, E. G., Abidemi, A., Oyewola, D. O., & Khammas, B. M. Metaheuristic algorithms for PID controller parameters tuning: review, approaches and open problems. Heliyon. 2022; vol. 8, no. 5. https://doi.org/10.1016/j.heliyon.2022.e09399.
29. Borase, R. P., Maghade, D. K., Sondkar, S. Y., & Pawar, S. N. A review of PID control, tuning methods and applications. International Journal of Dynamics and Control. 2021; vol. 9, pp. 818–827. https://doi.org/10.1007/s40435-020-00665-4.
30. Kherkhar, A., Chiba, Y., Tlemçani, A., & Mamur, H. Thermal investigation of a thermoelectric cooler based on Arduino and PID control approach. Case Studies in Thermal Engineering. 2022; vol. 36. https://doi.org/10.1016/j.csite.2022.102249.
31. Xu, F., Liang, X., Chen, M., & Liu, W. Robust Self-Learning PID Control of an Aircraft Anti-Skid Braking System. Mathematics. 2022; vol. 10, no. 8, p. 1290, 2022. https://doi.org/10.3390/math10081290.
32. Božek, P., & Nikitin, Y. The Development of an Optimally-Tuned PID Control for the Actuator of a Transport Robot. Actuators. 2021; vol. 10, no. 8, p. 195. https://doi.org/10.3390/act10080195.
33. Sun, J., Zhou, H., Ma, X., & Ju, Z. Study on PID tuning strategy based on dynamic stiffness for radial active magnetic bearing. ISA Transactions. 2018; vol. 80, pp. 458–474.
34. Fan, Y., Shao, J., Sun, G., & Shao, X. Improved Beetle Antennae Search Algorithm-Based Lévy Flight for Tuning of PID Controller in Force Control System. Mathematical Problems in Engineering. 2020; vol. 2020. https://doi.org/10.1155/2020/4287315.
35. Potnuru, D., Mary, K. A., & Babu, C. S. Experimental implementation of Flower Pollination Algorithm for speed controller of a BLDC motor. Ain Shams Engineering Journal. 2019; vol. 10, no. 2, pp. 287–295. https://doi.org/10.1016/j.asej.2018.07.005.
36. Alagoz, B. B., Deniz, F. N., & Koseoglu, M. An efficient PID-based optimizer loop and its application in De Jong's functions minimization and quadratic regression problems. Systems & Control Letters. 2022; vol. 159. https://doi.org/10.1016/j.sysconle.2021.105090.

37. Farag W. Complex Trajectory Tracking Using PID Control for Autonomous Driving. International Journal of Intelligent Transportation Systems Research. 2019; vol. 18, no. 2, pp. 356–366. https://doi.org/10.1007/s13177-019-00204-2.
38. Ulusoy, S., Nigdeli, S. M., & Bekdaş, G. Novel metaheuristic-based tuning of PID controllers for seismic structures and verification of robustness. Journal of Building Engineering. 2021; vol. 33. https://doi.org/10.1016/j.jobe.2020.101647.
39. Du, H., Liu, P., Cui, Q., Ma, X., & Wang, H. PID Controller Parameter Optimized by Reformative Artificial Bee Colony Algorithm. Journal of Mathematics. 2022; vol. 2022, pp. 1–16. https://doi.org/10.1155/2022/3826702.
40. Wang, H., Du, H., Cui, Q., & Song, H. Artificial bee colony algorithm based PID controller for steel stripe deviation control system. Science Progress. 2022; vol. 105, no. 1, pp. 1–22. https://doi.org/10.1177/00368504221075188.
41. Bhookya, J., Kumar, M. V., Kumar, J. R., & Rao, A. S. Implementation of PID controller for liquid level system using mGWO and integration of IoT application. Journal of Industrial Information Integration. 2022; vol. 28. https://doi.org/10.1016/j.jii.2022.100368.
42. Kommula, B. N., & Kota, V. R. Direct instantaneous torque control of Brushless DC motor using firefly Algorithm based fractional order PID controller. Journal of King Saud University - Engineering Sciences. 2020; vol. 32, no. 2, pp. 133–140. https://doi.org/10.1016/j.jksues.2018.04.007.
43. Rodríguez-Molina, A., Villarreal-Cervantes, M. G., Álvarez-Gallegos, J., & Aldape-Pérez, M. Bio-inspired adaptive control strategy for the highly efficient speed regulation of the DC motor under parametric uncertainty. Applied Soft Computing. 2019; vol. 75, pp. 29–45. https://doi.org/10.1016/j.asoc.2018.11.002.
44. Gani, M. M., Islam, M. S., & Ullah, M. A. Optimal PID tuning for controlling the temperature of electric furnace by genetic algorithm. SN Applied Sciences, 2019; vol. 1, no. 8, pp. 1–8, https://doi.org/10.1007/s42452-019-0929-y.
45. Bhookya, J., & Jatoth, R. K. Optimal FOPID/PID controller parameters tuning for the AVR system based on sine–cosine-algorithm.Evolutionary Intelligence. 2019; vol. 12, no. 4, pp. 725–733. https://doi.org/10.1007/s12065-019-00290-x.
46. Hekimoğlu B. Sine-cosine algorithm-based optimization for automatic voltage regulator system. Transactions of the Institute of Measurement and Control. 2018; vol. 41, no. 6, pp. 1761–1771 https://doi.org/10.1177/0142331218811453.
47. Zhou, Y., Zhang, J., Yang, X., & Ling, Y. Optimization of PID Controller Based on Water Wave Optimization for an Automatic Voltage Regulator System. Information Technology and Control, 2019; vol. 48, no. 1, pp. 160–171. https://doi.org/10.5755/j01.itc.48.1.20296.
48. Rahayu, E. S., Ma'arif, A., & Cakan, A. Particle swarm optimization (PSO) tuning of PID control on DC motor. International Journal of Robotics and Control Systems. 2022; Vol 2, No 2.
49. Kushwah, M., & Patra, A. Tuning PID controller for speed control of DC motor using soft computing techniques-A review. Advance in Electronic and Electric Engineering. 2014; 4(2), 141-148.
50. Ang, K. H., Chong, G., & Li, Y. PID control system analysis, design, and technology. IEEE transactions on control systems technology. 2005 13(4), 559-576.
51. Eberhart R, Kennedy J. A new optimizer using particle swarm theory. In: MHS'95 Proceedings of the Sixth International Symposium on Micro Machine and Human Science; 1995 Oct. p. 39–43.
52. Yıldırım, M. Y., & Akay, R. Mobil robotlar için çok engelli ortamlarda hızlı yol planlama. Gazi Üniversitesi Mühendislik Mimarlık Fakültesi Dergisi. 2021; 36(3), pp.1551-1564.
53. Garip, Z., Karayel, D., & Çimen, M. E. Parçacık Sürü Optimizasyon Tabanlı Mobil Robotlarda Global Yol Planlama. Journal of Smart Systems Research. 2021; Volume: 2 Issue: 1, pp. 18-26.
54. Ulusoy, A., & Güneş, M. Mobil robot kolunun PSO ile stabilizasyonu. Kahramanmaraş Sütçü İmam Üniversitesi Mühendislik Bilimleri Dergisi. 2019; 22(4), 288-297.
55. Sahib, M. A., & Ahmed, B. S. A new multiobjective performance criterion used in PID tuning optimization algorithms. Journal of Advanced Research. 2016; Vol.7, No.1, pp. 125-134.
56. Idir, A., Kidouche, M., Bensafia, Y., Khettab, K., & Tadjer, S. A. Speed control of DC motor using PID and FOPID controllers based on differential evolution and PSO. Int. J. Intell. Eng. Syst, 2018; Vol.11, No.4.
57. Ekinci, S., Hekimoğlu, B., Demirören, A., & Eker, E. Speed control of DC motor using improved sine cosine algorithm based PID controller. In 2019 3rd International Symposium on Multidisciplinary Studies and Innovative Technologies (ISMSIT). IEEE. 2019, October; (pp. 1-7).
58. Wu, C., Chen, L., Xiong, H., & Hu, J. USMN-SCA: A Blockchain Sharding Consensus Algorithm With Tolerance for an Unlimited Scale of Malicious Nodes. IEEE Transactions on Network and Service Management. 2024; Volume: 22 Issue: 2.
59. Nadimi-Shahraki, M. H., Taghian, S., Javaheri, D., Sadiq, A. S., Khodadadi, N., & Mirjalili, S. MTV-SCA: multi-trial vector-based sine cosine algorithm. Cluster Computing. 2024; 27(10), 13471-13515.
60. Shinde, V., Jha, R., & Mishra, D. K. Improved Chaotic Sine Cosine Algorithm (ICSCA) for global optima. International Journal of Information Technology. 2024; 16(1), pp. 245-260.
61. Kumar, M. S., Gopisetti, S., & Sujatha, P. Optimal PI controller parameter setting for torque ripple minimization in SVPWM–DTC based BLDC motor drive using sine cosine algorithm. Engineering Research Express. 2024; 6(4), 045359.
62. Yousef, A. M., Ebeed, M., Abo-Elyousr, F. K., Elnozohy, A., Mohamed, M., & Abdelwahab, S. M. Optimization of PID controller for hybrid renewable energy system using adaptive sine cosine algorithm. International Journal of Renewable Energy Research-IJRER. 2020; pp. 670-677.
63. Nanyan, N. F., Ahmad, M. A., & Hekimoğlu, B. Optimal pid controller for the dc-dc buck converter using the improved sine cosine algorithm. Results in Control and Optimization. 2024; 14, 100352.
64. Purnama HS, Sutikno T, Alavandar S, Subrata AC. Intelligent control strategies for tuning PID of speed control of DC motor—a review. In: 2019 IEEE Conference on Energy Conversion (CENCON); 2019 Oct. p. 24–30.

HITTITE JOURNAL OF SCIENCE AND ENGINEERING

e-ISSN: 2148-4171
Volume: 12 • Number: 2
June 2025

An Application on Electric Vehicle Charging Station Site Selection With Multi-Criteria Decision-Making Methods

Şeyma Sünbül[*1] | **Ahmet Tortum**[2]

[1]Erzincan Binali Yıldırım University, Urban and Regional Development Application and Research Center, Department of Environment, 24100, Erzincan, Türkiye.
[2]Atatürk University, Department of Civil Engineering, 25100, Erzurum, Türkiye.

Corresponding Author

Şeyma Sünbül
E-mail: seyma.sunbul@erzincan.edu.tr Phone: +90 553 610 07 04;
RORID[1]: https://ror.org/02h1e8605 RORID[2]: https://ror.org/03je5c526

Article Information

Article Type: Research Article
Doi: https://doi.org/10.17350/HJSE19030000355
Received: 18.12.2024
Accepted: 21.05.2025
Published: 30.06.2025

Cite As

Sünbül ş, Tortum A. An application on electric vehicle charging station site selection with multi-criteria decision-making methods . Hittite J Sci Eng. 2025;12(2):91-100.

Peer Review: Evaluated by independent reviewers working in at least two different institutions appointed by the field editor.
Ethical Statement: Not available.
Plagiarism Checks: Yes - iThenticate
Conflict of Interest: Authors approve that to the best of their knowledge, there is not any conflict of interest or common interest with an institution/organization or a person that may affect the review process of the paper.

CRediT AUTHOR STATEMENT
Şeyma Sünbül: Conceptualization, Methodology, Analysis, Formalization, Validation, Writing- original draft, Writing- review and editing. **Ahmet Tortum:** Data curation, Investigation, Supervision, Writing- review and editing.

An Application on Electric Vehicle Charging Station Site Selection With Multi-Criteria Decision-Making Methods

Şeyma SÜNBÜL[*1] | Ahmet TORTUM[2]

[1]Erzincan Binali Yıldırım University, Urban and Regional Development Application and Research Center, Department of Environment, 24100, Erzincan, Türkiye.
[2]Atatürk University, Department of Civil Engineering, 25100, Erzurum, Türkiye.

Abstract

As the population grows and vehicles are increasingly owned, emissions from fossil fuels are worsening environmental problems. In this context, electric vehicles (EVs) present a significant alternative for the development of sustainable transportation systems. However, for electric vehicles (EVs) to become a prevalent form of transportation, the establishment of an effective and efficient charging infrastructure is imperative. The primary objective of this study is to ascertain the most suitable location for the installation of an electric vehicle (EV) charging station within the Erzincan Binali Yıldırım University Yalnızbag Campus. During site selection, the analytical hierarchy process (AHP) and TOPSIS methods were used to evaluate the criteria. The study was conducted in two stages. In the first, seven active-use transformers on campus were weighed using the AHP method, then the most suitable one was selected using the TOPSIS method.In the second, seven parking areas were analysed using the same criteria. The parking lot selection used the AHP and TOPSIS methods, considering faculty and campus entrance distance, lot capacity and transformer preference score.

The findings of the study demonstrate the efficacy of the AHP and TOPSIS methods in the context of multi-criteria and multi-stage decision-making processes. The integration of these methods has been demonstrated to facilitate the optimisation of EV charging station location selection, both in technical and practical terms.

Keywords: Electric Vehicle, Transportation Planning, MCDM.

INTRODUCTION

The investigation of EVs commenced in the 19th century but was subsequently placed on the back burner for a multitude of reasons (1). The exponential growth in the use of EVs globally has created an imperative to develop innovative solutions and strategies for energy infrastructure, with the dual objective of reducing environmental pollution and addressing the pressing need for sustainable energy. The necessity for energy infrastructure is predominantly addressed in the context of urban energy planning, particularly regarding the provision of sustainable transportation and transport solutions. As EVs become increasingly prevalent, the availability, efficiency and effectiveness of charging infrastructure becomes a multifaceted question that is challenging to resolve. This assertion is supported by the findings reported by Xylia and colleagues in 2017 (2). The determination of the necessity for a charging station and the selection of an appropriate station location are not merely technical concerns; there are also multi-criteria problems that must be addressed in accordance with the requirements of the users. These issues require a technical solution, particularly for the more effective planning of urban transportation systems. MCDM is employed in situations where there are numerous options, and the decision-maker must evaluate more than one criterion collectively (3). The AHP and TOPSIS methodologies are two of the most effective and reliable methods for decision-making processes within the MCDM framework. The AHP method determines the most appropriate option by weighing the alternatives and comparing them according to the specified criteria (4). The TOPSIS method aims to ascertain the most suitable alternatives by identifying the positive ideal and negative ideal solutions and determining their proximity to these solutions (5). The combination of these methods, whether used together or separately, provides an effective solution in a multitude of contexts. Although other multi-criteria decision-making methods such as (Analytic Network Process) ANP, (The Preference Ranking Organization Method for Enrichment Evaluation) PROMETHEE, (Complex Proportional Assessment) COPRAS, Simple Multi Attribute Rating Technique (SMART) and (Weighted Aggregated Sum Product Assessment) WASPAS have been widely used in the literature, there are several main reasons why the AHP and TOPSIS methods have been preferred together in this study. Firstly, the AHP method produces reliable results by consistently modelling the subjective evaluations of decision makers during the weighting phase of the criteria. The TOPSIS method, on the other hand, provides a practical and applicable decision support mechanism by ranking the alternatives according to the identified criteria. In the literature, it has been observed that the use of these two methods together in studies on the determination of the location of EV charging stations is common and leads to successful results (6,7). In addition, the integration of AHP and TOPSIS makes the calculation process of the method simpler and more understandable. This makes it an effective solution in both academic and applied fields. Karabıçak et al. (2016) showed that by using AHP and TOPSİS methods together, practical and effective results were obtained in multi-criteria decision-making processes (6). Similarly, Saha and Roy (2021) conducted site selection by integrating geographic information systems (GIS) with AHP in planning suitable settlement areas (8). There are several studies in the literature that use different combinations of methods to determine the location of electric vehicle (EV) charging stations. While some of these studies used AHP alone, others evaluated AHP and TOPSIS together. In addition, more comprehensive and accurate solution methods have been provided by integrating additional analysis tools such as geographic information systems. To take one example, Erbaş et al. (2018) used Fuzzy AHP and TOPSIS together in her study and integrated them with the Geographical Information System (GIS) to determine the location of EV charging stations (9). Similarly, Bilgilioğlu (2022) optimised the siting of EV charging stations by integrating GIS with the fuzzy AHP method (10). On the other hand, Alkan et al. (2023) identified the criteria based

on expert opinion using the AHP method and determined the appropriate location of EV charging stations (7). In addition to the AHP method, Asnaz et al. (2021) used PROMETHEE and SMART methods to select EV charging stations (3).

In this context, the approach adopted in this study was to weigh the criteria using the AHP method and then to rank the alternatives using the TOPSIS method. As in this study, Khalkhali et al. (2015) used envelope analysis to determine EV charging stations. The locations and capacities of these stations were first decided based on grid benefits, then classified using envelopment analysis and technical indicators (11). In the present study, the transformer selection process was undertaken first, followed by the determination of the most suitable parking area depending on the previously selected transformer. Thanks to these methods, which have received positive feedback in the literature, the evaluation of different criteria together enables the production of more sustainable and versatile solutions. This ensured both consistent modelling of subjective judgements and determination of the most appropriate alternative.

This study designs a step-by-step decision-making process using both AHP and TOPSIS methods, unlike the studies in literature. This step-by-step approach has been addressed in a limited number of studies in the literature on EV sitting processes. In addition, the addition of demand forecasting analysis provides a more comprehensive methodological framework for determining station needs. In this respect, our study contributes to both academic literature and practical applications in the field of EV charging station sitting.

MATERIAL AND METHODS

Material

Erzincan Binali Yıldırım University, which is the subject of the study, started its higher education life in Türkiye with Erzincan Vocational School and Erzincan Education School, which were established in 1976, and became a university in 2006. The transition to Yalnızbağ Campus, which represents the largest campus of the university, was completed in 2021. The university, which has a campus that is still open to further development, employs a total of 1.750 staff, comprising 1.085 academic and 665 administrative personnel. The campus is home to a total of 14.485 students enrolled in a range of academic programmes, including associate degrees, undergraduate and graduate studies. These programmes are offered by the Faculty of Pharmacy, Faculty of Education, Faculty of Arts and Sciences, Faculty of Fine Arts, Faculty of Economics and Administrative Sciences, Faculty of Theology, Faculty of Engineering and Architecture, Faculty of Sports Sciences, Vocational School, Ali Cavit Çelebi Civil Aviation School, Institute of Science, Institute of Health Sciences and Institute of Social Sciences (12). Transportation to the campus, which is situated approximately 12 km from the city centre, is provided for students by city buses, while a shuttle service is available for administrative staff. The majority of academic staff utilise their own vehicles to reach the campus. The campus comprises seven transformers and seven parking lots.

Figure 1 Campus Area

The location of the EV e charging station was selected from among seven potential parking lots (figure 1). Furthermore, the requisite number of charging stations was estimated based on the number of vehicles entering and exiting the campus.

Method

MCDM was used to determine the location of the charging station. MCDM is a widely used method that allows a meaningful consensus to be reached by bringing together many criteria of varying quality and quantity. Criterion weights can be successfully obtained with MCDM methods in the most appropriate location selection problems in many different fields (8,13). The AHP method, one of the MCDM methods, is widely used to determine the weighting of criteria in site selection studies. In this study, AHP and TOPSIS methods were applied step by step. The reason why AHP and TOPSIS are preferred is that the AHP method provides a hierarchical structure in the weighting of criteria, allowing subjective judgements to be modelled consistently. TOPSIS, on the other hand, was preferred because it provides an effective decision support mechanism for determining the most appropriate option by ranking the alternatives according to their distance from positive and negative ideal solutions.

Analytical Hierarchy Process (AHP)

The AHP method is a MCDM method, initially proposed by Thomas L. Saaty of the University of Pennsylvania in the late 1970s (14). This method is the most frequently employed in location selection studies. Saaty posits that the five-step decision-making method can be applied in practice. The following steps are required: firstly, the issue must be defined and a hierarchical structure created; secondly, the pairwise comparison matrices and superiorities must be determined; thirdly, an eigenvector must be calculated; fourthly, the consistency of the eigenvector must be determined; and finally, the general result of the hierarchical structure must be obtained.

(3) (4) (9)

Step 1. Defining the Problem and Creating the Hierarchical Structure

The issue in question is duly identified, and a hierarchical structure is subsequently established, with the issue at the core of the structure. In this hierarchical structure, the purpose, criteria, sub-criteria and alternatives are interrelated and constitute a unified whole. The lowest level of the hierarchy comprises all potential alternatives, whereas the highest level delineates the overarching objective. The remaining levels represent the decision criteria and sub-criteria (15). Saaty's studies have often included examples of hierarchies that are appropriate for site selection studies (14). A similar hierarchical structure can be constructed based on the purpose and criteria identified in the problem.

Step 2. Pairwise Comparison of Matrices and Determination of Advantages

At this stage of the process, pairwise comparison matrices of dimension (nxn) are created to determine the relative importance levels of the selected criteria, as established in stage one. This decision-making process involves the comparison of criteria or alternative matrices on a pairwise basis (16). The sample matrix is defined in Equation 1.

$$A = \begin{bmatrix} 1 & a_{21} & a_{31} & \cdots & a_{n1} \\ 1/a_{21} & 1 & a_{32} & \cdots & a_{n2} \\ \vdots & \vdots & \ddots & \vdots & \vdots \\ 1/a_{n1} & 1/a_{n2} & 1/a_{n3} & \cdots & 1 \end{bmatrix}_{n\times n} \quad (1)$$

The relative importance of the factors is determined according to the Saaty scale (Table 1), and the resulting levels of importance are then placed in the matrix (4).

Table 1 Severity Table.

Value	Description	Explanation
1	Equally important	The two activities are of equal importance in achieving the desired outcome.
3	Moderately important	Experience and judgment slightly favor one activity over another.
5	Strongly important	Experience and judgment strongly favor one activity over another.
7	Very strong stream important	An activity is strongly preferred, and its dominance is clearly evident in practice.
9	Important	The evidence for preferring one activity over another is overwhelmingly reliable.
2,4,6,8	Intermediate values	In instances where a compromise is necessary, values that fall between the aforementioned judgments may be employed.

Step 3. Determination of Eigenvector

The objective of this phase is to identify the eigenvectors of the criteria, which have been assigned relative importance levels. The eigenvector of a matrix in an n x 1 dimension is determined through the following process:
In the case where i=1, 2, 3, ..., n and j=1, 2, 3, ..., n,

$$b_{ij} = \frac{a_{ij}}{\sum_{i=1}^{n} a_{ij}} w_i = \frac{\sum_{j=1}^{n} b_{ij}}{n} \quad (2,3)$$

In order to ascertain the relative importance of the criteria, it is necessary to calculate column vectors of the form W = $[w_i]_{nx1}$. The column vector W is obtained by calculating the arithmetic mean of the row elements of the matrix formed by the bijb_{ij}bij values specified in Equations 2 and 3 (16).

Step 4. Calculating the Consistency of Eigenvector

At this juncture, the consistency ratio (CR) of each binary matrix is calculated. It is desirable that the upper limit of the CR value should be 0.1. To calculate the CR ratio, it is necessary to calculate the basic value coefficient (λ). In such a case, the weighting matrix is multiplied by the eigenvector. Subsequently, the largest eigenvector (λmax) must be calculated. The pertinent operations are delineated in equations 4 and 5.
In the case where i=1, 2, 3,..., n and j=1, 2, 3,..., n,

$$D = [a_{ij}]_{n\times n} \times [w_i]_{n\times 1} = [d_i]_{n\times 1} \quad (4)$$

$$\lambda_{max} = \frac{\sum_{i=1}^{n} \frac{d_i}{w_i}}{n} \quad (5)$$

In order to calculate the consistency rate, it is necessary to determine the randomness index (RI). The data set comprising RI values, which are constant numbers determined according to the n value, is provided in Table 2. In accordance with the data, the calculation of the CR value is presented in equation number 6. To ascertain the randomness index, it is necessary to select the N value from Table 2.

$$CR = \frac{\lambda - n}{(n-1)\cdot RI} \quad (6)$$

Table 2 Randomness Index Calculation Table.

n	1	2	3	4	5	6	7	8	9	10
RI	0	0	0,58	0,9	1,12	1,24	1,32	1,41	1,45	1,49

Step 5. Obtaining the General Result of the Hierarchical Structure

In the final phase, the values calculated in the previous four phases are applied to the entire hierarchical structure. Consequently, a decision matrix of dimension m x n, designated as DW, is constructed. The R result vector is derived by multiplying the obtained matrix by the W superiority vector between the criteria (16). Given the data set in question, the following equation can be derived:

$$DW = [w_{ij}]_{m\times n} \quad (7)$$

This leads to the conclusion that;

$$R = DW \times W \quad (8)$$

Consequently, the overall outcome of the hierarchical structure is established, and the significance coefficients are ascertained.

TOPSIS Method

Hwan and Yoon (1981) introduced another multi-criteria decision-making method, the TOPSIS method. TOPSIS can be used for both selection and classification problems, as can AHP (17). The main objective of this method is to select the solution alternatives that are the shortest distance from the ideal solution, which is positive, and the farthest distance from the ideal solution, which is negative (5). To elucidate further, the positive ideal solution is formulated based on the most favourable values of the criterion, whereas the negative ideal solution is constructed on the foundation of the least favourable values of the criterion. In alternative selection processes, the optimal alternative is that which is closest to the positive ideal solution and furthest from the negative ideal solution (18). The Topsis method is typically conducted in six sequential steps.

Step 1. Creating The Decision Matrix

In the construction of the decision matrix, the rows represent the alternatives, while the columns represent the criteria. The matrix can be presented in the following format:

$$D = \begin{bmatrix} d_{11} & \cdots & d_{1k} \\ \vdots & \ddots & \vdots \\ d_{n1} & \cdots & d_{nk} \end{bmatrix} \quad (9)$$

In this context, the symbol (i = 1,2,...,n, j = 1,2,...,k) represents the score of the i. alternative based on the j. criterion (6).

Step 2. Normalizing The Decision Matrix

The matrix is normalised by taking the square root of the sum of the squares of the scores and features of the criteria in the created decision matrix (19). The normalization process can be demonstrated through the following formulas:

$$r_{ij} = \frac{a_{ij}}{\sum_{i=1}^{m} a_{ij}^2}, \left(i = 1, 2, \ldots, m \text{ve} j = 1, 2, \ldots, n\right) \quad (10)$$

The normalized matrix can be obtained by the following method:

$$R = \begin{bmatrix} r_{11} & \cdots & r_{1n} \\ \vdots & \ddots & \vdots \\ r_{m1} & \cdots & r_{mn} \end{bmatrix} \quad (11)$$

Step 3. Weighting The Normalized Matrix

In order to assign a weight to each value in the normalised matrix, it is first necessary to determine the weight value according to the importance levels assigned to the identified elements in relation to the specified criteria (W). The weighted matrix can be defined as follows:

$$W = \begin{bmatrix} w_{11} & \cdots & w_{1k} \\ \vdots & \ddots & \vdots \\ w_{n1} & \cdots & w_{nk} \end{bmatrix} \quad (12)$$

Here w_j: is the weight of each j. criterion.
Subsequently, the matrix with weight values is multiplied by the values in the normalised matrix, thereby providing the weighting of the matrix. The weighted matrix can be presented in the following manner:

$$V = \begin{bmatrix} v_{11} & \cdots & v_{1k} \\ \vdots & \ddots & \vdots \\ v_{n1} & \cdots & v_{nk} \end{bmatrix} \quad (13)$$

Step 4. Ideal And Non-Ideal Solutions

Once the weighted matrix has been identified, the subsequent step is to ascertain the ideal and non-ideal solutions. In this context, the positive ideal solution represents the optimal performance values of the weighted normalised decision matrix, whereas the negative ideal solution denotes the least favourable values (20). The solutions are calculated in accordance with the following formulae, where A^* represents the positive ideal solution and A^- denotes the negative ideal solution.

$$\begin{aligned} A^* &= \left\{(\max v_{ij} | j \in I), (\min v_{ij} | j \in J)\right\} \\ A^- &= \left\{(\min v_{ij} | j \in I), (\max v_{ij} | j \in J)\right\} \end{aligned} \quad (14)$$

The calculation of the distance to ideal and non-ideal solutions is performed in accordance with the principles set forth by Euclid. The ideal distance is represented by the symbol S_i^*, while the non-ideal distance is represented by S_i^-.

$$\begin{aligned} S_i* &= \sqrt{\sum_{j=1}^{n} (v_{ij} - v_{j*})^2} \qquad \mathrm{i} = 1, 2, \ldots, \mathrm{m} \\ S_i- &= \sqrt{\sum_{j=1}^{n} (v_{ij} - v_{j-})^2} \qquad \mathrm{i} = 1, 2, \ldots, \mathrm{m} \end{aligned} \quad (15)$$

Step 5. Relative Closeness To The Ideal Solution

The proximity according to the S_i^* ideal distance and S_i^- non-ideal distance values is calculated using the following formula:

$$C_i^* = \frac{S_i^-}{S_i^- + S_i^*} \qquad 0 \le C_i^* \le 1 \quad (16)$$

Step 6. Finding The Suitability Order of The Alternatives

Ultimately, the C_i^* values are sorted in ascending order to identify the optimal alternative.

RESULTS AND DISCUSSION

Determining the Number of Charging Stations Using Demand Forecast

The study began with a demand forecasting analysis to

determine how many charging points were needed. The number of vehicles entering the campus, the percentage of electric vehicles in the area and the daily usage requirements were considered when calculating the number of charging stations required. The number of charging points required was calculated based on the number of vehicles entering the campus, the proportion of electric vehicles in the area and the daily usage required. Based on the average daily mileage and battery capacity of electric vehicle users in Turkey, it was assumed that electric vehicles need to be charged every three days. According to TÜİK's 2024 data, the EV rate in Turkey has been determined as 1.5%. In consideration of the fact that the number of automobiles in Erzincan province in 2024 is 32.567, it can be estimated that approximately 489 vehicles can be utilized as EVs. Considering the potential for 10% of the estimated number of EVs in Erzincan to be deployed on campus, it is reasonable to assume that approximately 5 EVs will enter the campus daily. The number of vehicle entries was used to calculate the number of charging points required on campus and, taking into account the average daily mileage and battery capacity of electric vehicle users, it was estimated that a vehicle would be charged on average every 3 days (Table 3).

The necessity for a charging station was established on the premise that a maximum of five vehicles could be charged daily. Accordingly, the requisite number of EV charging stations has been calculated to be approximately two.

Table 3 Charging Station Need Demand Forecast.

Days	Vehicle Entry	Number of EVs	Daily Charging Request	Need for a Charging Station
Monday	1895	28.4	9.47	1.9
Tuesday	2007	30.1	10.04	2.0
Wednesday	1931	29.0	9.65	1.9
Thursday	2112	31.7	10.56	2.1
Friday	1717	25.8	8.59	1.7

Parking Lot Choice with AHP and TOPSIS

The criteria used in the study were determined based on similar studies in literature, expert opinion and field data. The most important factors in selecting a location for an electric vehicle charging station include the adequacy of the energy infrastructure, density of use, accessibility and parking capacity. Therefore, in the first stage, transformer power, distance to car parks and car park capacity were determined as transformer selection criteria. In the second stage, the distance to faculty entrances, distance to campus entrance gate, parking capacity and transformer preference score criteria determined in the first stage were evaluated for parking lot selection. Criteria were weighted using AHP and alternatives were ranked using TOPSIS. The initial stage involved the evaluation of three key criteria: the distances between transformers and parking lots (C1), parking lot capacities (C2) and transformer powers (C3). The relative significance of the primary criteria was established through the application of the AHP. The selection of transformers was conducted through the application of the TOPSIS method, utilising the identified importance coefficients and determining the derived preference scores. In the second stage of the process, several additional criteria were incorporated. The evaluation criteria were established based on the following parameters: the distances of the parking lots to the faculty entrances (FE) (C´1), the distances of the parking lots to the campus entrance (CE) gate (C´2), the parking lot capacities (C´3), and the transformer preference scores identified in the initial phase (C´4). Accordingly, the optimal transformer was selected, and the most suitable parking lot for the EV charging station was identified based on the selected transformer.

Finding the First Stage Criteria Weights with AHP Method

Step 1. Defining the Problem and Determining the Criteria

In selecting transformers, several criteria were taken into consideration, including the distances between transformers and parking lots, the capacities of the parking lots in question, and the powers of the transformers themselves. The distances between transformers and parking lots (PL) are provided in Table 4, while the capacities of the parking lots are presented in Table 5. The powers of the transformers are given in Table 6.

Table 4 Transformer-Parking Lots of Distances.

	PL1	PL2	PL3	PL4	PL5	PL6	PL7
T1	55.6	197	466	488	354	316	221
T2	416	175	108	324	510	555	562
T3	548	297	115	231	534	604	673
T4	896	693	612	368	644	758	931
T5	547	452	570	265	214	312	513
T6	356	370	601	401	34.8	79.8	277
T7	320	462	724	578	226	110	164

Table 5 Parking Lots Capacities

Parking Lots	Car Park Capacity
PL1	60
PL2	50
PL3	170
PL4	170
PL5	180
PL6	123
PL7	157

Table 6 Transformer Powers.

Transformer	Transformer Power
T1	630
T2	800
T3	800
T4	250
T5	630
T6	800
T7	800

Step 2. Determining Pairwise Comparison Matrices and Advantages

The relative importance of the criteria was determined using the AHP method, based on an analysis of the literature and the application of Saaty's pairwise comparison matrix (Table 7). The anticipated criteria are as follows: the location with the shortest distance, the highest parking capacity and the greatest transformer power.

Table 7 Pairwise Comparison Matrix.

	C1	C 2	C 3
C1	1	2	2
C2	1/2	1	1.5
C3	1/2	2/3	1

Step 3-4: Determining the Eigenvector and Calculating its Consistency.

The application of the AHP with a pairwise comparison matrix revealed that the criteria weights were 0.479 for distance, 0.285 for parking capacity, and 0.218 for transformer power. Furthermore, the consistency ratio (CR) was calculated to be 0.016. As the consistency ratio (CR) is less than 0.1, it can be demonstrated that the criteria weights have been calculated correctly.

Finding the First Stage Preference Scores with TOPSIS Method

Step 1-2. Creating And Normalizing The Decision Matrix

After determining the weights, the TOPSIS method was used to select the most ideal transformer, and normalisation was performed using the criteria data (Table 8).

Table 8 Transformer Decision Matrix Normalization

	C1	C2	C3
T1	0.190	0.190	0.190
T2	0.326	0.326	0.326
T3	0.389	0.389	0.389
T4	0.636	0.636	0.636
T5	0.378	0.378	0.378
T6	0.267	0.267	0.267
T7	0.297	0.297	0.297

Step 3. Weighting The Normalized Matrix

Following the creation of the normalisation matrix, a weighted matrix was constructed utilising the weights identified through the AHP (Table 9).

Table 9 Transformer Weighted Normalized Matrix.

	C1	C2	C3
T1	0.114	0.019	0.057
T2	0.196	0.033	0.098
T3	0.233	0.039	0.117
T4	0.381	0.064	0.191
T5	0.227	0.038	0.113
T6	0.160	0.027	0.080
T7	0.178	0.030	0.089

Step 4. Ideal And Non-Ideal Solutions

Following the acquisition of the weighted normalised matrix, an investigation was conducted into the positive ideal and negative ideal properties, with distances to the positive and negative solutions calculated for each transformer.

Table 10 Transformer Positive-Negative Ideal Solution.

Ideal Solutions	C1	C2	C3
Positive Ideal Solution	0.114	0.064	0.191
Negative Ideal Solution	0.381	0.019	0.057

Step 5. Relative Closeness to The Ideal Solution

At this stage, relative closeness to the ideal solution is calculated and presented in table 11.

Table 11 Distances to Transformer Positive Ideal and Negative Ideal Solutions

Transformer	Positive Ideal Solution	Negative Ideal Solution
T1	0.14	0.27
T2	0.13	0.19
T3	0.14	0.16
T4	0.27	0.14
T5	0.14	0.17
T6	0.13	0.22
T7	0.12	0.21

Step 6. Finding The Suitability Order of The Alternatives

In the final stage of the process, the preference scores were identified and organised in a ranked order, as illustrated in Table 12.

Table 12 Transformer Preference Scores.

Transformer	Preference Score
T1	0.65
T6	0.64
T7	0.62
T2	0.60
T5	0.54
T3	0.53
T4	0.35

4.5. Finding Second Stage Criteria Weights with AHP Method

In accordance with the results of this ranking, transformer 1 has been identified as the primary transformer requiring attention, with a score of 0.65. In the second stage of the study, the preference scores obtained at this stage were also incorporated into the criteria. The following criteria were identified: the distances of the parking lots to the faculty entrances (FE) (C´1), the distances of the parking lots to the campus entrance (CE) gate (C´2), the capacities of the parking lots (C´3), and the transformer preference scores (C´4). All steps applied for the first stage were also applied in the second stage according to the new criteria. A pairwise

comparison matrix was constructed in accordance with the classical AHP method, as detailed in Table 13.

Table 13 Parking Lot Pairwise Comparison Matrix.

	C´1	C´2	C´3	C´4
C´1	1	3	3	3
C´2	1/3	1	3	3
C´3	1/3	1/3	1	2
C´4	1/3	1/3	1/2	1

The RI value was calculated to be 0.90 in accordance with the matrix size. The values in the matrix were subjected to a process of normalisation, resulting in the determination of criterion weights as follows: 0.469 for C´1, 0.279 for C´2, 0.148 for C´3 and 0.104 for C´4. Furthermore, the consistency ratio (CR) was determined to be 0.08. Therefore, given that the consistency ratio (CR) is less than 0.1, it can be concluded that the calculated weight is both consistent and accurate.

Finding Second Stage Preference Scores with TOPSIS Method

After the application of AHP, the TOPSIS method was applied in the order of the first stage. Accordingly, the normalised decision matrix was calculated first and is shown in Table 14.

Table 14 Parking Decision Matrix Normalization.

	C´1	C´2	C´3	C´4
PL 1	0.392	0.215	0.182	0.182
PL 2	0.299	0.328	0.152	0.152
PL 3	0.525	0.450	0.379	0.379
PL 4	0.372	0.513	0.364	0.364
PL 5	0.227	0.432	0.546	0.546
PL 6	0.325	0.352	0.379	0.379
PL 7	0.431	0.264	0.476	0.476

The normalised values were weighted in accordance with the weights determined by the AHP method, as detailed in Table 15.

Table 15 Parking Lot Weighted Normalized Decision Matrix.

	C´1	C´2	C´3	C´4
PL 1	118.8	146.0	6.0	0.1
PL 2	90.5	222.8	5.0	0.1
PL 3	159.1	306.0	12.5	0.1
PL 4	112.6	348.8	12.0	0.0
PL 5	68.8	293.6	18.0	0.1
PL 6	98.5	239.6	12.5	0.1
PL 7	130.6	179.6	15.7	0.1

Following the acquisition of the weighted normalised matrix, an investigation was conducted into the positive ideal and negative ideal properties, with the distances to the positive and negative solutions calculated for each parking lot.

Table 16 Parking Lot Positive-Negative Ideal Solution.

	C´1	C´2	C´3	C´4
Positive Ideal Solution	159.12	146.00	5.00	0.07
Negative Ideal Solution	68.80	348.80	18.00	0.03

Table 17 Distances to Parking Lot Positive Ideal and Negative Ideal Solutions

Parking Lots	Positive Ideal Solution	Negative Ideal Solution
PL1	40.29	209.23
PL2	102.98	128.52
PL 3	160.18	100.10
PL 4	208.19	44.17
PL 5	173.53	55.20
PL 6	111.76	113.31
PL 7	45.38	180.13

Finally, the ranking was done by calculating the preference scores for the second stage (Table 18). According to this ranking, PL1 was identified as the first priority car park with a score of 0.84.

Table 18 Parking Lot Preference Scores

Parking Lots	Preference Score
PL1	0.84
PL 7	0.80
PL 2	0.56
PL 6	0.50
PL 3	0.38
PL 5	0.24
PL 4	0.18

Sensitivity Analysis

The present study has undertaken a sensitivity analysis with the objective of examining the effect of changes in the criteria weights on the ranking of the alternatives. The methodology employed in this study is founded upon the principle of re-ranking the alternatives with the TOPSIS method by altering the criteria weights that have been determined with the AHP method under a range of scenarios. For the sensitivity analysis, the criterion weights determined by AHP were taken as the starting point. Three distinct scenarios were formulated:

The distance criterion (C1) is given the greatest weighting: In this scenario, the distance of the parking lots to the faculty entrances and the campus entrance is the most significant criterion.

The significance of parking capacity (C2) is given as follows:

In scenarios characterised by intensive vehicle usage, where capacity is particularly salient, this factor assumes greater significance.

Weighting of transformer preference score (C3): Scenario where energy infrastructure is critical.
New criteria were calculated for each scenario. The criteria weights for each scenario are changed as in Table 9:

Table 19. Scenario Criterion Weights

Scenario	C1 (Distance)	C2 (Capacity)	C3 (Transformer Score)
Default	0.469	0.148	0.104
Distance Priority	0.600	0.100	0.100
Capacity Priority	0.300	0.400	0.100
Transformer Priority	0.300	0.100	0.400

An increase in the weight of C1 was accompanied by a decrease in the weights of the other criteria, thereby achieving a state of normalization. Similarly, when C2 or C3 was weighed, the weights for other criteria were balanced. The alternatives were then subjected to normalisation using the TOPSIS method with new weights. The determination of positive and negative ideal solutions was achieved. New preference scores were obtained by calculating the distances of the alternatives to the ideal solution. With these weights, the distances to the positive and negative ideal solutions were calculated for each alternative using the TOPSIS method (Table 20).

Table 20 Positive And Negative Ideal Solutions

Parking	Default Score	Distance Priority	Capacity Priority	Transformer Score Priority
PL1	0.84	0.86	0.79	0.82
PL2	0.56	0.58	0.60	0.55
PL3	0.38	0.35	0.40	0.37
PL4	0.18	0.15	0.22	0.19
PL5	0.24	0.20	0.30	0.25
PL6	0.50	0.52	0.47	0.51
PL7	0.80	0.82	0.75	0.78

Consequently, the sensitivity analysis demonstrated that, despite alterations in the ranking of the alternatives, the position of the parking lot with the highest score in the ranking remained unaltered. This finding serves to substantiate the model's resilience and dependability. The sensitivity analysis conducted in this study was undertaken to ascertain the impact of alterations in criteria weights on the ranking of alternatives. The criteria determined by the AHP method were subjected to modification under different scenarios, and the alternatives were re-ranked. This analysis resulted in the observation of some changes in the rankings of the alternatives. Specifically, in scenarios where the weight assigned to the distance criterion was augmented, parking lots near faculty entrances emerged as prominent contenders. Conversely, in scenarios where parking capacity was prioritized, larger parking lots were found to confer a distinct advantage. However, it was observed that the parking lot determined as the most suitable alternative maintained its first position. These results demonstrate the model's consistency and reliability in the decision-making process.

CONCLUSION AND DISCUSSION

This study used AHP and TOPSIS to choose the best parking lot for an EV charging station. In the first phase of the study, the distances between transformers and parking lots, parking lot capacities and transformer powers were evaluated for each alternative. The T1 transformer was the best choice after matrix weighting and preference score calculation. In the second stage, the scores from the first stage were used to evaluate the parking lots. Factors such as distance to entrances and gate, and capacity were also considered. The PL1 car park was identified as the optimal location based on the calculated weighting and preference scores at the conclusion of the second stage. The superior features of PL1, namely its advantageous position in terms of distance and the potential for increasing transformer power despite the latter's seemingly low capacity, have resulted in the creation of a competitive solution. The limited capacity of the PL1 car park has resulted in a reduction in the overall weight of the car park due to the comparatively low demand for EV charging stations in comparison to the current situation. Upon evaluation of the preference scores of alternative options, it becomes evident that the PL7 and PL2 car parks, situated near PL1, offer comparable advantages and can be considered for second phase installations as the campus development progresses in future projects. The distance effect in the selection of the PL1 parking lot demonstrates that distance weighting may be open to question in the context of the application scenario. In the case of longer-term projects, it would be prudent to undertake a re-evaluation of parking capacity and energy infrastructure. Considering the campus's relatively youthful status and ongoing development, it is possible to obtain disparate outcomes when environmental factors such as traffic density, user behaviour, parking accessibility and staff density are incorporated into the evaluation process. This situation demonstrates the potential for future expansion of study. To enhance the functionality and satisfaction of future parking facilities, it would be prudent to consider augmenting the parking capacity and utilising a multi-transformer power supply. The reliability of the results may be evaluated through a sensitivity analysis, which entails the consideration of alternative weight scenarios. Furthermore, the long-term sustainability of this study can be enhanced by the development of a more comprehensive model and the incorporation of data such as user demand forecasts and energy cost analysis. The findings of this study indicate that the application of a multi-criteria decision-making methodology would be advantageous in the context of the installation of an EV charging station at the Binali Yıldırım University Yalnızbağ Campus in Erzincan. Nevertheless, a more dynamic model that incorporates environmental factors could offer a more comprehensive framework for future research.

Acknowledgement

The author received no financial support for the research,

authorship or publication of this article.

References

1. Kaya Ö, Tortum A, Alemdar KD, Çodur MY. Site selection for EVCS in Istanbul by GIS and multi-criteria decision-making. Transp Res Part D Transp Environ. 2020; 80:102271.
2. Xylia M, Leduc S, Patrizio P, Kraxner F, Silveira S. Locating charging infrastructure for electric buses in Stockholm. Transp Res Part C Emerg Technol. 2017; 78:183–200.
3. Asnaz MSK, Özdemir B. Optimal positioning of electric vehicle charging stations using multi-criteria decision-making methods. J Intell Transp Syst Appl. 2021;4(2):175–87.
4. Saaty TL. The analytic hierarchy process (AHP). J Oper Res Soc. 1980;41(11):1073–6.
5. Uygurtürk H, Korkmaz T. Determination of financial performance with TOPSIS multi-criteria decision-making method: An application on basic metal industry enterprises. Eskişehir Osmangazi Univ J Econ Adm Sci. 2012;7(2):95–115.
6. Karabıçak Ç, Boyacı Aİ, Akay MK, Özcan B. Multi-criteria decision-making methods and an application on highway construction site selection. Kastamonu Univ J Fac Econ Adm Sci. 2016;13(3):106–21.
7. Alkan T, Atiz ÖF, Durduran SS. Selection of suitable locations for electric vehicle charging stations using AHP method: Konya example. Nigde Omer Halisdemir Univ J Eng Sci. 2023;12(1):1.
8. Saha A, Roy R. An integrated approach to identify suitable areas for built-up development using GIS-based multi-criteria analysis and AHP in Siliguri planning area, India. SN Appl Sci. 2021; 3:1–17.
9. Erbaş M, Kabak M, Özceylan E, Çetinkaya C. Optimal siting of electric vehicle charging stations: A GIS-based fuzzy multi-criteria decision analysis. Energy. 2018; 163:1017–31.
10. Bilgilioğlu SS. Electric vehicle charging station location selection using geographic information systems and fuzzy analytical hierarchy process. Afyon Kocatepe Univ J Sci Eng. 2022;22(1):165–74.
11. Khalkhali K, et al. Application of data envelopment analysis theorem in plug-in hybrid electric vehicle charging station planning. IET Gener Transm Distrib. 2015;9(7):666–76.
12. https://ebyu.edu.tr/ (Access Date: 06.12.2024)
13. Akar AU, Yalpir S, Sisman S, Goktepeli G, Yel E. A deterministic approach in waste management: Delineation of potential territories in Turkey for industrial symbiosis of olive pomace, marble wastes and plastics by integrating Fuzzy AHP to GIS. Environ Dev Sustain. 2023;25(6):5635–62.
14. Saaty TL. How to decide: the analytic hierarchy process. Eur J Oper Res. 1990;48(1):9–26.
15. Mikhailov L, Tsvetinov P. Evaluation of services using a fuzzy analytic hierarchy process. Appl Soft Comput. 2004;5(1):23–33.
16. Supçiller A, Çapraz O. Supplier selection application based on AHP-TOPSIS method. Istanbul Univ Econom Stat e-Journal. 2011;(13):1–22.
17. Hwang CL, Yoon K. Multiple attributes decision making methods and applications. Berlin: Springer; 1981.
18. Tsaur SH, Chang TY, Yen CH. The evaluation of airline service quality by fuzzy MCDM. Tourism Manag. 2002; 23:107–15.
19. Yurdakul M, İç YT. A case study using TOPSIS method for performance measurement and analysis of Turkish automotive companies. Gazi Univ Fac Eng Arch J. 2003;18(1):1–13.
20. Shyjith K, Ilangkumaran M, Kumanan S. Multi-criteria decision-making approach to evaluate optimum maintenance strategy in textile industry. J Qual Maint Eng. 2008;14(4):375–86.

HITTITE JOURNAL OF SCIENCE AND ENGINEERING

e-ISSN: 2148-4171
Volume: 12 • Number: 2
June 2025

Nonlinear MPC-Based Formation Control for Autonomous Ground Vehicles with Dynamic Geometric Patterns

Can Ulas Dogruer
Hacettepe University, Department of Mechanical Engineering, 06800, Ankara, Türkiye.

Corresponding Author

Can Ulas Dogruer
E-mail: cdogruer@hacettepe.edu.tr Phone: +90 312 2976208
RORID: https://ror.org/04kwvgz42

Article Information

Article Type: Research Article
Doi: https://doi.org/10.17350/HJSE19030000356
Received: 29.03.2025
Accepted: 26.05.2025
Published: 30.06.2025

Cite As

Dogruer C U. Nonlinear mpc-based formation control for autonomous ground vehicles with dynamic geometric patterns. Hittite J Sci Eng. 2025;12(2):101-110.

Peer Review: Evaluated by independent reviewers working in at least two different institutions appointed by the field editor.
Ethical Statement: Not available.
Plagiarism Checks: Yes - iThenticate
Conflict of Interest: Authors approve that to the best of their knowledge, there is not any conflict of interest or common interest with an institution/organization or a person that may affect the review process of the paper.

CRediT AUTHOR STATEMENT

Can Ulas Dogruer: Conceptualization, Methodology, Software, Validation, Writing- original draft, Data curation, Visualization, Investigation, Supervision, Writing- review and editing.

Nonlinear MPC-Based Formation Control for Autonomous Ground Vehicles with Dynamic Geometric Patterns

Can Ulas Dogruer

Hacettepe University, Department of Mechanical Engineering, 06800, Ankara, Türkiye.

Abstract

This paper presents a nonlinear model predictive control (NMPC) framework for real-time formation control of autonomous ground vehicles (AGVs) operating under dynamic geometric patterns. The proposed method integrates a nonlinear kinematic bicycle model with a time-varying linearization strategy and constrained quadratic optimization to compute control inputs for each follower agent. Formation references are generated online using geometric transformation functions, enabling flexible spatial configurations such as line, rectangular, half-circle, and V-shaped formations. An exponential convergence model ensures smooth trajectory tracking, while input constraints are enforced at each control step. The controller is decentralized and scalable, with each agent solving its own NMPC problem using leader pose information. Extensive simulations validate the approach across multiple formations, demonstrating accurate tracking, constraint satisfaction, and real-time feasibility. The results confirm that the proposed NMPC architecture provides a unified and modular solution for multi-AGV formation control under nonlinear dynamics.

Keywords: MPC, Formation Control, Tracking Control, AGV, Optimization

INTRODUCTION

Formation control for multiple autonomous ground vehicles (AGVs) has become increasingly significant, driven by diverse applications such as logistics, surveillance, exploration, and cooperative robotic tasks. Coordinated motion using precise geometric patterns allows a fleet of AGVs to execute complex tasks more efficiently and reliably compared to individual operation. Among the various methodologies explored for multi-agent coordination, Model Predictive Control (MPC) has emerged as a powerful approach due to its capability to systematically handle nonlinear dynamics, enforce operational constraints, and proactively plan trajectories within a predictive optimization framework.

Typically, in formation control scenarios, one vehicle-designated as the leader-follows a predefined trajectory, while the follower vehicles adjust their movements to maintain desired relative positions, forming structured patterns. Challenges arise particularly when the vehicle dynamics are inherently nonlinear, and when practical limitations such as velocity and steering constraints are considered. Additionally, ensuring smooth and adaptive convergence of followers to dynamically changing formation positions becomes crucial as the leader executes complex or time-varying maneuvers.

This paper contributes to addressing these issues by developing a nonlinear MPC-based control framework explicitly tailored for real-time formation control of AGVs. Specifically, the leader AGV navigates along a predefined figure-eight trajectory, while follower AGVs maintain formations including V-formation, rectangular, half-circle, and line shapes. A key contribution is the introduction of custom-designed formation generation functions, which calculate the follower positions dynamically based on the leader' s current position and orientation.

Another significant contribution is the implementation of exponentially convergent reference trajectories for each follower, ensuring smooth and monotonic transitions to their designated formation positions. The nonlinear kinematic bicycle model, representing the vehicle dynamics, is linearized at each time step around the current operating conditions, creating a computationally efficient, time-varying linear MPC formulation. Euler integration discretizes the system, and constraints on control inputs realistically capture physical vehicle limitations.

The proposed approach uniquely combines the adaptability of dynamic formation patterns with the robust, constraint-handling features inherent in MPC. Simulation results clearly demonstrate the method's effectiveness in real-time scenarios, showcasing stable and precise formation tracking across diverse geometric patterns. This research establishes a modular and flexible MPC framework, capable of further extensions such as dynamic obstacle avoidance, environmental adaptation, and seamless formation reconfiguration.

The remainder of this paper is structured as follows. Section II provides a focused review of related works in formation control and model predictive control, highlighting the limitations of prior approaches and motivating the need for flexible, real-time formation strategies under nonlinear dynamics. Section III outlines the theoretical methodology, detailing the use of time-varying linearized MPC, formation reference generation based on geometric transformations, and exponential convergence for reference trajectories. Section IV presents extensive simulation studies across four distinct formation types—line, rectangular, half-circle, and V-shape—validating the proposed approach in terms of tracking accuracy, constraint satisfaction, and control input smoothness. Finally, Section V concludes the paper with a summary of the key contributions and discusses potential future extensions, including real-time deployment and experimental validation.

RELATED WORKS

MPC has become a foundational strategy in multi-agent formation control due to its ability to handle constraints and nonlinear system dynamics predictively. Early works, such as Chen and Wang [1], laid the theoretical groundwork for formation strategies but lacked scalable implementations suitable for real-time operations. Since then, considerable advancements have been made across various domains including UAVs, AGVs, and marine vehicles. However, key limitations still persist.

In aerial domains, numerous studies have employed distributed MPC for UAV formation control [2–4]. While effective for decentralized navigation and obstacle avoidance, these approaches generally assume static formations and limited trajectory complexity. The emphasis has been on minimizing communication or energy usage [5], rather than enabling flexible formation morphologies or curvature-aware planning.

Others have integrated MPC with robust feedback linearization [6], neural optimization [7], or consensus-based strategies [8], but these often remain confined to homogeneous agent dynamics and fail to generalize to ground vehicle-specific kinematic constraints. UAV-specific schemes such as Ille and Namerikawa's MPC-based collision avoidance [9] or Droge's behavior-based MPC [10] further highlight this aerial-centric bias, providing limited relevance to the nonholonomic challenges of ground vehicle formations.

Ground-based formation control using MPC has gained traction more recently. Zhang et al. [11] demonstrated learning-enhanced MPC for trajectory tracking, while Oyelere [12] and Liu et al. [13] applied nonlinear MPC to high-speed AGV path planning. However, these studies predominantly addressed single-vehicle scenarios and lacked inter-agent formation logic. Similarly, Fukushima et al. [14] investigated centralized MPC formation control with collision avoidance, though at significant computational cost, hindering scalability. Formation reconfigurability remains underexplored. While Zang et al. [15] proposed a multi-objective distributed MPC for UGV formations, their framework lacked modularity and pattern switching capabilities. Some hybrid systems [16,17] have incorporated formation control under environmental disturbances or partial decentralization, yet still rely on fixed spatial templates or heuristic adaptations. Approaches integrating PSO or reinforcement learning [18,19] often prioritize optimization over geometric consistency.

Our work directly addresses these limitations by introducing a modular, nonlinear MPC framework specifically designed for real-time formation tracking of AGVs with dynamic geometric configurations. Key distinctions from prior works include: Unlike existing literature that assumes fixed or homogeneous patterns, our system supports seamless transitions among V-shape, line, half-circle, and rectangular formations. Unlike methods based on linear reference paths [4,20], we employ exponential convergence trajectories aligned with the leader's kinematic profile, allowing accurate tracking in sharp turns. Whereas many studies simplify AGV dynamics into linear or first-order systems [21,22], our use of a time-varying linearization of the kinematic bicycle model better captures real-world driving constraints and enhances prediction accuracy. Most prior efforts intertwine trajectory generation with control [23,24], limiting adaptability. Our architecture decouples the formation generation layer from the control layer, enabling better modularity, tuning, and potential platform transferability.

Additionally, while hierarchical MPC schemes [25] and cooperative hybrid frameworks [26,27] offer complex coordination strategies, they often overlook low-level control fidelity and formation morphology flexibility.

By bridging the gap between nonlinear predictive control and modular geometric formation design, our approach offers a scalable, curvature-sensitive, and structurally adaptive control strategy suitable for real-world AGV deployments.

THEORY

Multi-Agent Formation Control Framework

This study investigates the cooperative control of a multi-agent system composed of autonomous ground vehicles (AGVs), indexed by $i \in \{0, 1, \ldots, N\}$, where *i=0* denotes the leader and $i = 1, \ldots, N$ are followers. The leader AGV follows a predefined trajectory---specifically a figure-eight path---while each follower AGV is required to maintain a predefined geometric position within a dynamic formation, relative to the leader's real-time pose (position and heading angle).

The central control objective is to ensure that each follower AGV tracks its assigned formation position while respecting its nonlinear dynamics and control input constraints, adapting in real-time to changes in the leader's trajectory.

Nonlinear AGV Dynamics

Each AGV is modeled using a continuous-time nonlinear system:

$$\dot{x}_i = f(x_i, u_i) \tag{1}$$

where $x_i \in \mathbb{R}^4$is the state vector representing the AGV's global position, orientation, and speed:

$$x_i = \begin{bmatrix} x_i \\ y_i \\ \psi_i \\ V_i \end{bmatrix} \tag{2}$$

and $u_i \in \mathbb{R}^3$ is the control input vector:

$$u_i = \begin{bmatrix} a_i \\ \delta_{f,i} \\ \delta_{r,i} \end{bmatrix} \tag{3}$$

with a_i denoting the longitudinal acceleration, $\delta_{f,i}$ the front steering angle, and $\delta_{r,i}$ the rear steering angle. The nonlinear kinematic bicycle model is:

$$\begin{aligned} \dot{x}_i &= V_i \cos(\psi_i + \beta_i) \\ \dot{y}_i &= V_i \sin(\psi_i + \beta_i) \\ \dot{\psi}_i &= \tfrac{V_i}{L} \sin\left(\beta_i\right) \\ \dot{V}_i &= a_i \end{aligned} \tag{4}$$

where β_i is the effective sideslip angle:

$$\beta_i = \tan^{-1} \tfrac{L_r \tan(\delta_{f,i}) + L_f \tan(\delta_{r,i})}{L} \tag{5}$$

and $L = L_f + L_r$ is the wheelbase, with L_f and L_r being the distances from the center of mass to the front and rear axles, respectively.

Figure 1 illustrates the lateral vehicle kinematics described by the nonlinear kinematic bicycle model. It visually represents how the AGV's velocity vector, heading angle, and effective sideslip angle β_i interact in determining the vehicle's trajectory.

This nonlinear kinematic bicycle model represents a non-holonomic system, as it imposes non-integrable constraints on the motion—specifically, lateral slipping is not allowed. The vehicle's trajectory is constrained to evolve along its heading direction, making sideway motion impossible without reorientation. This inherent non-holonomic nature introduces additional challenges in trajectory planning and formation control, as the system's feasible motions are geometrically restricted.

Furthermore, the model is overactuated, since the control input vector includes three degrees of control—longitudinal acceleration (a_i), front steering angle ($\delta_{f,i}$), and rear steering angle ($\delta_{r,i}$)—while the system has only two degrees of underactuated mobility in the plane. This redundancy can be exploited to enhance control flexibility. In the context of formation control, having both front and rear steering allows the AGV to follow tighter curvature paths with smaller turning radii, improve convergence to dynamic references, and maintain geometric alignment with fewer oscillations in heading or velocity. This is particularly advantageous in dense or dynamic multi-agent formations, where rapid and precise reconfiguration is essential.

This nonlinear kinematic model serves as the predictive foundation for the Model Predictive Control (MPC) framework applied to each AGV. At each control iteration, the nonlinear dynamics are linearized online around the current operating point yielding a local affine approximation of the system. This linear model is discretized and used to predict the future evolution of the AGV over a finite prediction horizon. A reference trajectory, derived from the desired formation geometry relative to the leader's real-time pose, is also constructed for each agent. The MPC then solves a constrained quadratic optimization problem, which minimizes the deviation between predicted and reference states while ensuring that control inputs (acceleration and steering angles) remain within feasible bounds. The optimal control action obtained from this procedure is applied in real-time, and the process repeats at the next time step, allowing each AGV to continuously adjust its trajectory and maintain formation despite nonlinearities and dynamic updates in the formation geometry.

Formation Geometry and Reference Trajectory Generation

At each time step t, the reference position for follower i in the global frame is computed using a rotation-translation transformation based on the leader's pose:

$$p_{i,\text{ref}}(t) = R(\psi_0(t)) \cdot \Delta_p i + p_0(t) \tag{6}$$

where: $\Delta_p i \in \mathbb{R}^2$: desired relative position of follower i in the leader's local frame, $p_0(t) = [x_0(t), y_0(t)]^\top$: global position of the leader, $\psi_0(t)$: heading angle of the leader at time t $R(\psi_0) \in \mathbb{R}^{2\times 2}$: rotation matrix:

$$R\left(\psi_0\right) = \begin{bmatrix} \cos(\psi_0) & -\sin(\psi_0) \\ \sin(\psi_0) & \cos(\psi_0) \end{bmatrix} \tag{7}$$

Relative positions Δp_i are generated by one of the four formations. Figures 2 and 3 support the formation generation logic. Figure 2 presents the four geometric formation types used in this study—line, rectangular, half-circle, and V-shaped. These layouts correspond to the relative position vectors Δp_i introduced in the formation equations. Figure 3 expands this by showing the information flow in the leader–follower framework. It maps how the leader's pose is used to compute global reference positions for each follower, which are then used as inputs for the individual MPC controllers.

Leader Trajectory: Figure-Eight Path

The leader AGV is assigned a predefined smooth trajectory in the shape of a figure-eight, which allows both straight and curved segments for evaluating follower tracking performance. The trajectory is parameterized as:

$$\begin{aligned} x_0(t) &= A\sin(\omega t) \\ y_0(t) &= B\sin(\omega t)\cos(\omega t) \end{aligned} \tag{8}$$

where: A, B: amplitude parameters controlling width and height, ω: angular frequency, $x_0(t)$, $y_0(t)$: global leader position. The heading angle of the leader is:

$$\psi_0\left(t\right) = \tan^{-1}\left(\frac{y_0(t)}{x_0(t)}\right) \tag{9}$$

AGV Fleet Formations

Each follower AGV is assigned a relative position Δp_i in a formation centered on the leader. The global reference position is:

$$p_{i,\text{ref}} = R(\psi_0) \cdot \Delta p_i + p_0 \tag{10}$$

where $p_0 = [x_0, y_0]^\top$ is the leader's position and $R(\psi_0)$ is the rotation matrix:

$$R\left(\psi_0\right) = \begin{bmatrix} \cos(\psi_0) & -\sin(\psi_0) \\ \sin(\psi_0) & \cos(\psi_0) \end{bmatrix} \tag{11}$$

V-Formation

Followers are split along two symmetric arms with spacing d and angle ϕ:

Left Arm: $\Delta p_i = \begin{bmatrix} -id\cos\left(\frac{\phi}{2}\right) \\ id\sin\left(\frac{\phi}{2}\right) \end{bmatrix}$;

Right Arm: $\Delta p_i = \begin{bmatrix} -id\cos\left(\frac{\phi}{2}\right) \\ -id\sin\left(\frac{\phi}{2}\right) \end{bmatrix}$

Rectangular Formation

Let r be rows, c columns, with spacing δ_x, δ_y. Follower i at row r_i, column c_i

$$\Delta p_i = \begin{bmatrix} -r_i\delta_y \\ \left(c_i - \frac{c}{2}\right)\delta_x \end{bmatrix} \tag{12}$$

Half-Circle Formation

Followers are on a semicircle of radius R:

$$\Delta p_i = \begin{bmatrix} -R\cos(\theta_i) \\ R\sin(\theta_i) \end{bmatrix}, \quad \theta_i \in [-\pi/2, \pi/2] \tag{13}$$

Line Formation

Followers are spaced by d directly behind the leader:

$$\Delta p_i = \begin{bmatrix} -i \cdot d \\ 0 \end{bmatrix} \tag{14}$$

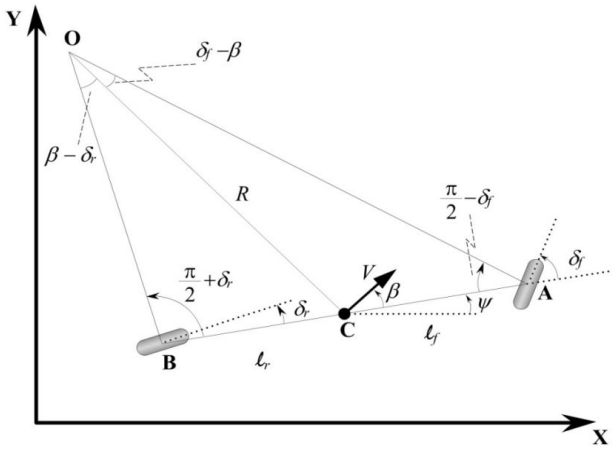

Figure 1 Kinematics of lateral vehicle motion

Each layout is rotated by ψ_0 and translated to p_0 for global positioning.

Model Predictive Control (MPC) Formulation

The nonlinear system is linearized around the current state and control $\left({x_i}^0, {u_i}^0\right)$:

$$\dot{\delta x}_i = A_i\left(t\right)\delta_x i + B_i\left(t\right)\delta_u i \tag{15}$$

where:

$$A_i(t) = \left.\frac{\partial f}{\partial x_i}\right|_{x_i^0, u_i^0}, \quad B_i(t) = \left.\frac{\partial f}{\partial u_i}\right|_{x_i^0, u_i^0} \tag{16}$$

After Euler discretization with step Δt :

$${x_i}^{k+1} = {A_i}^k {x_i}^k + {B_i}^k {u_i}^k \tag{17}$$

where:

$${A_i}^k = I + A_i\left(t\right)\Delta t, \quad {B_i}^k = B_i\left(t\right)\Delta t \tag{18}$$

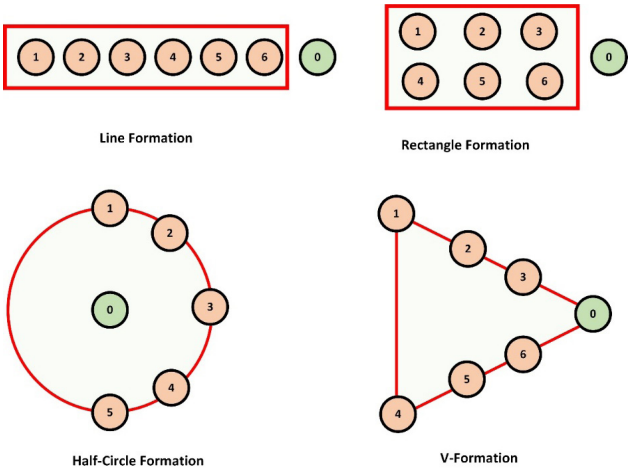

Figure 2 Four different formation patterns for AGV fleet formation.

The MPC optimization problem becomes:

$$\min_{\{u_i^k\}} \sum_{k=0}^{N-1} \left\|x_i^k - \hat{x}_i^k\right\|_Q^2 + \left\|u_i^k\right\|_R^2 \tag{19}$$

subject to:

$$x_i^{k+1} = A_i^k x_i^k + B_i^k u_i^k, u_{ik} \in [\min, \max] \tag{20}$$

A reference trajectory $\hat{x}_i^k$ over a prediction horizon N is constructed:

$$\hat{x}_i^k = x_i^0 + \left(x_{i,\text{ref}} - x_i^0\right)\left(1 - e^{-\lambda \cdot k/N}\right), \quad k = 0, 1, \ldots, N$$

where $\lambda > 0$ is the convergence rate. Thus a smooth uniform convergence to the desired position in the formation is achieved. Virtual exponential path for MPC cost function that implements a tracking control problem is illustrated in Figure 4.

Figures 5 and 6 detail the MPC structure implemented on each follower AGV. Figure 5 illustrates the high-level flow of the MPC algorithm, including

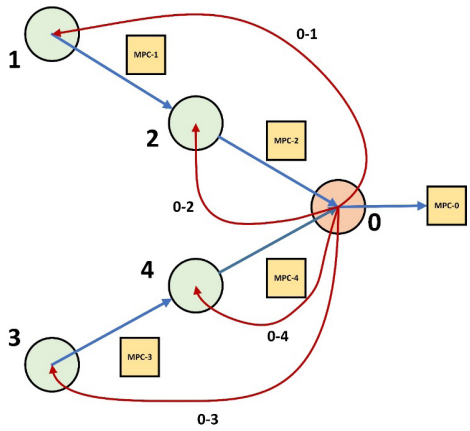

Figure 3 Information flow between leader and follower agents and independent agent-MPC following the formation pattern: Red arrow shows information flow for pattern generation. Blue line represents local agent-MPC controllers. Circles represent agents.

linearization, discretization, and optimization steps executed at each time instant. Figure 6 breaks this process into the computational steps taken by each agent: predicting future states over the horizon, comparing them to the reference trajectory $\widehat{x}_i^k$, and computing the optimal input sequence u_i^k.

The control inputs---longitudinal acceleration a_i, front steering angle $\delta_{f,i}$, and rear steering angle $\delta_{r,i}$ ---are not determined by explicit analytical expressions. Instead, they are computed as the optimal solution to the constrained quadratic program solved at each time step by the NMPC controller. This optimization minimizes the cost function

$$J = \sum_{k=0}^{N-1} \|x_i^k - \widehat{x}_i^k\|_Q^2 + \|u_i^k\|_R^2 \qquad (21)$$

subject to the discretized linearized system dynamics

$$x_i^{k+1} = A_i^k x_i^k + B_i^k u_i^k, u_{\min} \le u_i^k \le u_{\max} \qquad (22)$$

The optimization yields a sequence of future control actions $\{u_i^0, u_i^1, \ldots, u_i^{N-1}\}$, but only the first input $u_i{}^0 = [a_i{}^0,\ \delta_{f,i}{}^0,\ \delta_{r,i}{}^0]^\top$ is applied to the AGV in real time. This

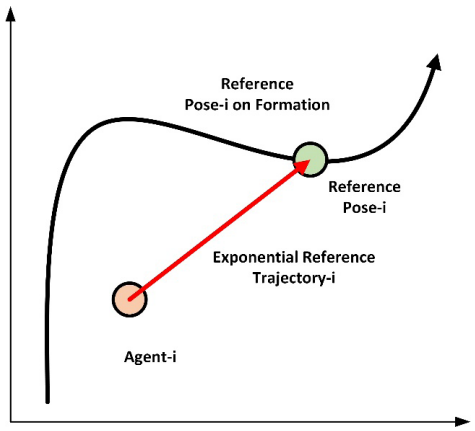

Figure 4. Virtual exponential path for MPC cost function that implements a tracking control problem.

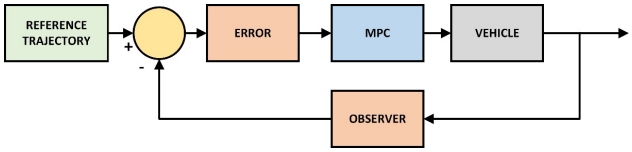

Figure 5 A general block diagram of an agent-MPC for formation pattern following.

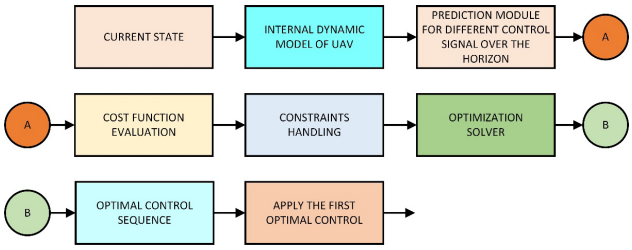

Figure 6 Details of an agent-MPC controller optimization cycle.

receding horizon strategy ensures that the control inputs account for nonlinear vehicle behavior, dynamic formation references, and actuator constraints at every control cycle.

RESULTS AND DISCUSSION

This section presents a detailed evaluation of the proposed nonlinear model predictive control (NMPC) strategy applied to a fleet of AGVs operating under varying geometric formations. The controller is tested under four formation types—line, rectangle, half-circle, and V-shape—generated using relative position functions defined in the theory section. The leader AGV follows a predefined figure-eight trajectory, and each follower tracks a dynamic reference generated based on the leader's pose. The decentralized NMPC controller for each follower is constructed via online linearization and operates in real-time under input and state constraints.

To determine optimal control gains for follower AGVs, a nonlinear constrained optimization is performed using MATLAB's $\mathrm{fmincon}$ solver. The objective function evaluates the formation tracking error using a polynomial and exponential convergence model.

The optimization is initialized with a baseline control vector and executed under strict tolerance conditions to ensure convergence and accuracy:: Max-Iterations:2x10^4; Function Tolerance / Step Tolerance / Constraint Tolerance / Optimality Tolerance}: 1x10^{-6}; Control bounds: $\mathbf{u} \in [-1, +1]$ The predictive model uses a sampling time of $T_s = 0.2$ seconds and a prediction horizon of $_{\text{N=20}}$. The AGV kinematic parameters are defined as $l_f = l_r = 0.2$ meters, corresponding to the distances from the vehicle's center of gravity to the front and rear axles, respectively. The weighting matrices used in the MPC cost function are defined as:

$$Q = \mathrm{diag}\left(10^4, 10^4, 10^6, 10^2\right), \quad R = 10 \cdot I_3 \qquad (24)$$

where Q penalizes errors in global position, heading, and speed, and R penalizes control input effort across the three input channels.

The simulation spans a total duration of 128 seconds, yielding

641 discrete time steps. All seven follower AGVs are initialized at the same state:

$$x_0 = [2, -1, 1, 0]^T \tag{25}$$

and are simultaneously controlled and monitored throughout the simulation. This simulation setup ensures high-fidelity closed-loop behavior under nonlinear dynamics, allowing rigorous evaluation of both the controller's performance and the system's ability to maintain formation geometry under realistic constraints and convergence expectations.

In the line formation scenario, the results confirm the accurate and stable convergence of all agents to their assigned positions behind the leader. As shown in Figure 7, the global trajectories of the leader align with the figure-eight path, and the spatial consistency of the formation is preserved throughout. Figure 8 highlights the positional tracking errors for leader. These errors decay rapidly, illustrating the effectiveness of the exponential convergence-based reference design. Figure 9 shows the control signals of the leader AGV—longitudinal acceleration and steering angles—which remain smooth and well-behaved, indicating the feasibility of the leader trajectory itself.

Figure 10 visually depicts the agents maintaining line formation through turns, further validating the effectiveness of formation control. In the rectangular formation, depicted in Figure 11, followers are arranged in rows and columns behind the leader. The simulation demonstrates that the fleet preserves both lateral and longitudinal spacing across dynamic maneuvers. The half-circle formation, shown in Figure 12, introduces curved relative positioning for the follower agents. This pattern is particularly demanding due to the asymmetric turning radii it introduces. Yet, the agents manage to preserve the arc structure while tracking the leader's figure-eight path. In the V-formation scenario, shown in Figure 13, the agents are symmetrically distributed along two angled arms extending from the leader. This configuration challenges the control architecture due to its symmetry sensitivity and turning dynamics. Nevertheless, the system maintains stable inter-agent spacing and heading alignment.

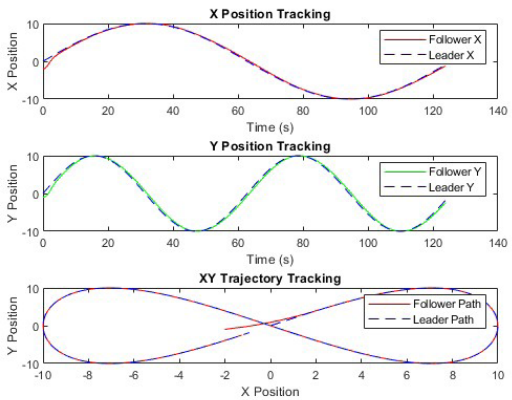

Figure 7 Line formation control: x/y tracking and trajectory tracking graphs of leader

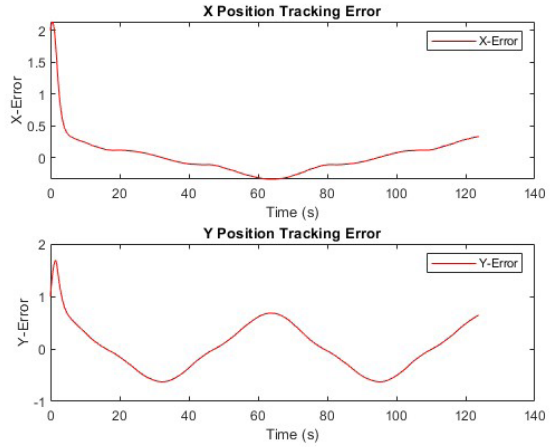

Figure 8 Line formation control: Leader x/y position error.

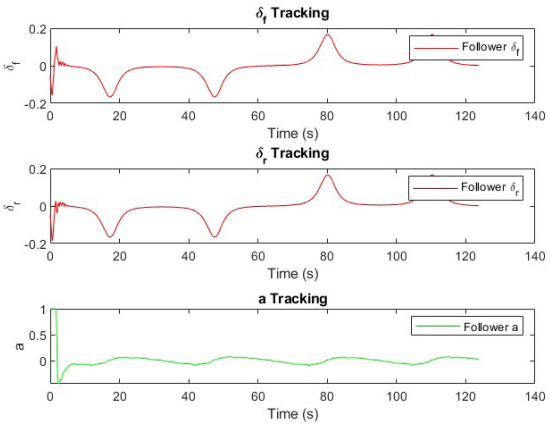

Figure 9 Line formation control: Leader control signal.

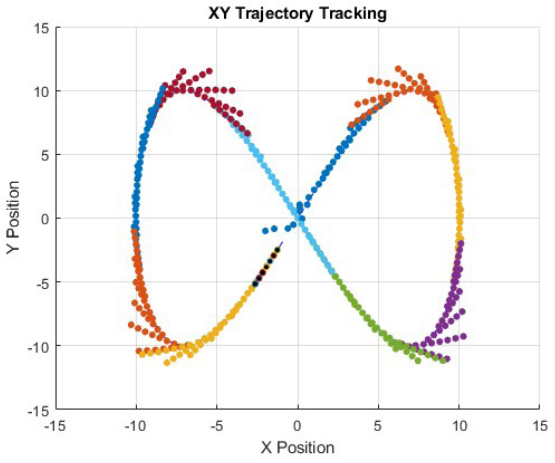

Figure 10 Line formation control: AGV fleet formation on the path.

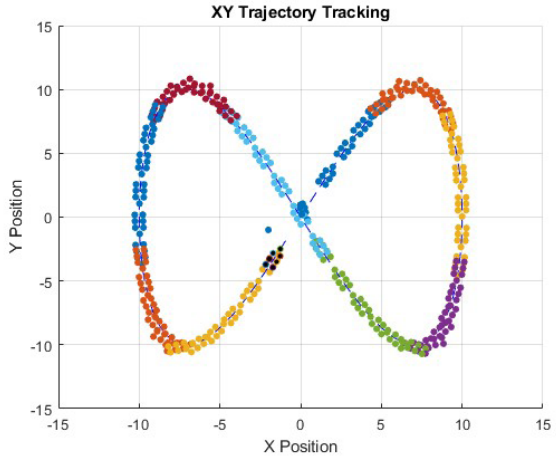

Figure 11 Rectangle formation control: AGV fleet formation on the path.

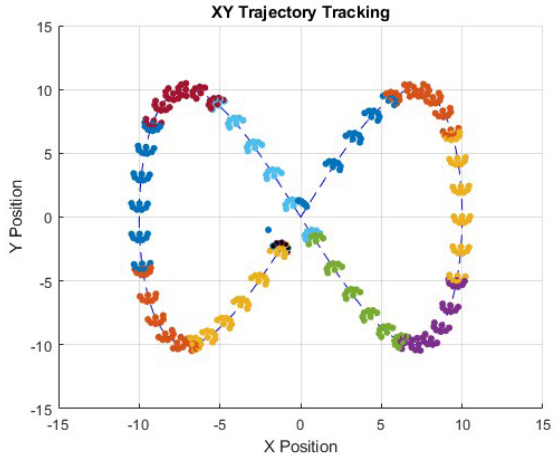

Figure 12 Half-Circle formation control: AGV fleet formation on the path.

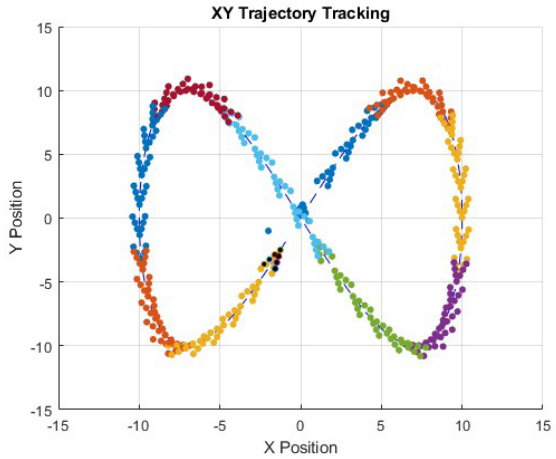

Figure 13 V- formation control: AGV fleet formation on the path.

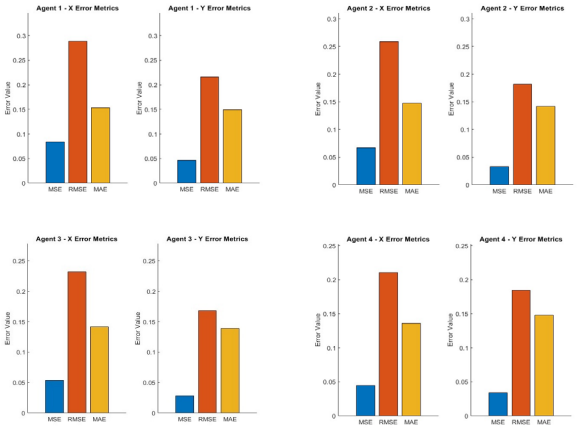

Figure 14 Error metrics for AGV line formation agent's position

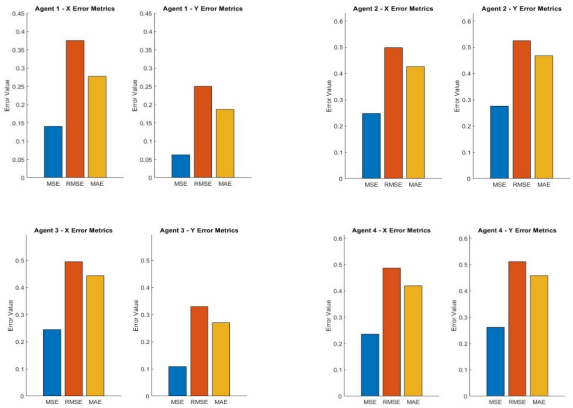

Figure 15 Error metrics for AGV rectangle formation agent's position

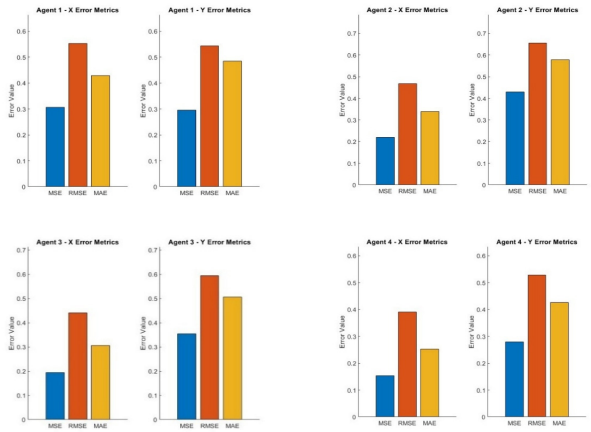

Figure 16 Error metrics for AGV half-circle formation agent's position

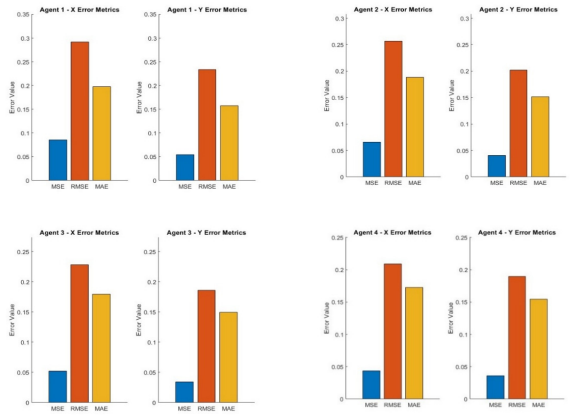

Figure 17 Error metrics for AGV V-formation agent's position

Quantitatively, Figure 14 presents the error metrics for line formation scenario (MSE, RMSE, and MAE), demonstrating uniformly low values across all agents and confirming the accuracy of the MPC tracking scheme. Error metrics in Figure 15 show slight increases compared to the line formation, which is expected due to the added geometric complexity. Nonetheless, the errors remain bounded and small, verifying that the MPC controller generalizes well across different spatial configurations. F igure 16 confirms the accuracy of this performance, showing low and consistent tracking errors even under rapid changes in leader heading. Figure 17 reports the error metrics for this scenario, showing only a modest increase compared to simpler geometries, with overall tracking performance remaining robust and stable.

Overall, the simulations confirm that the proposed NMPC framework ensures stable formation tracking under nonlinear dynamics and tight control constraints. The modular reference generation logic—paired with exponential trajectory convergence—provides consistent behavior across all formation types. Control inputs remain bounded and smooth in all cases, as verified by the time histories and error metrics. Most importantly, the same NMPC structure applies uniformly across all geometric formations without requiring structural changes to the controller, highlighting both the scalability and flexibility of the proposed approach.

CONCLUSION

In this study, a NMPC strategy was developed for the formation tracking of AGVs operating in a leader-follower configuration. The proposed method enables follower vehicles to track dynamically assigned positions in a geometric formation relative to a leader AGV that moves along a predefined figure-eight trajectory. Multiple formation types-V-shape, rectangle, half-circle, and line-were supported through modular formation generation functions, allowing for adaptable and structured coordination.

To address the inherent nonlinearity in AGV dynamics, the system was linearized at each time step using a time-varying approach, and discretized via Euler integration to derive a computationally tractable prediction model. Reference trajectories for each follower were generated through an exponential convergence scheme toward their target positions, ensuring smooth and stable transitions into the desired formation. Input constraints on steering and acceleration were also incorporated within the MPC framework to ensure realistic control behavior.

The proposed approach provides a scalable and flexible formation control solution, capable of adapting to different formation geometries and leader paths in real-time. Simulation results demonstrate that follower AGVs can converge reliably to their formation positions while respecting dynamic and input constraints.

Future work will focus on extending the framework to dynamic obstacle avoidance, decentralized control architectures, and experimental validation on real robotic platforms.

Acknowledgement

The author received no financial support for the research, authorship, and/or publication of this article.

References

1. Chen YQ, Wang Z. Formation control: a review and a new consideration. In: 2005 IEEE/RSJ International Conference on Intelligent Robots and Systems; 2005 Aug 2-6; Edmonton, Canada. New York (US): IEEE; 2005. p. 3181–6.
2. Xu T, Liu J, Zhang Z, Chen G, Cui D, Li H. Distributed mpc for trajectory tracking and formation control of multi-uavs with leader-follower structure. IEEE Access. 2023;11:128762–128773.
3. Cai Z, Wang L, Zhao J, Wu K, Wang Y. Virtual target guidance-based distributed model predictive control for formation control of multiple uavs. Chin J Aeronaut. 2020;33(3):1037–56.
4. Vargas S, Becerra HM, Hayet J-B. MPC-based distributed formation control of multiple quadcopters with obstacle avoidance and connectivity maintenance. Control Eng Pract. 2022;121:105054.
5. Cai Z, Zhou H, Zhao J, Wu K, Wang Y. Formation control of multiple unmanned aerial vehicles by event-triggered distributed model predictive control. IEEE Access. 2018;6:55614–27.
6. Zhao W, Go TH. Quadcopter formation flight control combining mpc and robust feedback linearization. J Franklin Inst. 2014;351(3):1335–55.
7. Xiao H, Li Z, Chen CP. Formation control of leader–follower mobile robots' systems using model predictive control based on neural-dynamic optimization. IEEE Trans Ind Electron. 2016;63(9):5752–62.
8. Kuriki Y, Namerikawa T. Formation control with collision avoidance for a multi-uav system using decentralized mpc and consensus-based control. SICE J Control Meas Syst Integr. 2015;8(4):285–94.
9. Ille M, Namerikawa T. Collision avoidance between multi-uav-systems considering formation control using mpc. In: 2017 IEEE International Conference on Advanced Intelligent Mechatronics (AIM); 2017 Jul 3-7; Munich, Germany. New York (US): IEEE; 2017. p. 651–6.
10. Droge G. Distributed virtual leader moving formation control

using behavior-based mpc. In: 2015 American Control Conference (ACC); 2015 Jul 1-3; Chicago, US. New York (US): IEEE; 2015. p. 2323–8.
11. Zhang K, Sun Q, Shi Y. Trajectory tracking control of autonomous ground vehicles using adaptive learning mpc. IEEE Trans Neural Netw Learn Syst. 2021;32(12):5554–64.
12. Oyelere SS. The application of model predictive control (mpc) to fast systems such as autonomous ground vehicles (agv). IOSR J Comput Eng. 2014;3(3):27–37.
13. Liu J, Jayakumar P, Stein JL, Ersal T. A nonlinear model predictive control formulation for obstacle avoidance in high-speed autonomous ground vehicles in unstructured environments. Veh Syst Dyn. 2018;56(6):853–82.
14. Fukushima H, Kon K, Matsuno F. Model predictive formation control using branch-and-bound compatible with collision avoidance problems. IEEE Trans Robot. 2013;29(5):1308–17.
15. Zang Z, Gong J, Li Z, Song J, Liu H, Gong C, et al. Formation trajectory tracking control of utvs: A coupling multi-objective iterative distributed model predictive control approach. IEEE Trans Intell Veh. 2022;8(3):2222–32.
16. Dong Z, Zhang Z, Qi S, Zhang H, Li J, Liu Y. Autonomous cooperative formation control of underactuated usvs based on improved mpc in complex ocean environment. Ocean Eng. 2023;270:113633.
17. Eskandarpour A, Majd VJ. Cooperative formation control of quadrotors with obstacle avoidance and self collisions based on a hierarchical mpc approach. In: 2014 Second RSI/ISM International Conference on Robotics and Mechatronics (ICRoM); 2014 Oct 15-17; Tehran, Iran. New York (US): IEEE; 2014. p. 351–6.
18. Huang J, Ji Z, Xiao S, Jia C, Jia Y, Wang X. Multi-agent vehicle formation control based on mpc and particle swarm optimization algorithm. In: 2022 IEEE 6th Information Technology and Mechatronics Engineering Conference (ITOEC); 2022 Mar 25-27; Chongqing, China. New York (US): IEEE; 2022. p. 288–92.
19. Li S, Song Q. Cooperative control of multiple agvs based on multi-agent reinforcement learning. In: 2023 IEEE International Conference on Unmanned Systems (ICUS); 2023 Mar 27-29; Beijing, China. New York (US): IEEE; 2023. p. 512–7.
20. Van Parys R, Pipeleers G. Distributed mpc for multi-vehicle systems moving in formation. Robot Auton Syst. 2017;97:144–52.
21. Yu S, Hirche M, Huang Y, Chen H, Allgöwer F. Model predictive control for autonomous ground vehicles: A review. Autom Intell Syst. 2021;1:1–17.
22. Shen W, Wu D. Path planning of an agv based on artificial potential field and model predictive control. In: 2021 33rd Chinese Control and Decision Conference (CCDC); 2021 May 28-30; Kunming, China. New York (US): IEEE; 2021. p. 6925–30.
23. Zhang J, Yan J, Zhang P. Multi-uav formation control based on a novel back-stepping approach. IEEE Trans Veh Technol. 2020;69(3):2437–48.
24. Wang Y, Yang Y, Pu Y, Manzie C. Path following by formations of agents with collision avoidance guarantees using distributed model predictive control. In: 2021 American Control Conference (ACC); 2021 May 26-28; New Orleans, US. New York (US): IEEE; 2021. p. 3352–7.
25. Qian X, De La Fortelle A, Moutarde F. A hierarchical model predictive control framework for on-road formation control of autonomous vehicles. In: 2016 IEEE Intelligent Vehicles Symposium (IV); 2016 Jun 19-22; Gothenburg, Sweden. New York (US): IEEE; 2016. p. 376–81.
26. Alonso-Mora J, Baker S, Rus D. Multi-robot formation control and object transport in dynamic environments via constrained optimization. Int J Robot Res. 2017;36(9):1000–21.
27. Wei H, Shi Y. MPC-based motion planning and control enables smarter and safer autonomous marine vehicles: Perspectives and a tutorial survey. IEEE/CAA J Autom Sin. 2022;10(1):8–24.